Evidence of Dynamic Thinning and Grounding Line Retreat over the Last Two Decades in Porpoise Bay, Wilkes Land, East Antarctica

Matilda Weatherley

Evidence of Dynamic Thinning and Grounding Line Retreat over the Last Two Decades in Porpoise Bay, Wilkes Land, East Antarctica

Matilda Weatherley

Thesis submitted for M.Sc. By Research Degree

Department of Geography

Durham University

August 2025

Abstract

Over the last four decades, the Antarctic Ice Sheet has been losing mass, largely from West Antarctica. Though the East Antarctic Ice Sheet (EAIS) is often considered less vulnerable to climate change, recent studies suggest that some regions of the EAIS have lost mass at accelerating rates over recent decades. In particular, Wilkes Land, which overlies the marine-based Aurora Subglacial Basin, has been referred to as the 'weak underbelly' of the EAIS. Whilst several large outlet glaciers drain this region, few have been studied in detail, including the four glaciers that drain Porpoise Bay. This thesis presents new data on the understudied Porpoise Bay outlet glacier dynamics observed between 1963 and 2025. Optical satellite imagery, differential synthetic aperture radar interferometry, and a range of previously published datasets are used to explore changes in the ice-shelf front, grounding line position, ice surface velocity and ice surface elevation over the last three decades. The results reveal evidence of dynamic changes in the region, characterised by extreme thinning of grounded ice and rapid grounding line retreat, albeit with large uncertainties, across Holmes East and West glaciers and Frost Glacier. This thesis finds that Holmes West Glacier was recently grounded at the edge of a steep retrograde slope that continues inland for tens of kilometers. Rapid grounding line retreat may therefore be predicted at this glacier over the coming decades. Analysis of ocean temperatures and salinity are consistent with the notion that warm Circumpolar Deep Water proximal to the continental shelf break could access the glaciers through deep cross-shelf troughs, which could drive the previously estimated high rates of basal melting beneath their floating tongues/ice shelves. Observations of ice-shelf frontal change and sea-ice concentration across Porpoise Bay's ice shelves support a previous study of near-synchronous ice-shelf calving that correlates with the break-out of sea ice. This study finds an additional recent calving event, further highlighting the vulnerability of this region to ongoing and future changes in ocean and sea-ice conditions.

Table of Contents

List of Tables

List of Figures

List of Abbreviations

auto-RIFT – autonomous Repeat Image Feature Tracking

AIS – Antarctic Ice Sheet

ASAID - Antarctic Surface Accumulation and Ice Discharge

CDW – Circumpolar Deep Water

CTD-SRDL – Conductivity Temperature Density Satellite Relay Data Logger

DInSAR – Differential Interferometric Synthetic Aperture Radar

EAIS – East Antarctic Ice Sheet

ENSO – El Niño Southern Oscillation

IMBIE – Ice sheet Mass Balance Inter-comparison Exercise

mCDW – modified Circumpolar Deep Water

MEaSUREs – Making Earth Science Data Records for Use in Research Environments

MEOP – Marine Mammal Exploring the Oceans Pole to Pole

MOA – Mosaic Of Antarctica

MICI – Marine Ice Cliff Instability

MISI – Marine Ice Shelf Instability

RCP – Respective Concentration Pathways

SAM – Southern Annular Mode

SLE – Sea Level Equivalent

SMB – Surface Mass Balance

WAIS – West Antarctic Ice Sheet

Statement of Copyright

Acknowledgements

I would like to thank my supervisors, Professor Chris Stokes and Professor Stewart Jamieson, for their guidance and support throughout the year. I am also grateful to Sindhu Ramanath for producing the DInSAR grounding lines around Porpoise Bay and to Alessandro Silvano for providing insight into the oceanography datasets.

Chapter 1: Introduction

1.1 Background

The Antarctic Ice Sheet (AIS) is the largest ice sheet worldwide, containing 57.9 m of global mean sea level equivalent (SLE) (Morlighem et al., 2020). The AIS comprises three regions: the East Antarctic Ice Sheet (EAIS), the West Antarctic Ice Sheet (WAIS), and the Antarctic Peninsula. Recent work has mostly focused on changes in the Antarctic Peninsula (van den Broeke, 2005; Berthier et al., 2012; Cook et al., 2014, 2016; Leeson et al., 2020) and pronounced mass loss in the WAIS (Pritchard et al., 2009; Mouginot et al., 2014; Rignot et al., 2014; McMillan et al., 2015; Feldmann and Levermann, 2015; Pattyn and Morlighem, 2020), which contains 5.3 m SLE (Morlighem et al., 2020). Comparatively less work has focused on the stability of the EAIS, containing 52.2 m SLE, an order of magnitude larger than the WAIS (Morlighem et al., 2020; Stokes et al., 2022).

Recent mass balance studies show accelerating mass loss from the AIS over recent decades; the most recent assessment estimates 2,671 ± 530 Gt of ice lost between 1992 and 2020, equating to 7.4 ± 1.5 mm of global mean sea-level rise (Otosaka et al., 2023). This mass loss is dominated by loss from the WAIS (82 ± 9 Gt yr^{-1}) and the Antarctic Peninsula (13 ± 5 Gt yr^{-1}), with the EAIS remaining close to balance (3 ± 25 Gt yr^{-1}), albeit with larger uncertainties (Otosaka et al., 2023). Mass loss from the WAIS accelerated from −37 ± 19 Gt yr^{-1} (1992–1996) to −131 ± 21 Gt yr^{-1} (2012–2016) then slowed to −94 ± 25 Gt yr^{-1} (2017–2020) (Otosaka et al., 2023). Mass loss from the WAIS is concentrated in the Amundsen Sea Embayment, primarily from Pine Island and Thwaites glaciers (Mouginot et al., 2014; Gardner et al., 2018; Shepherd et al., 2019). Ice sheet mass is lost through ice flow acceleration, thinning, and grounding line retreat, which is predominantly driven by ice-shelf debuttressing due to warm ocean water melting the base of ice shelves (Mouginot et al., 2014; Rignot et al., 2014; Fürst et al., 2016; Pattyn and Morlighem, 2020).

Comparatively, the EAIS has often been considered to be much less vulnerable to recent climate change, with the IMBIE mass balance estimates (e.g., Otosaka et al., 2023) revealing it is largely in balance or slightly increasing in mass (albeit with greater uncertainties than the WAIS). It has been noted that mass gain is generally concentrated in Dronning Maud Land and mass loss in Wilkes Land, with other areas close to balance (Gardner et al., 2018; Smith et al., 2020a; Otosaka et al., 2023). However, there is emerging evidence of a longer-term trend of regional mass loss from Wilkes Land (Rignot et al., 2019; Smith et al., 2020a; Wang et al., 2021; Stokes et al., 2022), referred to as the ‘weak underbelly’ of the EAIS (Miles et al., 2016; Pelle et al., 2020). Wilkes Land is drained by 39

outlet glaciers and has received growing attention in the past three decades due to the emerging signal of mass loss (Gardner et al., 2018; Rignot et al., 2019; Schröder et al., 2019a; Shepherd et al., 2019; Smith et al., 2020a; Nilsson et al., 2022; Stokes et al., 2022, 2025). Mass loss has been linked to the intrusion of warm modified Circumpolar Deep Water (mCDW) in sub-ice cavities through deep cross-shelf troughs, driving melt rates (up to 20 m yr^{-1} between 1994 and 2018) that are comparable to the Amundsen Sea Embayment (Rintoul et al., 2016; Silvano et al., 2016, Miles et al., 2016; Rignot et al., 2019). Indeed, direct observations have confirmed mCDW proximal to three key glaciers in Wilkes Land: Vanderford, Totten, and Moscow University glaciers (Greenbaum et al., 2015; Rintoul et al., 2016; Silvano et al., 2017; Picton et al., 2023). A recent study by Rignot et al. (2019) estimated the cumulative mass loss from each drainage basin in East Antarctica between 1979 and 2017, with Totten (236 Gt) and Denman (191 Gt) glaciers contributing the greatest, followed by Frost (159 Gt) and Holmes (152 Gt) glaciers that both feed Porpoise Bay in Wilkes Land. However, despite Frost and Holmes glaciers losing mass at potentially high rates, there have been few studies of these major outlet glaciers. Furthermore, Wilkes Land is underlaid by a bed that lies below sea level and deepens inland to the Aurora Subglacial Basin (ASB), containing several deep troughs (Morlighem, 2022). This makes it potentially vulnerable to Marine Ice Sheet Instability (MISI), which may have occurred during past warm periods (Cook et al., 2013).

1.2 Study Area

Porpoise Bay (76°S, 128°E) is a 150 km wide bay that lies east of Moscow University Glacier (~300 km) and Totten Glacier (~550 km). The bed overlies the eastern ASB and is approximately 600 m below sea level (Fig. 1.1a), featuring some reverse-sloping beds (Pritchard et al., 2024; Rignot et al., 2024). Porpoise Bay is drained by several marine-terminating outlet glaciers, of which the largest (by catchment area and volume) are Holmes (0.12 m SLE) and Frost glaciers (0.84 m SLE) (Rignot et al., 2019). Holmes Glacier has two distinct outlets that feed the same ice shelf (Fig. 1.1b); the outlets are referred to as Holmes East and Holmes West glaciers (Miles et al., 2017). In addition, a further enhanced area of flow lies between Frost and Holmes East glaciers and is referred to as Glacier 1 in this study.

Recent studies suggest a mass imbalance from the marine-based glaciers entering Porpoise Bay. Rignot et al. (2019) found a potential combined sea level contribution of 0.8 mm from Holmes and Frost catchments between 1979 and 2017. Ice surface thinning was recorded between −0.07 m yr^{-1} and −0.87 m yr^{-1} (2003−2019) (Smith et al., 2020a). Ice-shelf retreat has been linked to sea-ice break-out events (Miles et al., 2017). Finally, records

show ice-shelf thinning (Smith et al., 2020a; Miles and Bingham, 2024), grounding line retreat (Konrad et al., 2018), and ice flow speed up (Rignot et al., 2022). Despite these studies suggesting that dynamic change may be occurring (Miles et al., 2017; Konrad et al., 2018; Rignot et al., 2019; Smith et al., 2020; Rignot et al., 2022; Miles and Bingham, 2024), Porpoise Bay's glaciers have not been studied in detail.

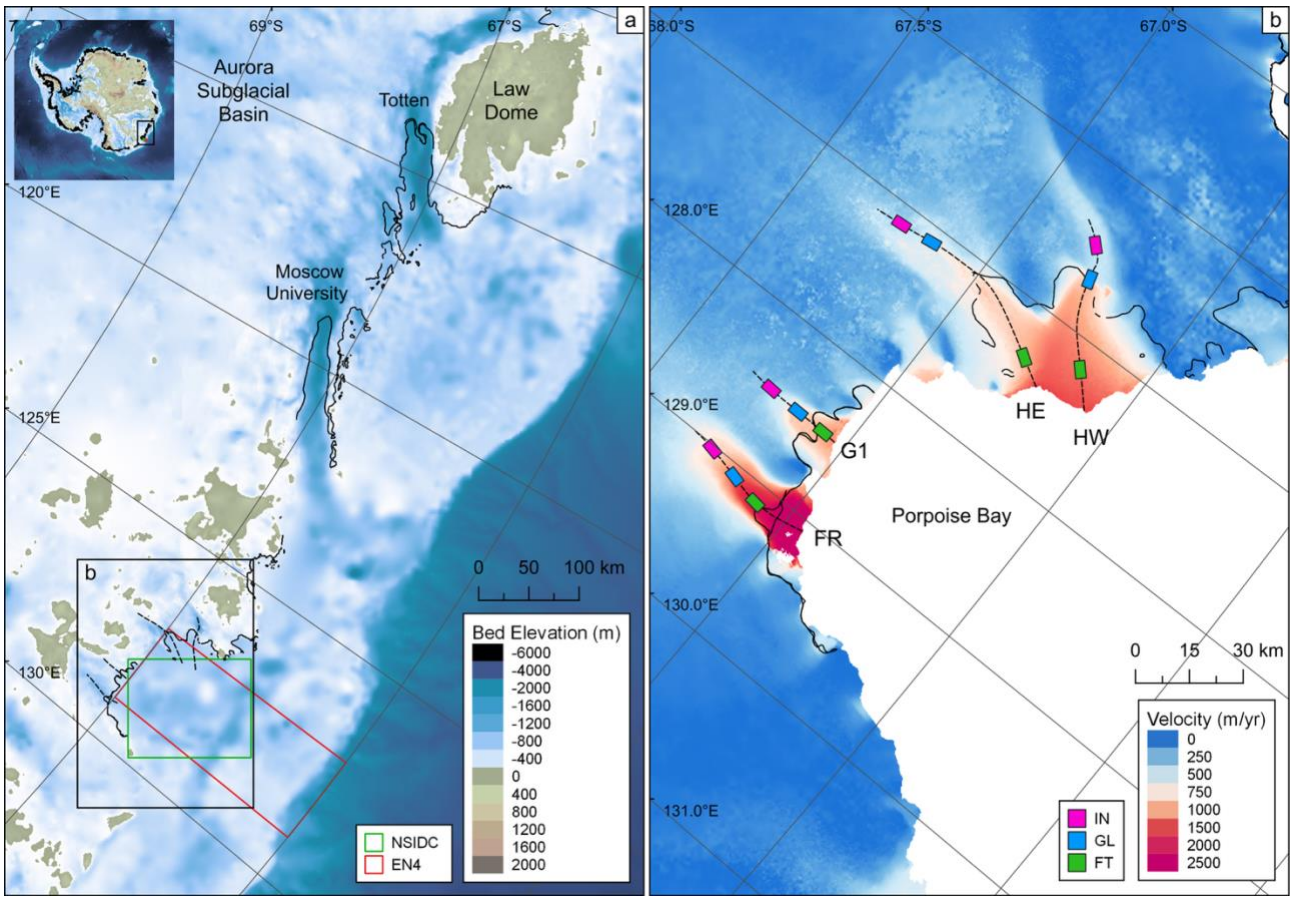

Figure 1.1: (a) Ice sheet bed elevation and bathymetry of Porpoise Bay and the surrounding Wilkes land from Bedmap3 (Pritchard et al., 2024). (b) Ice velocity map of Porpoise Bay extracted from the 2021 ITS_LIVE ice velocity mosaic (Gardner et al., 2025). Central flowlines and sampling boxes are shown across the inland (IN), grounding line (GL), and floating ice tongue (FT) at each of the studied glaciers: Frost (FR), Glacier 1 (G1), Holmes East (HE), and Holmes West (HW). Black lines show the 1996 MEaSUREs grounding line (Rignot et al., 2016).

1.3 Aims and Objectives

This thesis aims to improve our understanding of the recent changes in the ice dynamics of the outlet glaciers in largely unstudied Porpoise Bay, East Antarctica. The following objectives were defined to achieve this aim:

1. To delineate the ice-shelf frontal position using optical satellite imagery between 1963 and 2025.

2. To assess changes in ice surface elevation from 1985 to 2020, assessed from published elevation change datasets from Schröder et al. (2019b), Smith et al. (2020b) and Nilsson et al. (2023).
3. To examine the ice surface velocity of the outlet glaciers, extracted from ITS_LIVE between 2000 and 2022 (Gardner et al., 2025).
4. To explore changes in the grounding line position in Porpoise Bay using a range of datasets, including MEaSUREs (Rignot et al., 2016), ASAID (Bindschadler and Choi, 2011) and MOA (Haran et al., 2018; 2021a; 2021b).
5. To consider potential controls on dynamic changes, including ocean temperature from MEOP (Treasure et al., 2017) and EN4 (Good et al., 2013), sea-ice conditions (Fetterer et al., 2017), and bedrock bathymetry (Morlighem, 2022; Pritchard et al., 2024; Rignot et al., 2024).

1.4 Thesis Structure

This thesis contains six chapters, including the introduction (*Chapter 1*). *Chapter 2* reviews previously published literature on the AIS, providing an insight into the mass balance of the AIS, WAIS and EAIS ice sheet dynamics, including ice-ocean interactions and the potential for ice sheet instabilities, followed by a review of the literature on the outlet glaciers in Porpoise Bay. *Chapter 3* describes the methods employed to address objectives 1 to 5, including the acquisition and delineation of the ice-shelf edge from satellite imagery, processing steps to extract ice surface elevation, ice surface velocity, and grounding lines from secondary datasets, as well as the use of DInSAR to extract grounding line information. The results from these methods are presented in *Chapter 4*, according to the fundamental glacier parameters assessed: ice-shelf frontal position, ice flow velocity, ice surface elevation, and grounding line position. These findings are discussed in *Chapter 5*, exploring signals and potential ocean-climate drivers of dynamic change, the controls on ice-shelf change, mechanisms of glacier flow, and potential future changes in the system. *Chapter 5* also provides recommendations for future work on Porpoise Bay. *Chapter 6* summarises and concludes the finding of this thesis. *Chapters 3, 4, 5,* and *6* were submitted (in August 2025) as a research paper for publication in *The Cryosphere*, which was drafted and lead-authored by MW (Weatherley et al., 2025).

Chapter 2: A Review of the Recent East Antarctic Ice Sheet Change

In order to place Porpoise Bay glacier change in context, changes in the overall ice sheet and examples from specific locations, including previous work in Porpoise Bay, are outlined below.

2.1 Mass Balance of the Antarctic Ice Sheet

2.1.1 Recent Mass Balance Trends

The beginning of satellite-era observations in the late 1970s enabled the first estimations of the AIS mass balance (Brooks et al., 1978; Zwally et al., 1983; Wingham et al., 1998; Rignot and Thomas, 2002; Zwally et al., 2005; Wingham et al., 2006). Currently, AIS mass balance is estimated using three techniques (Fig. 2.1a): (1) radar and laser altimetry, which infers mass change from change in elevation over time (Rémy and Parouty, 2009; McMillan et al., 2015; Schröder et al., 2019a; Shepherd et al., 2019; Smith et al., 2020a), (2) the input-output method, which calculates individual components of the mass balance, such as accumulation versus ablation/calving (Gardner et al., 2018), and (3) satellite gravimetry, which directly measures mass change through variations in gravitational pull (Velicogna and Wahr, 2006; Velicogna, 2009; Chen et al., 2009; Luthcke et al., 2013). Regardless of method, these studies all show that the AIS is losing mass over recent decades, albeit with different estimated magnitudes. The Ice Sheet Mass Balance Inter-comparison Exercise (IMBIE) uses a combination of estimates from each technique (Fig. 2.1b); a recent publication found a clear mass loss trend from the AIS, losing 92 ± 18 Gt yr^{-1} between 1992 and 2020 (Otosaka et al., 2023).

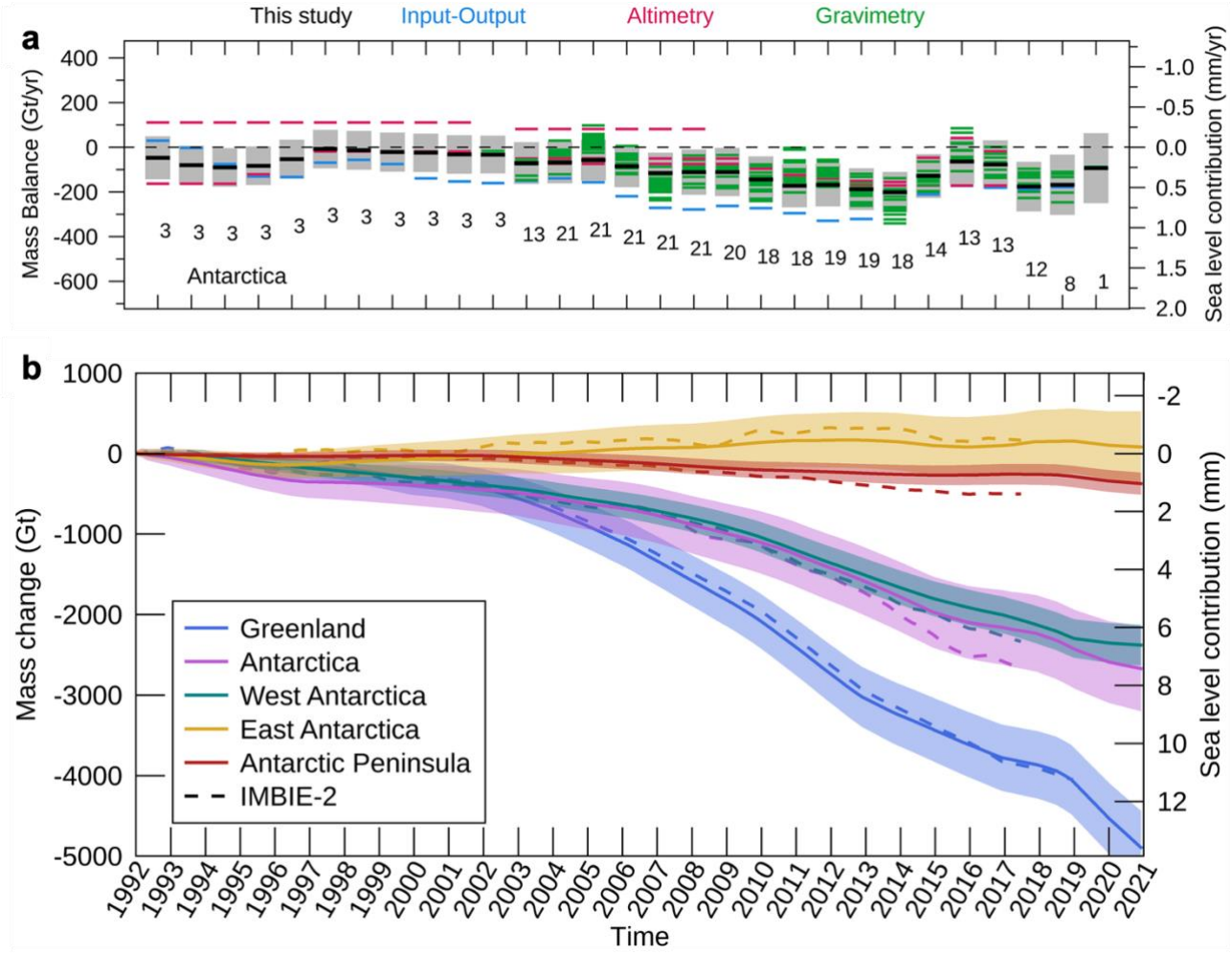

Figure 2.1: (a) Annual rates of mass change (left) and sea level contribution (right) for the AIS from the input-output (blue), altimetry (pink), and gravimetry (green) estimates included in (b) and the reconciled estimates (thick black) with uncertainty (grey). The values below each bar are the number of individual mass balance estimates at each epoch. (b) Cumulative mass change (Gt) and sea level contribution (mm) for Antarctica and Greenland between 1992 and 2020. Figures from Otosaka et al. (2023)

There is a significant spread of mass balance estimates for the EAIS across methods (Fig. 2.1b and Fig. 2.2). For example, Otosaka et al. (2023) estimated that the EAIS remained close to balance (+3 ± 25 Gt yr^{-1}) between 1992 and 2020, whilst Rignot et al. (2019) used the inout-output method to calculate that the EAIS lost considerable mass (–57 ± 2 Gt yr^{-1}) between 1979 and 2017. Another study by Smith et al. (2020a) used laser altimetry to calculate that the EAIS mass balance was –90 ± 21 Gt yr^{-1} between 2003 and 2019, detecting a strong mass loss signal from the Amundsen Sea Embayment in WAIS and Wilkes Land in EAIS (Fig. 2.3).

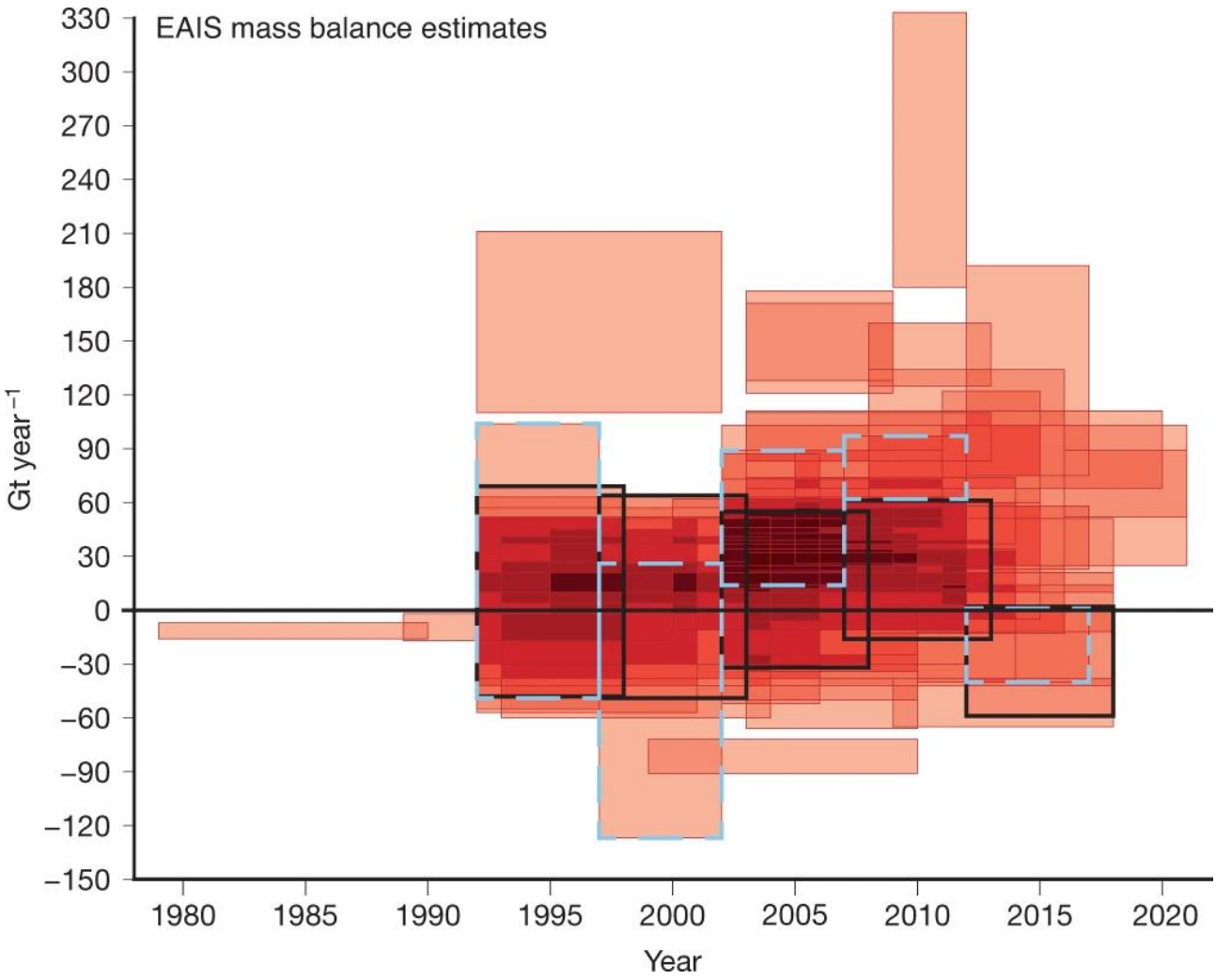

Figure 2.2: The spread of published EAIS mass balance estimates from studies published between 2002 and 2021 from Stokes et al. (2022). Each box is a mass balance estimate; box width represents the survey period; box height represents the stated uncertainty. Black box are the estimate from The IMBIE Team (2018) and blue dashed boxes are the estimate from Bamber et al. (2018): both attempts to reconcile data from several methods.

2.1.2 Drivers of Mass Loss from the Antarctic Ice Sheet

There are two components that influence the mass balance of Antarctica: surface mass loss/gain (e.g., through snowfall and melting) and dynamic mass loss (e.g., through changes in ice flow and iceberg calving). The large spread in EAIS mass balance estimates in Figure 2.2, with estimates varying within a range of +330 to –120 Gt yr^{-1}, is largely due to uncertainties in surface mass input (i.e., precipitation), rather than ice discharge, an issue primarily focused in the large, dry basins of Adelie Land and Victoria Land (Stokes et al., 2022). Estimating surface mass balance (SMB) is challenging due to an absence of direct snowfall observations in East Antarctica, meaning that studies rely on atmospheric datasets, global reanalyses, and regional climate models that, in turn, lack observational data

constraints (Stokes et al., 2022). Antarctic SMB is highly variable, both temporally and spatially across Antarctica, with a recent study by Mottram et al. (2024) reporting no clear long-term trend. Studies show that Antarctic SMB is influenced by the Southern Annular Mode (SAM), pressure anomalies and precipitation in the Southern Hemisphere (Fogt and Bromwich, 2006; Vannitsem et al., 2019; Hansen et al., 2021). SAM controls the strength and latitudinal position of the southern westerly winds, thus how moisture and ocean circulation intersects the Antarctic coast, influencing Antarctic precipitation (van den Broeke and Van Lipzig, 2004; Marshall et al., 2017; Medley and Thomas, 2019), temperature (Thompson and Solomon, 2002; Van Lipzig et al., 2008), and pressure (van den Broeke and Van Lipzig, 2004).

Dynamic ice loss is due to changes in ice flow dynamics that cause greater ice discharge into the ocean (e.g.,via iceberg calving), primarily affecting coastal regions. Mass loss from outlet glaciers in Amundsen Sea Embayment and Wilkes Land has been attributed to the ocean-induced basal melting of ice shelves and grounding line retreat, driven by mCDW intrusion (see *Section 2.3.1*) (Alley et al., 2015; Greenbaum et al., 2015; Rintoul et al., 2016; Miles et al., 2016; Silvano et al., 2017; Rignot et al., 2019; Brancato et al., 2020; Picton et al., 2023). However, evidence of the presence of CDW in East Antarctica is limited and, unlike the WAIS, mass loss in the EAIS is highly variable between drainage basins; extensive mass loss recorded from Wilkes Land and substantial mass gain elsewhere, particularly in the Dronning Maud Land, driven by increased precipitation (Velicogna et al., 2014; Harig and Simons, 2015; Gardner et al., 2018; Smith et al., 2020a). Although the overall mass balance signal from the EAIS is unclear, there is an opportunity to explore the ice flow dynamics at a basin or individual glacier level in greater detail to examine any individual change and the controls on ice dynamics.

The scientific community has been uncertain about the relative role of internal variability and external forcing as drivers of dynamic mass loss in Antarctica. A study by King et al. (2023) found that approximately 40% of total ice mass loss from Antarctica (2002–2021) was forced by a more positive SAM and El Niño Southern Oscillation (ENSO), driven by ozone and greenhouse forcing (Fogt and Marshall, 2020). Positive SAM periods feature circumpolar westerly wind anomalies that increase the flow of CDW onto the continental shelf and contribute to ice-shelf thinning, affecting dynamic mass loss, alongside less precipitation over the EAIS, affecting SMB (Walker and Gardner, 2017; Paolo et al., 2018; King et al., 2023). Critically, King et al. (2023) suggest that anthropogenic-caused global carbon dioxide emissions are an attributable driver of both surface and dynamic mass loss.

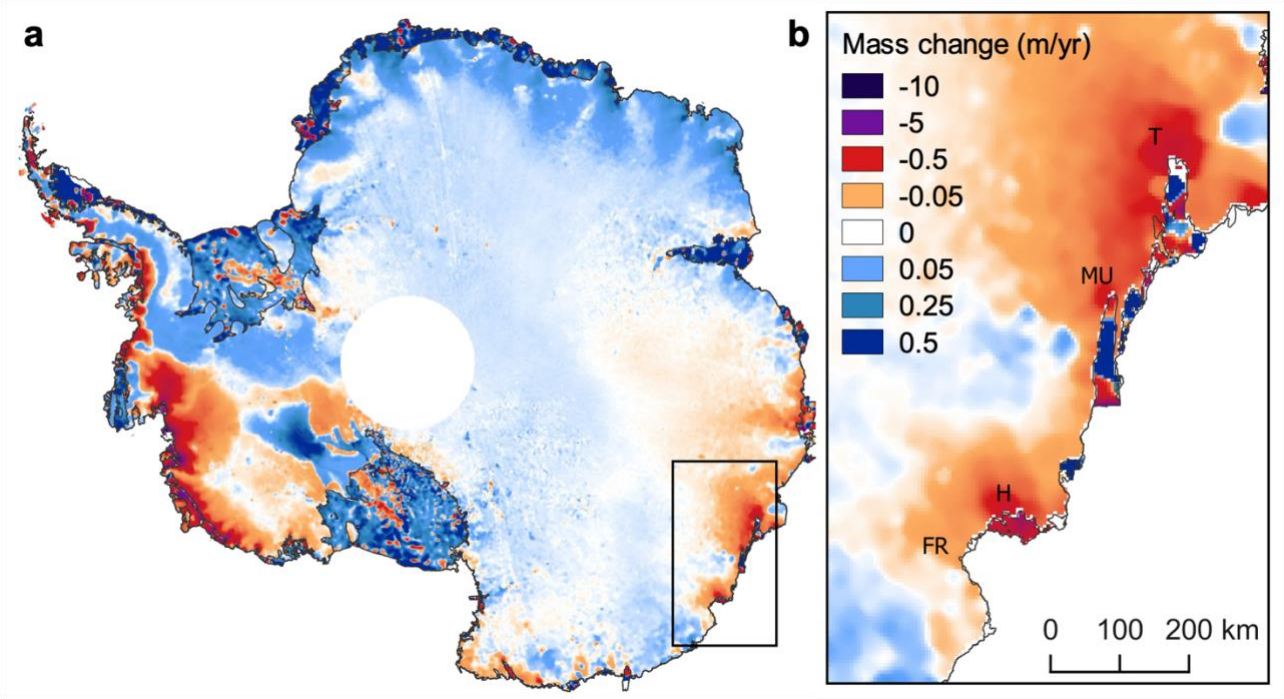

Figure 2.3: Mass change in (a) Antarctica, and (b) Wilkes Land between 2003 and 2019. Data from Smith et al. (2020b). FR: Frost, H: Holmes, MU: Moscow University, T: Totten.

2.2 East Antarctic Ice Sheet Dynamics

2.2.1 The Perceived Stability of the East Antarctic Ice Sheet

Substantial fluctuations in EAIS extent have occurred since the onset of widespread glaciation during the Eocene-Oligocene transition (Fig. 2.4) (Zachos et al., 1993), influenced by climatic changes (Naish et al., 2001; Gulick et al., 2017). Sediment records provide evidence of orbitally paced advance and retreat during the early- to mid-Miocene (24–14 Ma) (Lewis et al., 2008; Passchier et al., 2011; Levy et al., 2016; Stokes et al., 2022). During this period, the erosion of the land and deposition of eroded material offshore led to an increasingly reverse-sloping bed, heightening the vulnerability of this region to MISI (see *Section 2.3.2*) (Paxman et al., 2020). The EAIS underwent major retreat in the mid-Miocene Climatic Optimum (17–14.8 Ma), during which temperature and CO_2 concentrations were much higher (7–8°C and 600–800 ppm); ice-sheet modelling simulates tens of meters of mass loss from the EAIS marine-subglacial basins at this time (Fig. 2.4a: Gasson et al., 2016).

There are two historical (but geologically recent) warm periods, in which global temperatures were similar to present and atmospheric CO_2 concentrations were similar, or slightly lower: the mid-Pliocene (3.3–2.6 Ma) and the Last Interglacial (~129–116 ka). During the mid-Pliocene Warm Period, global mean temperatures were 2–5°C warmer than present

(Haywood et al., 2016). Records show considerable retreat occurred from Antarctica, with the WAIS and marine basins in the EAIS losing considerable mass (Fig. 2.4b), contributing 13–17 m of global mean sea level (Scherer et al., 2016; Grant et al., 2019; Stokes et al., 2022). The response of parts of the AIS during the Last Interglacial is argued in the literature, but geological records (ice cores, coral reefs, coastal sediment, deep-sea sediment, and octopus DNA) show the AIS contributed up to 5 m of global mean sea level; likely from the WAIS, but possibly from marine basins in the EAIS, such as George V Land, Wilkes Land, and Coats Land, which are grounded on beds below sea level that partly deepen inland (Bradley et al., 2012; Dutton et al., 2015a; Dutton et al., 2015b; Rohling et al., 2019; Turney et al., 2020; Barnett et al., 2023; Lau et al., 2023).

Geological evidence and modelling from previous warm periods are an important method of understanding the vulnerability of EAIS marine basins to both atmospheric and oceanic processes (Stokes et al., 2022). These records aid our understanding of how the AIS will respond to future climate change, which is especially important given a recent study that highlighted the dangers of warming to just +1.5°C above pre-industrial temperatures (Stokes et al., 2025).

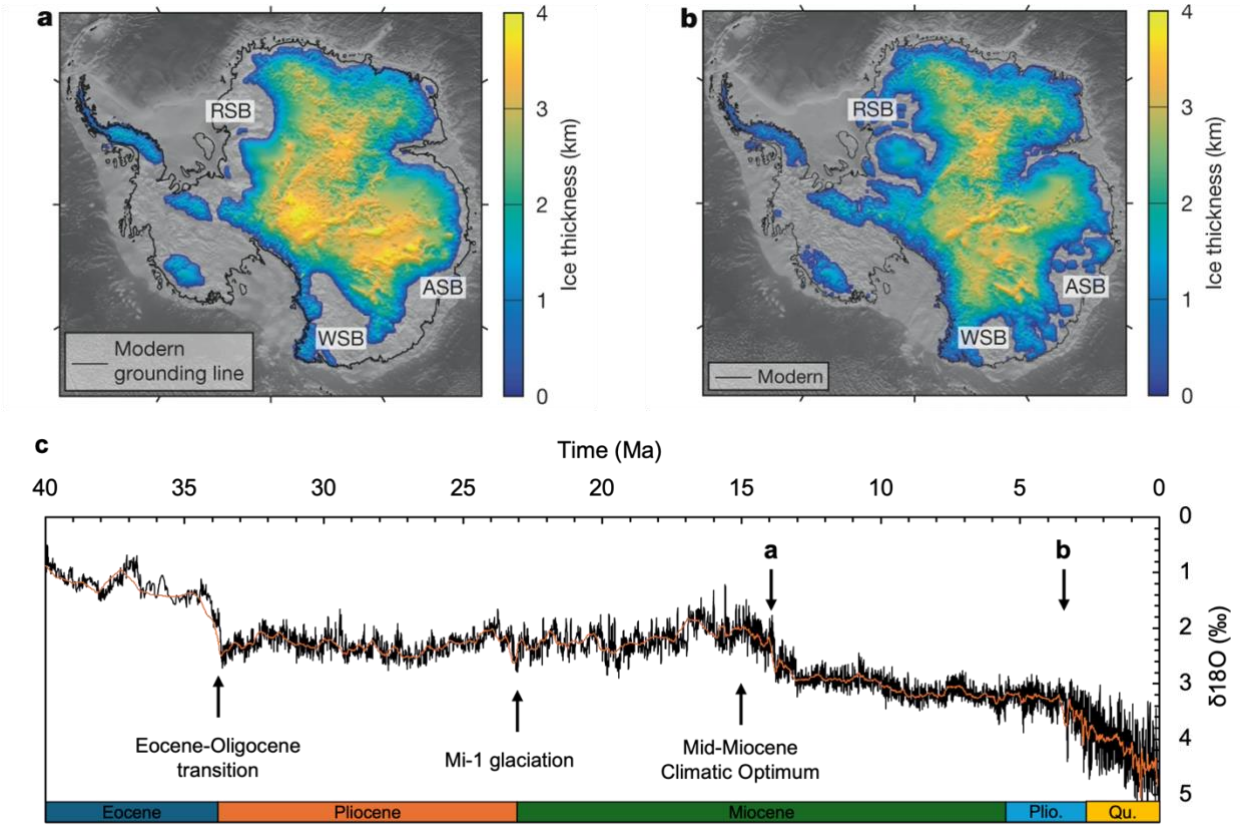

Figure 2.4: (a) Modelled ice thickness during the mid-Miocene (Gasson and Keisling, 2020). (b) Modelled ice thickness during the warm mid-Pliocene interglacial (DeConto et al., 2021). (c) Global benthic oxygen isotope curve through the Cenozoic, data from Zachos (2001). Figures (a) and (b) from Stokes et al. (2022).

2.2.2 The Vulnerability of Marine-Based Basins

The intrinsic instability of the marine-based WAIS was initially recognised in the 1970s (Weertman, 1974; Mercer, 1978), driven by bed geometry meaning the ice sheet is predominately grounded on bed topography that lies below sea-level and deepens inland (Morlighem et al., 2020). Similar bed geometries exist beneath marine-based sectors of the EAIS, such as the ASB and Wilkes Subglacial Basin (Morlighem et al., 2020). Several papers have mentioned that the present behaviour of the WAIS can serve as an analogue for future instability in the EAIS (DeConto and Pollard, 2016; Rignot et al., 2019; Fox-Kemper et al., 2021).

Mass loss from the WAIS is driven by accelerated ice discharge from the Amundsen Sea Embayment since the 1990s (Fig. 2.3a) (Rignot et al., 2019; Smith et al., 2020a), driven by increased discharge from fast flowing Thwaites and Pine Island glaciers (Mouginot et al., 2014; Medley et al., 2014; Christianson et al., 2016; Yu et al., 2018). This mass loss has been attributed to ice thinning, grounding line retreat and increased ice discharge due to enhanced ice-shelf thinning and reduced buttressing, a process forced by the intrusion of warm, salty, modified CDW onto the continental shelf towards sub-ice-shelf cavities (see *Section 2.3.1*), which causes enhanced melting where the glaciers and ice shelves contact the ocean (Rignot et al., 2011; 2013; 2014; 2019; Pritchard et al., 2009; 2012; Depoorter et al., 2013; Feldmann and Levermann, 2015; Paolo et al., 2015; Fürst et al., 2016; Scambos et al., 2017; Konrad et al., 2018; Gudmundsson et al., 2019; Pattyn and Morlighem, 2020; Naughten et al., 2023). Studies show substantial grounding line retreat from Thwaites and Pine Island glaciers down retrograde bed slopes, at a rate of 0.8 km yr^{-1} between 1992 and 2017 (Millio et al., 2019) and 1.6 km yr^{-1} between 1992 and 2011 (Rignot et al., 2014).

A mass loss signal has likewise emerged from marine-based Wilkes Land in the EAIS, featuring similarly retrograde slopes. Mass loss is driven by losses from several key outlet glaciers: Totten, Denman, Frost, Holmes, Dibble, and Moscow University glaciers (Fig. 2.3 and Fig. 2.5). Totten Glacier is the most studied glacier in Wilkes Land. Studies found deep troughs beneath the glacier (Greenbaum et al., 2015) and observed mCDW in front of Totten that causes basal melting (Rintoul et al., 2016; Silvano et al., 2016; Gwyther et al., 2018; Hirano et al., 2023), which drives grounding line retreat (Flament et al., 2012; Li et al., 2016; Konrad et al., 2018) and ice flow acceleration (Pelle et al., 2021; Li et al., 2023). Given Totten's large basin (385 cm of SLE) and high mass loss (–236 Gt between 1979 and 2017), these results are concerning (Rignot et al. 2019). The nearby Moscow University Glacier, is similarly thinning, retreating, and flowing at increasingly high ice velocities (Mohajerani et

al., 2018; Li et al., 2023; Xia et al., 2023; Ross et al., 2024). The glacier lost –93 Gt from 1979 to 2017 (Rignot et al., 2019). However, both Totten and Moscow University glaciers are presently 'protected' from unstable retreat, as they are grounded on prograde slopes that extend 50–60 km inland (Li et al., 2016; Morlighem et al., 2020).

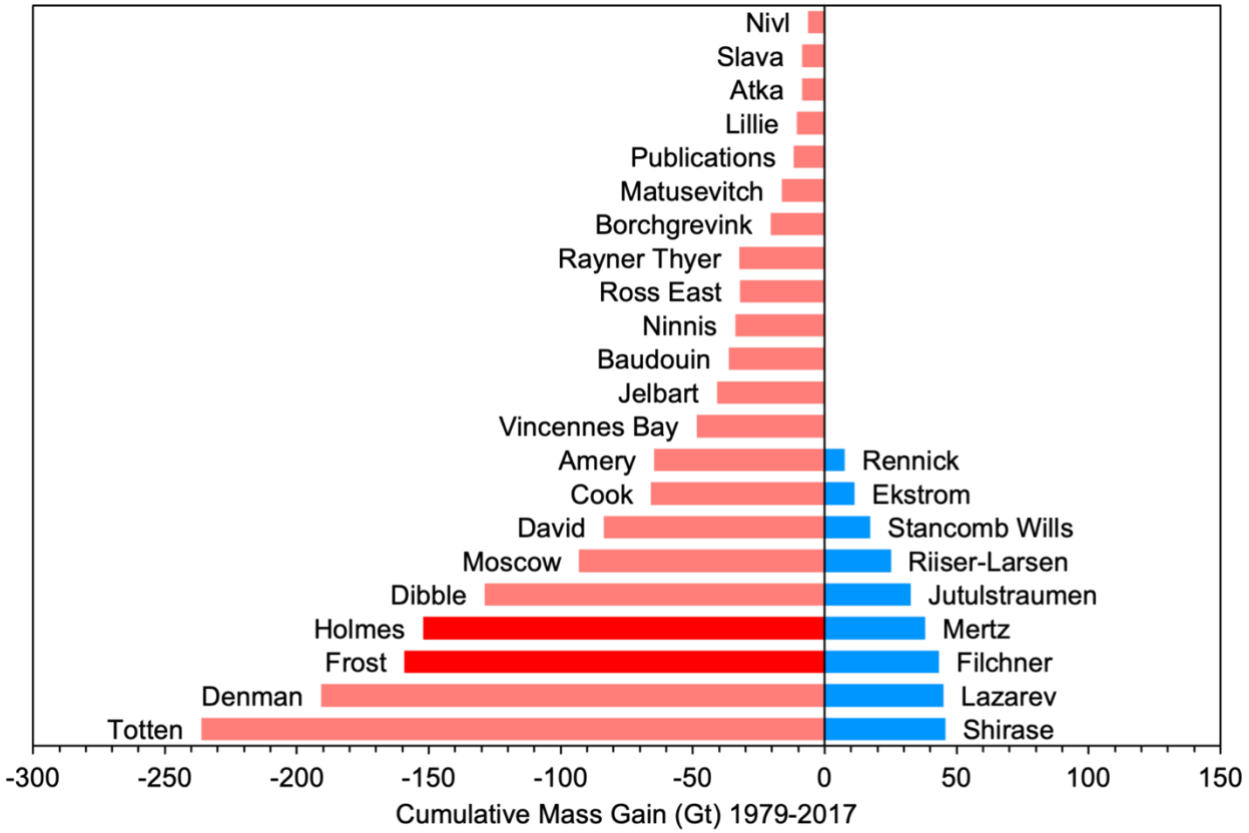

Figure 2.5: Cumulative mass gain in billions of tons for 1979–2017 for drainage basins in East Antarctica. Basins in red display mass loss, whilst blue shows gain. Basins in bold are those explored in this thesis. Data from Rignot et al. (2019).

Another key outlet glacier, Denman Glacier, has undergone similar grounding line retreat and ice velocity acceleration (Brancato et al., 2020; Miles et al., 2021). The glacier is grounded on a ridge, with a deep canyon positioned immediately upstream, containing the lowest elevation (below –3,500 m) on continental Earth (Morlighem et al., 2020). Although there are no oceanographic data near the glacier, the ice shelf experiences high melt rates, suggesting a presence of mCDW (Rignot et al., 2019; Miles et al., 2021). Denman's basin is large (149 m SLE), and Rignot et al. (2019) estimated mass loss of –191 Gt over the ca. 40 year period (1979–2017) (Fig. 2.5).

Further east are Holmes and Frost glaciers that flow into Porpoise Bay. Rignot et al. (2019) reported these glaciers lost the third and fourth most mass in EAIS (1979–2017), losing 159 and 152 Gt, respectively (Fig. 2.5). Though Miles et al. (2017) reported on the ice

shelves in Porpoise Bay, finding they regularly disintegrate in low sea-ice conditions/warmer-than-usual summers, there is little work directed at the mass loss in Porpoise Bay or the individual glacier dynamics.

2.2.3 Future Projections of East Antarctic Ice Sheet Mass Balance

Numerical ice sheet modelling is used to explore the sea level contribution from the AIS under different scenarios, largely focusing on the IPCC's low (RCP2.6), medium (RCP4.5), and high (RCP8.5) emission scenarios (Fox-Kemper et al., 2021). The response of the EAIS to future warming is the most significant source of uncertainty in future sea level projections from the AIS; modelling studies generate a range of positive and negative projections for 2100, depending on the emission scenario (Golledge et al., 2015; DeConto and Pollard, 2016; Edwards et al., 2021; Lowry et al., 2021; Stokes et al., 2022). A recent Ice Sheet Model Intercomparison Project (ISMIP6), using ice flow simulations from 13 different international modelling groups, estimated the future sea level contributions from EAIS between –7 to +15 cm at 2100 (Seroussi et al., 2020). In a more recent study, Seroussi et al. (2024) assessed Antarctica's SLR contribution up to 2300, highlighting the considerable increase in AIS mass loss after 2100; up to +0.28 m by 2100, up to +1.7 m by 2200 and +4.4 m by 2300, under high-emission scenarios (Fig. 2.6). The study found that thinning in the coastal EAIS increases rapidly by 2200, focused in the Wilkes Subglacial Basin and ASB where extensive thinning extends 400 km into the interior by 2300 (Fig. 2.6), with thinning hotspots located at Totten Glacer, Moscow University Glacier, Vincennes Bay, and Porpoise Bay (Seroussi et al., 2024). Regarding grounding line projections, Seroussi et al. (2024) estimated that the retreat will be concentrated at Totten, Moscow University, Cook, and Ninnis glaciers and the speed of grounding line retreat is primarily controlled by bed topography in regions of retrograde bed (Seroussi et al., 2024). However, despite recent progress, few ice sheet models can accurately reproduce the rapid mass loss from the AIS (or Greenland Ice Sheet) over the last few decades, indicating that uncertainties are greater than assumed (Aschwanden et al., 2021; Stokes et al., 2025).

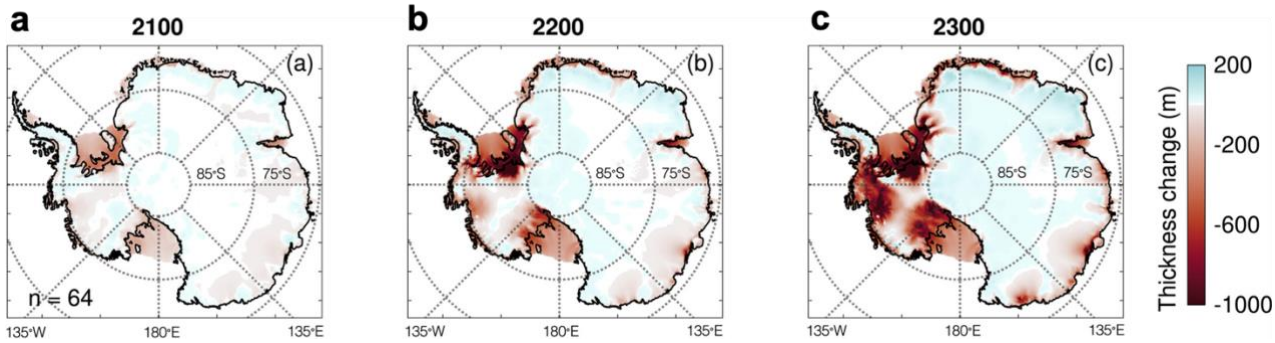

Figure 2.6: Antarctic ice thickness change across in (a) 2100, (b) 2200, and (c) 2300 for high-emission scenario from Seroussi et al. (2024). Red represents ice thinning and blue represents thickening. Black line shows the modern-day grounding line from BedMachine2 (Morlighem et al., 2020).

2.3 Ice-Ocean Interactions and Instabilities

2.3.1 Pathways and Impact of Circumpolar Deep Water

Most of coastal East Antarctica is characterised by a 'fresh shelf' regime (Fig. 2.7a) caused by strong easterly winds that drive onshore Ekman transport of cold, fresh Antarctic Surface Water onto the continental shelf that induce downwelling circulation and strong Antarctica Slope Current, limiting CDW intrusion (Thompson et al., 2018; Stokes et al., 2022). However, the coast of Wilkes Land is characterised by a 'warm shelf' regime where weaker easterly winds facilitate CDW intrusion close to the ice margin (Fig. 2.7c). Although direct shelf water temperature observations are sparse, studies have recorded warm ocean temperatures close to Totten Glacier, Moscow University Glacier, and Vincennes Bay (Greenbaum et al., 2015; Rintoul et al., 2016; Silvano et al., 2017; Ribeiro et al., 2021). Using Lagrangian particle tracking in an ocean-ice model, Tamsitt et al. (2021) modelled the mCDW residency time in East Antarctica (Fig. 2.8), finding mCDW resided for 200-400 days around Porpoise Bay and other areas of Wilkes Land, suggesting the ice margins are protractedly exposed to warm waters even if CDW inflow is intermittent.

Warm mCDW enhances melting on base of ice shelves, causing thinning and reduced buttressing (see *Section 2.3.3*) (Pritchard et al., 2012; Depoorter et al., 2013; Rignot et al., 2013; Paolo et al., 2015; Fürst et al., 2016; Adusumilli et al., 2020). Furthermore, warm water can also form basal channels under an ice shelf, causing local incision and structural weakening, which can lead to calving (Alley et al., 2016; Dow et al., 2018).

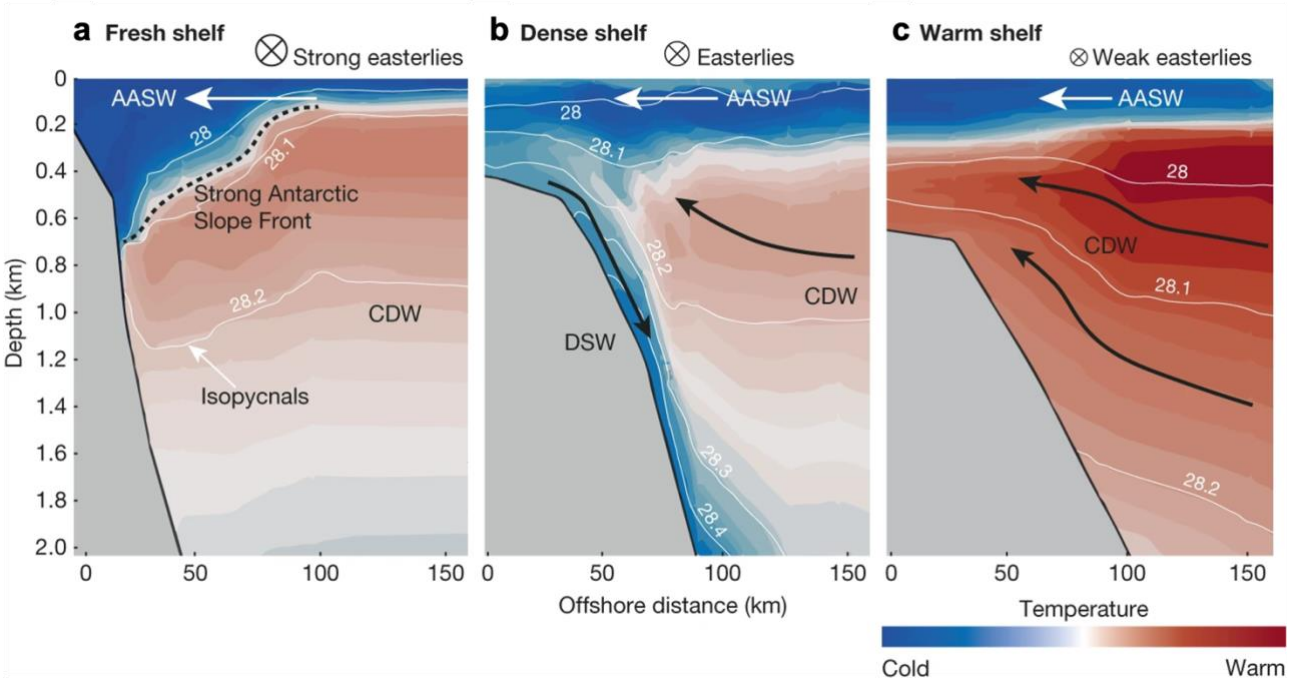

Figure 2.7: Schematic latitude-depth transects showing wind, subsurface ocean circulation, temperature, and density structure in (a) fresh shelf, (b) dense shelf, (c) warm shelf regimes from Stokes et al. (2022), modified from Thompson et al. (2018). Colours signify temperature, white contours are isopycnals of neutral density, dashed black line in (a) is the sharp density gradient, black and white arrows show cross-slope circulation, arrow tails represent wind strength and direction.

Bathymetry influences the intrusion of CDW onto the continental shelf and under ice-shelf cavities: where bathymetry is shallow (<300 m) at the shelf edge, CDW may be blocked; where bathymetry is deeper (650–750 m) at the shelf edge, CDW can flow over the lip and follow any cross-shelf trough to the glacier terminus, ice shelf, and grounding line (Dutrieux et al., 2014; Charrassin et al., 2025). Icebreaker ships are predominantly used to measure bathymetry using acoustic multibeam or single beam echo sounders (Dorschel et al., 2022). However, Antarctica's coastlines and sub-ice-shelf cavities are some of the least surveyed areas across the globe; large areas of the continental shelf and most ice shelves have no direct bathymetry measurements (Morlighem et al., 2020; Pritchard et al., 2025). As a result, undiscovered bathymetric troughs or overdeepenings likely exist on the continental shelf and upstream of grounding lines that could transfer water to the ice margin, causing rapid mass loss (Stokes et al., 2022; Stokes et al., 2025).

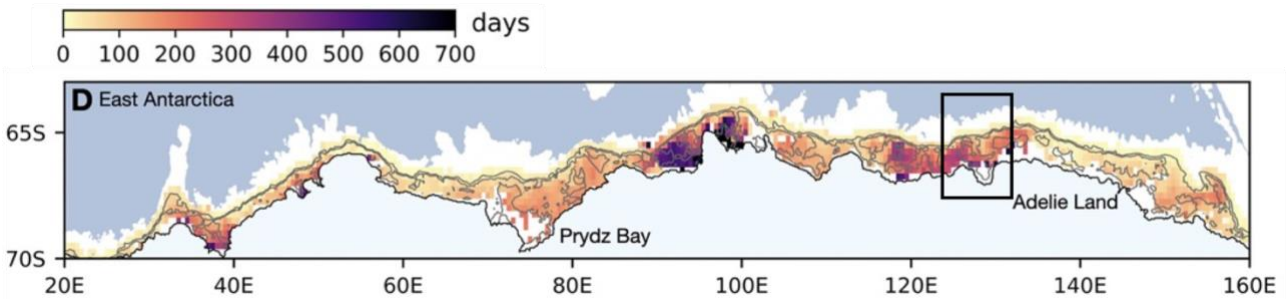

Figure 2.8: Mean residence time of mCDW in on the continental shelf in East Antarctica. Grey lines show the 500- and 1,000-m-depth contours and blue shows bathymetry deeper than 3,000 m. Figure from Tamsitt et al. (2021). Porpoise Bay is shown in a the black box.

East Antarctic bathymetry is disproportionately unsurveyed, but there has been some recent progress using new methods. The recent release of Bedmap3 revealed hundreds of better-defined troughs under the grounded ice sheet and more highly resolved bed, compared to BedMachine3 and Bedmap2 (Fig. 2.9: Pritchard et al. 2025). A recent study by Charrasin et al. (2025) employed a novel method using gravity anomalies (AntGG2021) to infer bathymetry on the continental shelf and ice margins around Antarctica. Another study by McMahon et al. (2023) used seal dive depth to redefine bathymetry on the EAIS continental shelf, revealing troughs off the Shackleton Ice Shelf and Underwood Glacier, and a deep canyon near Vanderford Glacier that was recently confirmed by multi-beam echo sounder survey on icebreaker RSV *Nuyina* (Picton et al., 2023) At Porpoise Bay, the bed is approximately 600 m below sea level on the continental shelf and there appears to be a reverse-sloping bed with suggestions of cross-shelf troughs which may provide pathways for CDW under appropriate conditions (Pritchard et al., 2024; Rignot et al., 2024).

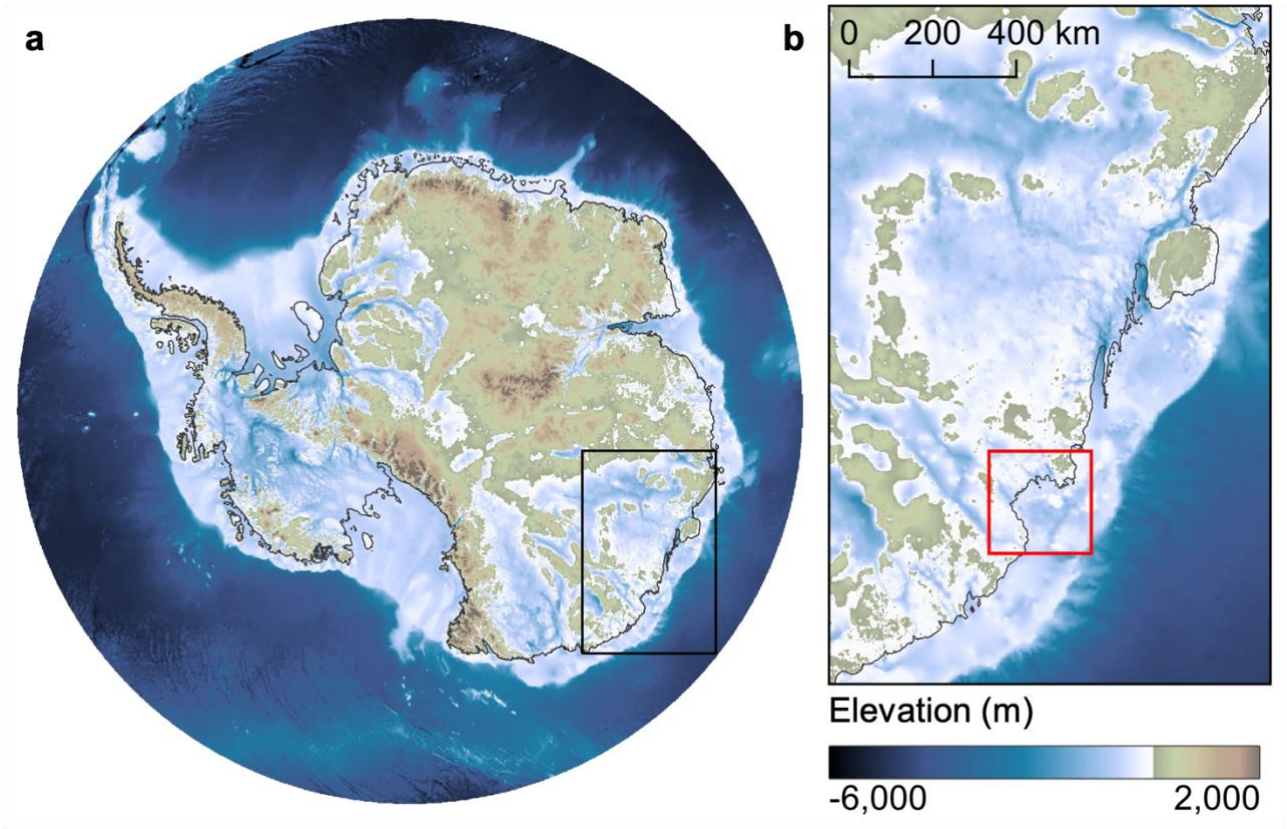

Figure 2.9: Bed topography in (a) Antarctica and (b) Wilkes Land from Bedmap3, with Porpoise Bay in the red box. Data from Pritchard et al. (2025). Ice sheet edge from MEaSUREs (Rignot et al., 2016).

2.3.2 Marine Ice Sheet and Ice Cliff Instabilities

There are two positive feedback mechanisms that produce rapid ice loss in ice sheet models: MISI and Marine Ice Cliff Instability (MICI) (Fig. 2.10). MISI can occur when an ice sheet is grounded on a retrograde slope (Fig. 2.10a). Initial retreat is triggered by ice-shelf thinning due to warm ocean currents proximal to the grounding line, causing the grounding line retreat, leading to greater ice thickness grounded in deeper water, resulting in floatation, basal melting and further retreat, forcing the grounding line further into deeper water (Joughin and Alley, 2011). The resultant grounding line cross-sectional area is larger, causing greater ice discharge into the ocean (Schoof, 2007). This positive feedback continues until grounding line reaches a stabilising bedrock pinning point or prograde slope (Durand et al., 2009; Pattyn and Morlighem, 2020).

Studies back in the 1970s warned that outlet glaciers in the WAIS were vulnerable to MISI (Mercer, 1978), with some studies now suggesting it is already underway in the WAIS (Joughin et al., 2014; Rignot et al., 2014). Parts of the EAIS are potentially vulnerable to MISI, particularly along the coastline of the three major marine basins (ASB, Wilkes

Subglacial Basin, and Recovery Subglacial Basin), which hold ice that is grounded on retrograde slopes (Brancato et al., 2020; Picton et al., 2023; Stokes et al., 2025).

MICI is a more recent hypothesis (Fig. 2.10b: Pollard et al., 2015; DeConto and Pollard, 2016; DeConto et al., 2021). MICI could theoretically occur when ice shelves are removed, revealing large, mechanically unstable ice cliffs at the grounding line that progressively collapse due to greater ice thicknesses further inland (Bassis and Walker, 2012; Pollard et al., 2015). There is no evidence that MICI is currently underway, and the mechanism's validity is argued, with a recent study suggesting it will not occur in the 21st century (Morlighem et al., 2024). Despite this, ice sheet modelling has used MICI to resolve the AIS sea-level contribution in past warm periods, though even models that do not use MICI find the ASB is responsive to change (Pollard et al., 2015; DeConto and Pollard, 2016).

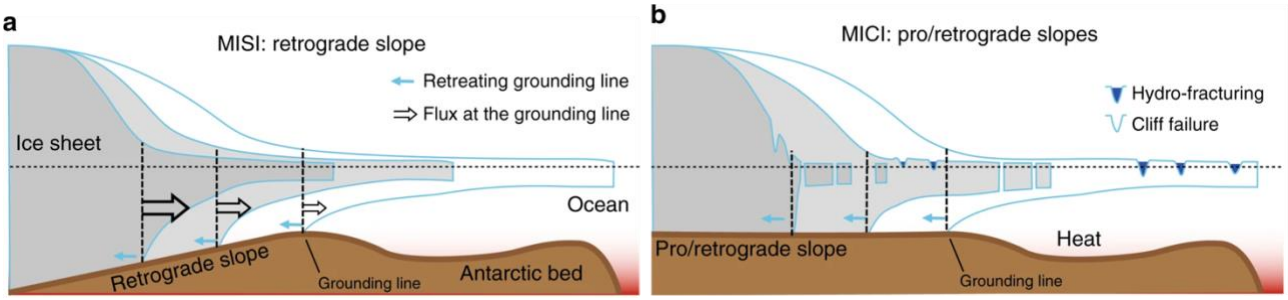

Figure 2.10: Conceptual models of (a) MISI and (b) MICI from Pattyn (2018).

2.3.3 Ice-Shelf Processes and Glacier Stability

Ice shelves are the floating portion of the ice sheet that form where the grounded ice meets the ocean; sometimes referred to as the 'safety band' of the AIS (Fürst et al., 2016). This is because some floating ice shelves and glacier tongues apply a buttressing force on glacier flow by exerting back stress from basal pinning points or side-wall friction; the weakening or removal of these ice shelves can induce inland ice flow acceleration due to a reduction in backstress exerted on grounded ice inland (Rignot et al., 2004; Scambos et al., 2004; Gudmundsson et al., 2019). Numerical modelling suggests the process of debuttressing will be a key control on the timing and magnitude of future sea level rise (Golledge et al., 2015; DeConto and Pollard, 2016).

Ice-shelf retreat in Antarctica is driven by various interactive processes (Fig. 2.11): thinning from basal melting (Shepherd et al., 2004; Pritchard et al., 2012; Adusumilli et al., 2020; Baumhoer et al., 2021), sea-ice/mélange breakup (Miles et al., 2017; 2018; Arthur et al., 2021), surface meltwater-induced flexure and hydrofracture (Banwell et al., 2013; 2019;

Banwell and MacAyeal, 2015; Lhermitte et al., 2020), ocean swell and wave damage (Massom et al., 2018), and the propagation of pre-existing structural weaknesses (Massom et al., 2015; Miles et al., 2020). A recent study by Greene et al. (2022) found that Antarctica lost 36,701 ± 1,465 km^2 of ice-shelf area (1997–2021) that will not be regained for at least another decade. Using CryoSat-2 altimetry, Adusumilli et al. (2020) estimated basal melt rates for Antarctica's ice shelves, finding rapid melt rates across the Amundsen Sea Embayment and Wilkes Land (Fig. 2.12).

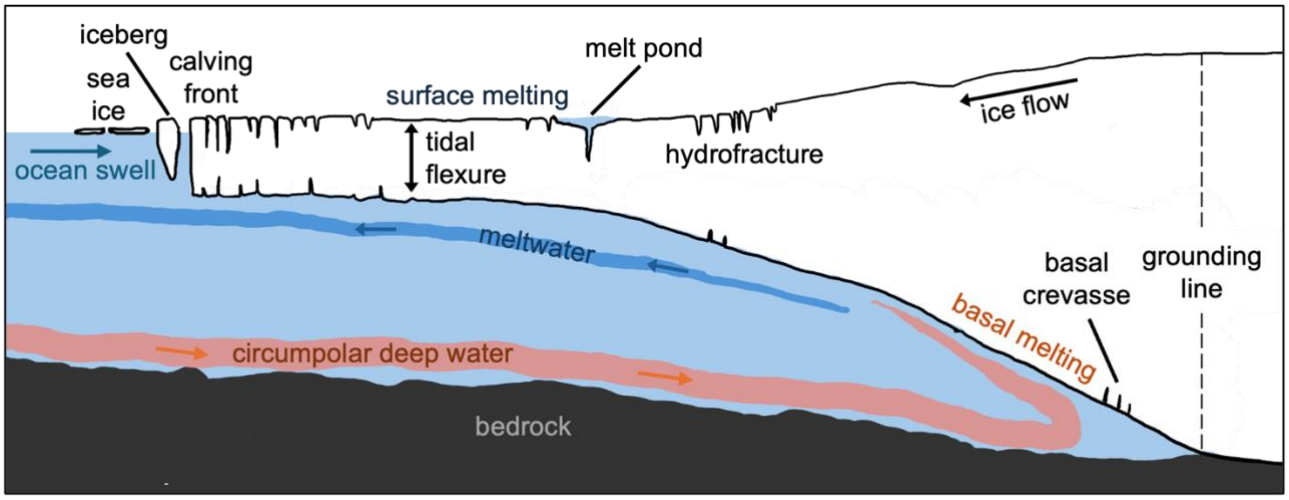

Figure 2.11: Conceptual model of the processes driving ice-shelf retreat and thinning.

Ice shelves in the Antarctic Peninsula dominate the literature on ice-shelf stability and ice-shelf collapse (Rott et al., 1996; Scambos et al., 2000; 2003; Rignot et al., 2004; Glasser and Scambos, 2008; Hulbe et al., 2008; Glasser et al., 2011; Wille et al., 2022). There are relatively fewer studies on ice shelves in EAIS, with limited observation on the timing and drivers of calving events (Massom et al., 2015; Miles et al., 2017; 2018; Cheng et al., 2021; Saunderson et al., 2022; Li et al., 2023). There are two ice shelves in EAIS that have received recent attention: the Conger Ice Shelf that collapsed in 2022, driven by an atmospheric river and structural weaknesses (Walker et al. 2024) and the Voyekov Ice Shelf, located between Porpoise Bay and Moscow University Glacier, that disintegrated in 2007, triggered by mélange removal due to an atmospheric warm anomaly (Arthur et al., 2021). The outlet glaciers in Porpoise Bay flow into small ice shelves, with Holmes East and Holmes West glaciers terminating in one large ice shelf.

2.4 A Review of Previous Work on Porpoise Bay

2.4.1 The Outlet Glaciers

There are two glacier catchments, from which several glaciers feed into Porpoise Bay. Frost catchment contains 84 cm of SLE (Rignot et al., 2019) and is drained by Frost Glacier and Glacier 1, alongside several other minor glaciers. Frost Glacier is roughly 20 km wide, flowing around 2,000 m yr^{-1} through a wide bedrock trough (800–900 m below sea level) into a small ice shelf. Glacier 1 is about 15 km wide, flowing up to 1,000 m yr^{-1} across a flat bed (500 m below sea level) into a small ice shelf. Neighbouring Holmes catchment is relatively smaller, containing 12 cm of SLE (Rignot et al., 2019), drained by Holmes East and West glaciers. Holmes East is roughly 25 km wide, heavily crevassed, flowing through a bedrock trough (700–900 m below sea level). Holmes West is about 15 km wide, also heavily crevassed, flowing through a bedrock trough down a reverse slope (up to 1,500 m below sea level). Holmes East and West glaciers join near the terminus to feed a large ice shelf. Porpoise Bay contains considerable sea ice that disintegrates every 5–10 years (Miles et al., 2017). The proximity of the Frost and Holmes catchments to the deeper parts of the ASB (Fig. 2.9b) is concerning as continued mass loss in Porpoise Bay may increase the potential risk of significant grounding line retreat down retrograde bedslopes (Young et al., 2011; Stokes et al., 2022).

2.4.2 Observed Behaviour of Porpoise Bay Outlet Glaciers

The glaciers flowing into Porpoise Bay have received very little attention. As mentioned in *Section 2.2.2*, Frost and Holmes glaciers lost 159 and 152 Gt, respectively, between 1979 and 2017, contributing almost a quarter of the total sea level input from the EAIS over the study period (Rignot et al., 2019). Observations show that Holmes Glacier is thinning (>1 m yr^{-1}) more than Frost Glacier (<0.5 m yr^{-1}), the second fastest long-term thinning rate in East Antarctica (Schröder et al., 2019a; Shepherd et al., 2019; Smith et al., 2020a; Stokes et al., 2022). Despite observations of ice surface thinning and mass loss, findings show relatively steady ice discharge (Rignot et al., 2019; Miles et al., 2022). However, a weak ice flow speed up was recorded at Holmes and Frost glaciers of approximately 10–40 m yr^{-1} between 2007–2009 and 2020–2022 (Rignot et al., 2022). In a study of grounding line retreat across Antarctica, Konrad et al. (2018) found Frost Glacier retreated >200 m yr^{-1} between 2010 and 2016, the EAIS's fourth most rapidly retreating grounding line.

Porpoise Bay is occupied by several ice shelves, of which the largest is Holmes Ice Shelf (fed by Holmes East and West glaciers). Miles et al. (2017) reported the ice shelves

underwent two near-synchronous breakup events in 2007 and 2016 associated with low sea-ice conditions. Studies using laser and radar altimetry and firn-layer models suggest that Holmes Ice Shelf is thinning by enhanced basal melt (Prichard et al., 2012; Adusumilli et al., 2020). Pritchard et al. (2012) used laser altimetry with a firn-layer model to calculate that the ice shelf thinned by >0.3 m yr^{-1} from 2003 to 2008. More recent work used radar altimetry, ice-flow velocities, and a novel firn-layer model to calculate an average ice-shelf basal melt of 13.3 ± 2.9 m yr^{-1} between 1994 and 2018, the highest in Wilkes Land and one of the highest in Antarctica (Fig. 2.12b*:* Adusumilli et al., 2020). Furthermore, in a study using the expression of basal pinning points as a proxy for ice thickness, Miles and Bingham (2024) reported basal pinning point loss from the Holmes Ice Shelf since 1973, suggesting a 50-year thinning trend. Although the ice shelf was still pinned in 2022, accelerated basal pinning point loss reveals ice-shelf thinning that may have de-buttressing implications (Miles and Bingham, 2024). There is a lack of ocean data near Porpoise Bay, making it challenging to assess the relationship between ocean temperature forcing and mass loss (Silvano et al., 2016).

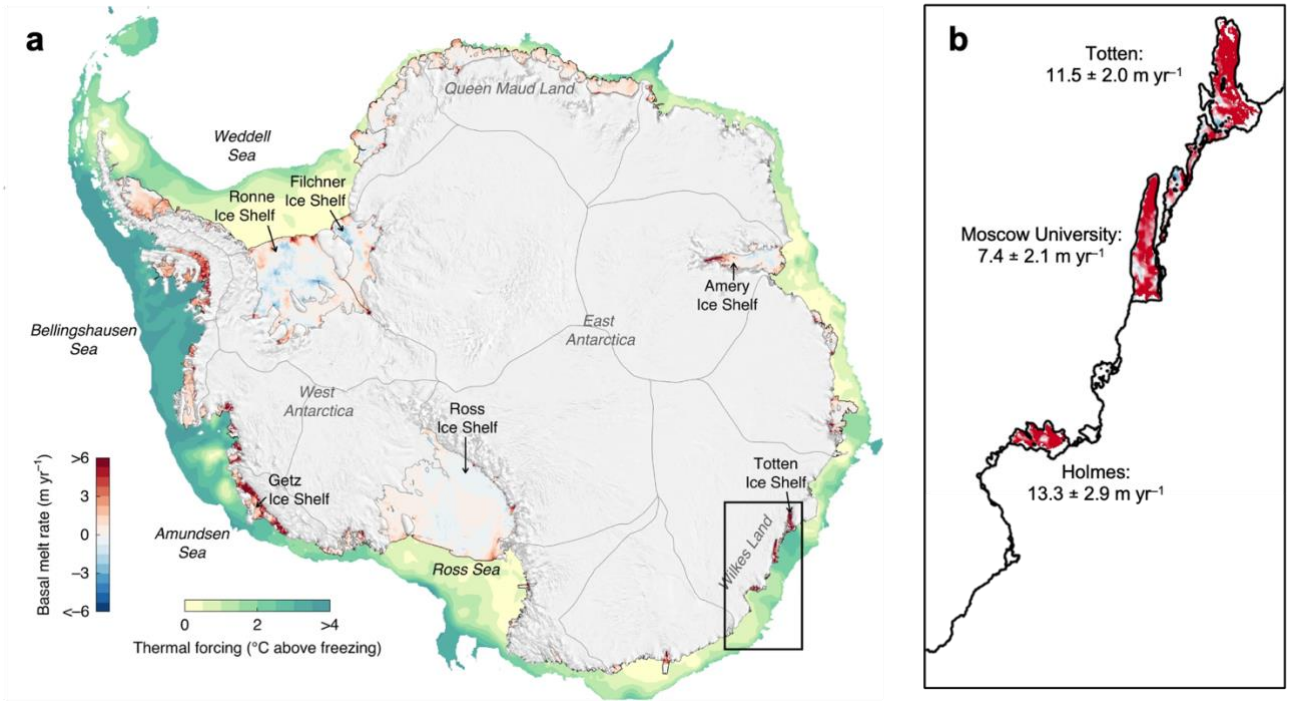

Figure 2.12: (a) Basal melt rates of Antarctica's ice shelves and thermal forcing on the continental shelf from Adusumilli et al. (2020) between 1994 and 2018. (b) Basal melt rates of ice shelves in Wilkes Land.

2.4.3 Knowledge Gaps and Research Justification

In an assessment of the EAIS response to climate change, Stokes et al. (2022) specifically mentioned that Porpoise Bay's glaciers warrant monitoring due to their large catchments, high ice discharge, and potential sensitivity to ocean processes. Furthermore, Rignot et al. (2022) mentioned Frost Glacier, out of six EAIS glaciers, as being important for future investigation due to its recently recorded speed up.

The studies in *Section 2.4.2* do not fully elucidate the relationship between the mass loss and the dynamic processes in Porpoise Bay and several are pan-ice sheet studies that are not focused on the bay. Many of the datasets are temporally limited, contain contradictory data (i.e., Frost Glacier ice discharge of >45 Gt yr^{-1} from Rignot et al. (2019) and <25 Gt yr^{-1} from Miles et al. (2022)) or have missing regions (i.e., lack of grounding line for Holmes Glacier from Konrad et al. (2018)). These knowledge gaps limit our understanding of the magnitude of, and controls upon, changes in these outlet glaciers. Interpreting the relative roles of the driving mechanisms of mass loss (ocean warming, dynamic change at the terminus, and evolving sea-ice conditions) is crucial given the scale of the glaciers and the uncertainty around future projections in this area. New measurements of glacier change would improve our understanding of the physical processes that are taking place, clarify the extent of dynamic imbalance in the system, and illuminate future change in the region.

Chapter 3: Methodology

The recent ice dynamics of Porpoise Bay's outlet glaciers were examined by combining a range of remote sensing approaches to measure four key glacier parameters (ice-shelf position, ice surface elevation, ice surface velocity, and grounding line position) between the 1960s and the present day. This depicts the scale of change and enables assessment of the potential driving mechanisms.

3.1 Ice-Shelf Frontal Position

The Google Earth Engine Digitisation Tool (GEEDiT) was used to manually map the calving front of each outlet glacier following the criteria outlined in Table 3.1. GEEDiT uses imagery from Landsat 4, 5, 7, 8, and 9, ASTER, and Sentinel 1 and 2, spanning from 1982 to the present day (Lea, 2018). In addition, co-registered and orthorectified Landsat 1 (Miles and Bingham, 2023) and declassified ARGON (Kim et al., 2007) imagery were used to extend our measurements back to 1963. Images were preferentially selected from austral summertime (December to February) to minimise complications with digitising sea ice. Cloud cover thresholds were not applied to avoid unnecessarily omitting images with visible ice-shelf edges. Instead, the images were manually checked to ensure the calving front was visible. The failure of the Scan Line Corrector onboard the Landsat 7 satellite resulted in striped data losses (Paul et al., 2017), but parts of the glaciers were still visible. In such images, the ice-shelf position was, where possible, digitised across gaps, using an adjacent image with a differently striped pattern of data losses to inform digitisation (Black and Joughin, 2022). The spatial resolution of imagery ranged from 140 m (Landsat-1) to 10 m (Sentinel-2).

Table 3.1: Ice-shelf features and identifying criteria adapted from Holt et al. (2013) and Arthur et al. (2021). Examples of ice-shelf features from Sentinel-2 are provided.

Feature	Example	Structure	Identification on satellite imagery
Ice calving front (ice-free conditions)	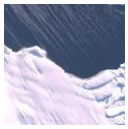	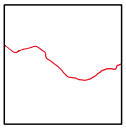	Abrupt transition from ice-shelf calving margin (bright feature) to open ocean (dark feature).
Ice calving front (mélange presence)	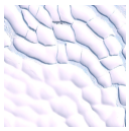		Transition from ice shelf (smooth feature) to mélange (tightly packed calved ice blocks with other calved materials); transition often marked by shadow.
Ice calving front (sea ice presence)	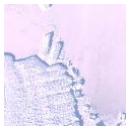		Sharp transition from ice shelf ('thick' feature) to sea ice (darker than glacial ice, 'flat' feature); transition often marked by shadow.
Calved ice blocks/icebergs	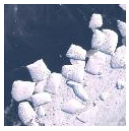		Distinct blocks detached from ice-shelf edge and surrounded by mélange or open ocean
Mélange	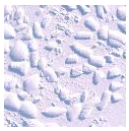		Amalgamation of sea ice, marine ice, firn, and densely packed calved icebergs

The outcomes of the mapping were exported to ArcGIS. The ice-shelf position change was quantified using the box method outlined by Moon and Joughin (2008), which calculates the mean frontal change using the difference in ice-shelf geometry as measured by the area within an open-ended box across the central region of ice flow. This method accounts for asymmetric changes across glacier termini.

The availability of cloud-free digital satellite imagery limits this method as it conceals the ice-shelf edge. When mapping the ice-shelf edge, digitisation errors were minimised by using the highest-resolution imagery available and applying contrast stretching filters to improve the shelf-ice-mélange and ice-water boundary visibility; the resultant digitisation uncertainty was estimated to be similar to Miles et al. (2021) at 1 pixel. A particular challenge was identifying the mélange from the calving front, due to the blocky nature of the mélange. To minimise the subjectivity of the mapping this boundary, the feature identification criteria outlined in Table 3.1 were used.

3.2 Ice Surface Elevation

Monthly surface elevation changes from 1985 to the present day were extracted from the following published ice surface elevation change datasets: Schröder et al. (2019b), Smith et al. (2020b) and Nilsson et al. (2023). The error associated with each annual velocity mosaic was provided at pixel scale, representing the standard deviation of the elevation values. Schröder et al. (2019b) calculated the monthly surface elevation changes between 1978 and 2017, relative to September 2010, at a horizontal resolution of 10 km. The associated monthly uncertainties range from ±0.3 to ±9.7 m yr^{-1} (Schröder et al., 2019b). The data were obtained from altimetry data from Seasat, Geosat, ERS-1, ERS-2, Envisat, ICESat, and CryoSat-2 satellite missions (Schröder et al., 2019b). Nilsson et al. (2023) calculated monthly surface elevation changes between 1985 and 2020, relative to December 2013, at a horizontal resolution of 1920 m. The monthly error ranges from 0.06 to 3.8 m yr^{-1} (Nilsson et al., 2023). This dataset includes additional data from the ICESat-2 mission, extending the temporal coverage between 2018 and 2020.

The mean rate of elevation change was extracted from two 10 km^2 sampling boxes that were drawn to capture changes at key points along flow: at the grounding line (GL) and 10 km inland (IN) (Fig. 1.1b). Sampling from two boxes facilitates the recognition of dynamic thinning (propagation of thinning from the glacier front to the inland portion of the glacier). The measurements were calculated relative to the earliest shared time period (September 1992), to enable comparison across the datasets. The elevation anomalies were calculated relative to the 1992–2017 mean and a 24-month moving average was produced for the datasets.

The dataset from Smith et al. (2020b) shows the rate of surface elevation change between 2003 and 2019, at a horizontal resolution of 5 km. The dataset uses altimetry data from ICESat and ICESat-2 satellite missions (Smith et al., 2020b). The dataset quantifies the root mean square error in each grid cell, which stems from instrument precision, grounding finding errors, and interpolation errors; the error from the sampling boxes ranges from 0.004 to 0.08 m. To compare the datasets, mean rates of elevation change were calculated for Nilsson et al. (2023) between 2003 and 2019 and for Schröder et al. (2019b) between 2003 and 2017.

3.3 Ice Surface Velocities

The Making Earth Science Data Records for Use in Research Environments (MEaSUREs) ITS_LIVE product was used to extract ice surface velocity at an annual resolution between

2000 and 2022 (Gardner et al., 2025). The ITS_LIVE mosaics were derived from Landsat 4, 5, 7, and 8 imagery using autonomous Repeat Image Feature Tracking (auto-RIFT) algorithms, an open-source Python module that analyses pixel displacement between two images to calculate ice velocity (Gardner et al., 2018).

The mean annual velocities were extracted from the GL and IN sampling boxes alongside a box positioned on the floating ice tongue (FT) (Fig. 1.1b). Sampling from multiple boxes depicts the spatial variability in ice velocity over time to reveal any pattern or propagation of dynamic change up-ice. Ice surface velocity profiles were extracted along the central flowlines using the 2021 annual velocity mosaic for each outlet glacier and sampled at 240 m intervals to reflect the spatial resolution of the ITS_LIVE data. The 2021 mosaic was selected due to a relatively lower indicated error. The flowlines were clipped at the 2021 manually digitised ice-shelf position.

The error associated with each annual velocity mosaic was provided at pixel scale, representing the standard deviation of the difference between the image-pair component velocities and the mean annual component velocities (Gardner et al., 2018). The mean annual velocity error was extracted from each FT, GL, and IN box; the error ranged from 0.7 to 467 m yr^{-1}. The annual velocity data measurements were disregarded where the mean percentage error was over 50 % of the velocity magnitude, resulting in the loss of 1 % of data.

Data scarcity is a limiting factor of the early ITS_LIVE product as the auto-RIFT processing chain is limited by the availability of image pairs across a given year. Incomplete coverage was seen across Holmes East and West before the launch of Landsat 8 in 2013. The annual velocity values were disregarded if less than 25 % data coverage was observed spatially within the sample boxes, resulting in the removal of 8 % of values.

3.4 Grounding Line Position

Grounding line positions were provided by Sindhu Ramanath (DLR). They were derived using DInSAR interferograms from Sentinel-1 imagery collected between 2019 and 2021 (Table 3.2) to enable comparison with older, previously published datasets (described below). DInSAR interferograms were generated by differencing two interferograms, each produced from three or more consecutive repeat pass SAR acquisitions. Assuming constant velocity over the observed time period, the phase change from tidal flexure at the ice sheet-ice-shelf boundary can be detected from the resulting differential interferograms. These ice-shelf flexure zones are characterised by a dense fringe in the DInSAR phase.

To automatically delineate the grounding line, a Holistically-Nested Edge Detection (HED) neural network was applied to the DInSAR interferograms (Ramanath et al., 2025). The neural network was trained on the real and imaginary interferometric features, achieving a median and mean offset of 265 m and 421 m, respectively, from manual grounding line delineations, and a predictive uncertainty of 401 m (Ramanath et al., 2025). The uncertainty was derived by calculating the pixel-wise standard deviations of each DInSAR interferogram of an ensemble of five HED neural networks, configured with the same hyperparameters, but differing in the initialization and trained with randomly shuffled training samples (Ramanath et al., 2025). No coherent interferograms were extracted over Glacier 1 or Frost glaciers because the ice flow was too rapid to get coherence within the 6-day repeat-pass interval of the Sentinel-1 constellation. At Holmes West Glacier, a 2020 grounding line was identified, but its implausibility relative to secondary datasets and very wide uncertainty buffer from a highly de-correlated interferogram led us to disregard the line.

The grounding line positions were also extracted from several secondary datasets in the published literature. The MEaSUREs grounding line product was generated using similar DInSAR techniques applied to ERS-1 and ERS-2 imagery collected in 1996 (Rignot et al., 2016). This dataset has a standard error of ±100 m (Rignot et al., 2016). The Antarctic Surface Accumulation and Ice Discharge (ASAID) grounding line dataset was produced by manually delineating the most seaward continuous break in slope using Landsat 7 images between 1999 and 2003 and surface elevation data from ICESat satellite mission (Bindschadler et al., 2011). This dataset has an estimated positional error of ±502 m for outlet glacier boundaries (Bindschadler and Choi, 2011). The Mosaic Of Antarctica (MOA) grounding lines were also produced using manual delineation of the most seaward break in slope, observed in 2004, 2009, and 2014 (Haran et al., 2018; 2021a; 2021b). The MOA grounding line products have associated errors of ±250 m. The change in grounding line position was measured along the central flowline from the most seaward MEaSUREs 1996 position.

The DInSAR results and MEaSUREs product represent the hinge line, an approximation of the grounding line position (Rignot et al., 2016). Contrastingly, the ASAID and MOA datasets represent the break-in-slope; the change in ice surface at the transition from grounding and floating ice (Bindschadler et al., 2011). The hinge line and break-in-slope are different components of the grounding zone (the break-in-slope is observed seaward of the grounding line). Hence, caution must be exercised when interpreting changes in grounding line position acquired from the different methods.

Table 3.2: Imagery used in the DInSAR grounding line extraction.

Satellite	**T1**	**T2**	**T3**
Sentinel 1	03/11/2019	09/11/2019	15/11/2019
Sentinel 1	21/11/2020	27/11/2020	03/12/2020

3.5 Bed and Ice Surface Topography

To interpret grounding line migration in the context of the wider subglacial topography, bed and ice surface elevation profiles for the Porpoise Bay outlet glaciers were extracted. Bedrock elevation profiles were derived from BedMachine3 (Morlighem, 2022) and Bedmap3 (Pritchard et al., 2024) along the digitised flowlines. Bed elevation and the associated error were sampled at 500 m intervals (the horizontal resolution of the dataset). Although there are 47,492 line-kilometres of airborne radar profiles over the ASB (Young et al., 2011), including over Porpoise Bay, the roughness and shape of the bed are not well characterised, and the presence of inland pinning points that may restrict future grounding retreat are unknown. The bed elevation error associated with Bedmap3 ranges from ±7 to ±276 m for the grounded bed and ±60 m to ±306 m for the interpolated seabed (Pritchard et al., 2024). For BedMachine3, the typical uncertainties are ±36 m in well-constrained regions (driven by radar vertical resolution); uncertainties can exceed ±200 m where data are sparse due to reliance on interpolations and can exceed ±500 m beneath floating ice where sub-ice bathymetry data are lacking (Morlighem, 2022).

Bed elevation profiles along the marine area in front of the glaciers were digitised from the AntGG2021 dataset which is based on a 3D inversion of a circumpolar compilation of gravity anomalies constrained by measurements from BedMachine3, the International Bathymetric Chart of the Southern Ocean, and discrete seafloor measurements from seismic and ocean robotic probes (Rignot et al., 2024; Charrassin et al., 2025). This dataset provides insight into the seafloor elevation of ice-shelf cavities and continental shelf. The potential error of the estimated bathymetry for the Sabrina region, where Porpoise Bay is situated, is 185 m (Charrassin et al., 2025).

Surface topography profiles were extracted along each central flowline from the Reference Elevation Model of Antarctica (REMA) mosaic (Howat et al., 2022). The surface

elevation product from REMA is provided at 100 m resolution with errors of less than 1 m (Howat et al., 2019). These were sampled at 500 m intervals to match the bedrock elevation. The ice-shelf base elevation was calculated by subtracting the Bedmap3 ice thickness from the Bedmap3 ice surface elevation (Pritchard et al., 2024). The uncertainty of the Bedmap3 ice thickness dataset ranges between ±0 m for rock cells, ±10 m for ice shelves, ±10–20 m in surveyed cells, ±73–272 m in interpolated or poorly constrained cells (Prichard et al., 2025). The Bedmap3 ice surface elevation error is, on average, ±7 m (Pritchard et al., 2025).

3.6 Ocean and Sea-Ice Conditions

Ocean temperature and sea-ice conditions were analysed to understand their potential influence on any observed changes in ice dynamics. Due to an absence of direct, observational ocean temperature data across the continental shelf in Wilkes Land, the EN4.2.2 subsurface ocean temperature objective analysis data were used (Good et al., 2013), accessed from the UK Met Office (https://www.metoffice.gov.uk/hadobs/en4/). The data are available monthly at 1º × 1º spatial resolution. The mean monthly temperature from four cells between 65º and 66ºS, 127º and 128ºE were extracted, located on the continental shelf proximal to Porpoise Bay (Fig. 1.1a), for each month between January 1990 and March 2025 at 24 depths. It should be acknowledged that the nature of EN4 analysis data creates very high uncertainty estimates, but these data provide the only consistently-derived indication of ocean temperature through time.

The EN4 data were supplemented with direct measurements of ocean temperature collected by instrumental marine mammals between 2004 and 2021, available from the Marine Mammal Exploring the Oceans Pole to Pole (MEOP) Consortium (Treasure et al., 2017). Each mammal is equipped with a Conductivity Temperature Density Satellite Relay Data Logger (CTD-SRDL) and deployed for 72 to 136 days (Roquet et al., 2014; Treasure et al., 2017). Data are collected throughout a dive and once the mammal surfaces the data are processed by the CTD-SRDL sensors and telemetered through the Argo satellite system. The geolocation of each dive is extracted by the Argo satellite triangulation, and collected with an accuracy of 4 km. The data are not spatially or temporally continuous: there are numerous casts near the edge of the continental shelf but none within 130 km of the Porpoise Bay ice margin.

Sea-ice conditions in Porpoise Bay were analysed using the NSIDC Sea-ice Index, Version 3 (Fetterer et al., 2017). The data are available at 25 km spatial resolution. Monthly sea-ice concentrations from a 12,500 km^2 polygon between November 1979 and April 2025 were extracted (Fig. 1.1a). This region may include ice mélange and shelf ice, so is likely to

capture mélange and ice-shelf breakup as well as sea-ice concentration changes. The data are obtained from satellite passive micro-wave derived datasets (the Near-Real-Time DMSP SSMIS Daily Polar Gridded Sea-ice Concentrations and the Sea-ice Concentrations from Nimbus-7 SMMR and DMSP SMM/I-SSMIS Passive Microwave Data). The accuracy of the sea-ice concentration is usually cited within ±5 % in winter and ±15 % in summer (Fetterer et al., 2017). The error is reduced for thicker and higher sea-ice concentrations due to the reduced influence of open water or high cloud liquid on the measured brightness temperature (Cavalieri, 1995; Spreen et al., 2008; Fetterer et al., 2017).

Chapter 4: Results

4.1 Ice-Shelf Position

The ice-shelf position of Frost, Glacier 1, Holmes East, and Holmes West glaciers fluctuated between 5.7 km and 11.3 km over the study period (1963–2025), with no clear trend of advance or retreat, but with several major calving events, followed by advance (Fig. 4.1 and 15). All four glaciers advanced between 1963 and 1973, at a mean rate of 281 m yr^{-1}, and retreated between 1973 and 1991, at a mean rate of −386 m yr^{-1}, with Glacier 1 and Holmes East Glacier retreating by over ~9 km. Contrastingly, 1991 to 2001 saw an advance from Frost Glacier (177 m yr^{-1}), Glacier 1 (329 m yr^{-1}), and Holmes East Glacier (545 m yr^{-1}) and a retreat from and Holmes West Glacier (52 m yr^{-1}). However, data scarcity before 2000 is likely to mask smaller-scale periods of advance and retreat, so these trends are evaluated with caution. The ice shelves advanced to a similar maximum position within 2 km of the previous advance limit (Fig. 4.1), before rapidly calving and beginning to advance once more.

The ice shelves in Porpoise Bay underwent almost synchronous cycles of advance and retreat between 2006 and 2025 (Fig. 4.2). Initially, the glaciers advanced from a post-calving position: 5.4 km at Frost Glacier (2008–2016), 6.2 km at Glacier 1 (2007–2015), 2.7 km at Holmes East Glacier (2006–2016) (underwent another calving event between 2010 and 2011), and 6.8 km at Holmes West Glacier (2006–2016). Between 2016 and 2017, the outlet glaciers underwent a calving event, retreating 2.8 km at Frost Glacier, 8 km at Glacier 1, 0.9 km at Holmes East Glacier, and 4.5 km at Holmes West Glacier. Subsequently, Frost, Glacier 1, Holmes East and West glacier gradually advanced 0.6 km, 3.7 km, 3.1 km, and 4.2 km, respectively, between 2017 and 2021. Glacier 1, Holmes East, and Holmes West glaciers calved between 2021 and 2022 by 2.7 km, 7 km, and 5.4 km, respectively, whilst Frost Glacier retreated 3.6 km between 2022 and 2023. Finally, the glaciers advanced 2.4 km (Frost), 1.2 km (Glacier 1), 3.7 km (Holmes East), and 0.6 km (Holmes West) by 2025.

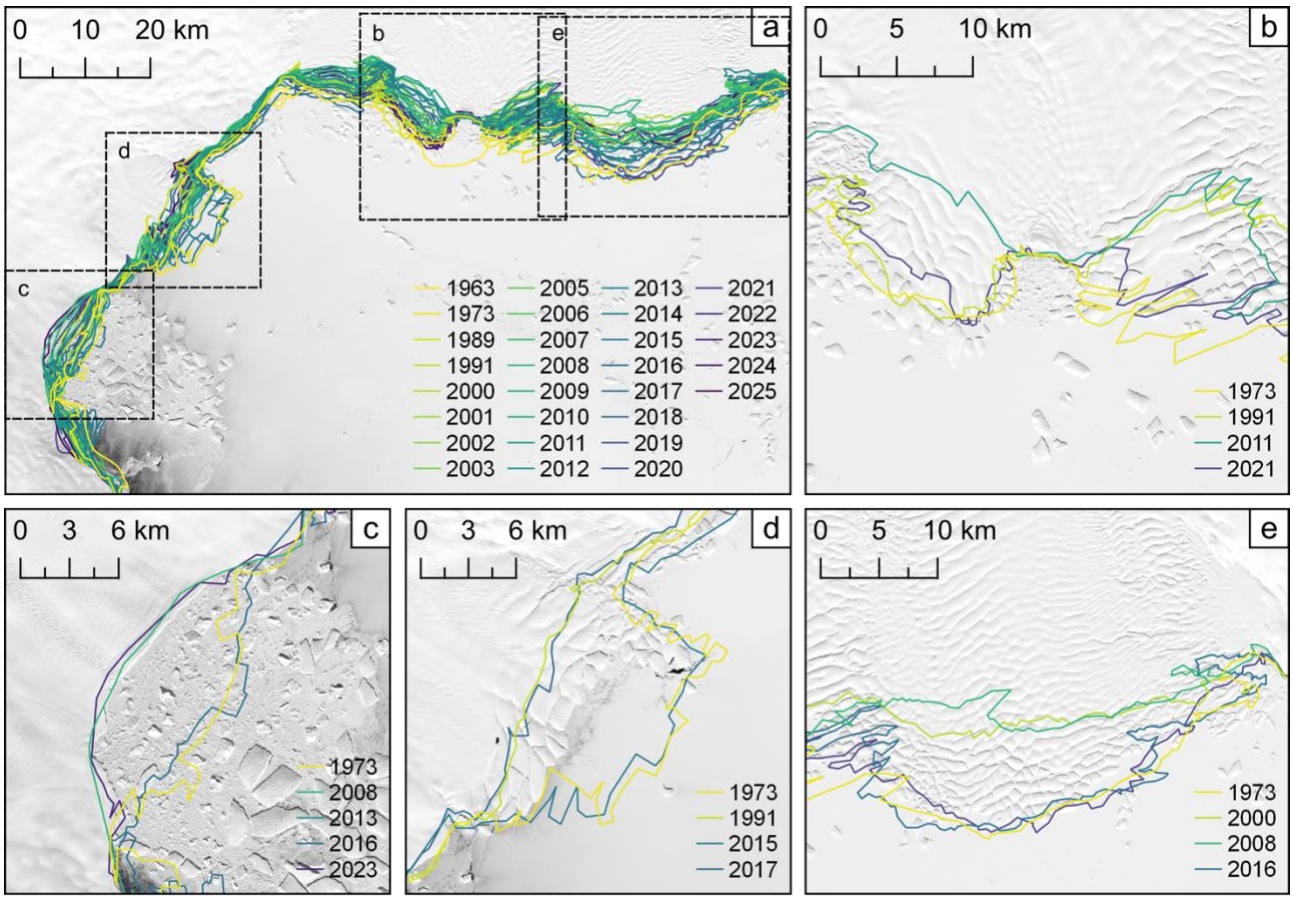

Figure 4.1: (a) Minimum and maximum ice shelf positions manually digitised across Porpoise Bay: (b) Holmes East Glacier, (c) Frost Glacier, (d) Glacier 1, and (e) Holmes West Glacier. The background satellite imagery is a Landsat image from 2024 and was downloaded from USGS EarthExplorer.

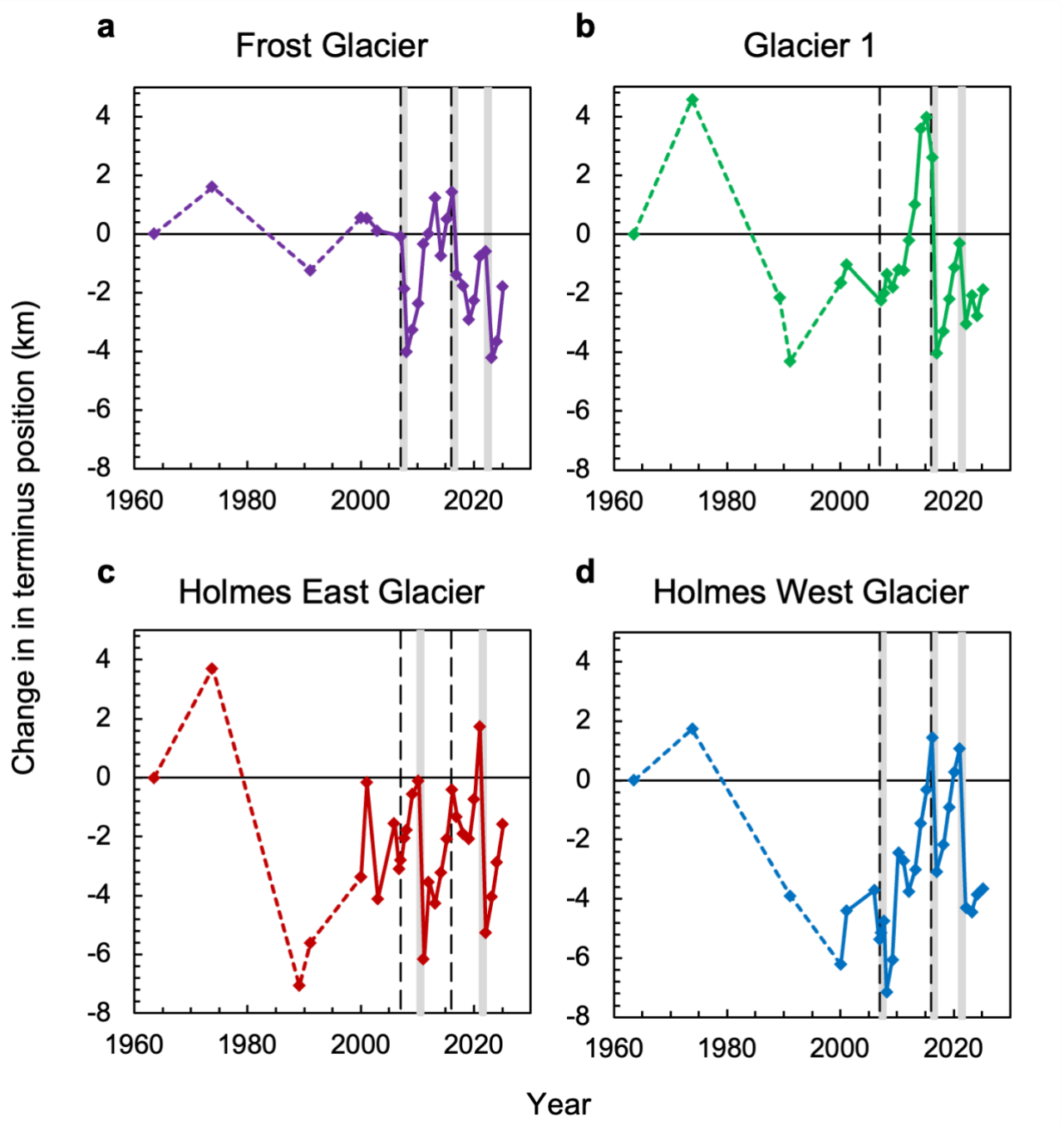

Figure 3: Width-averaged ice-shelf calving position changes relative to the first measurement in 1963 at (a) Frost Glacier, (b) Glacier 1, (c) Holmes East Glacier, and (d) Holmes West Glacier. Terminus positions before 2000 are joined by dashed lines due to large gaps in satellite imagery availability. Vertical dashed lines display the 2007 and 2016 sea-ice break-out event from Miles et al. (2017). Grey lines show the timing of major calving events.

4.2 Ice Surface Velocity

4.2.1 Temporal Variability

Temporal variations in ice surface velocity were observed between 2000 and 2022 (Fig. 4.3). All three glaciers saw an increase in ice flow velocity over the study period, across parts of the glacier flowlines. Observations showed the greatest speed up at Holmes East Glacier (Fig. 4.3c), with ice surface velocity at the IN box increasing 32 % overall from 382.3 ±37 in 2013 to 504 ±121 m yr^{-1} in 2022. However, the absolute value of velocity increase (122 m yr^{-1}) is similar to the associated error. Significant ice surface velocity variations were recorded in the GL and IN boxes at Holmes East and West glaciers, with a period of slowdown measured between 2017 and 2020, followed by a subsequent speed-up. Interestingly, this variation in ice surface velocity was not translated to the floating tongue for either glacier. Glacier 1 increased to peak velocity in 2010 before slowing down to a lower constant velocity (Fig. 4.3b). The ice surface velocity at Frost Glacier consistently increased 7 % to 10 % over the study period (Fig. 4.3a).

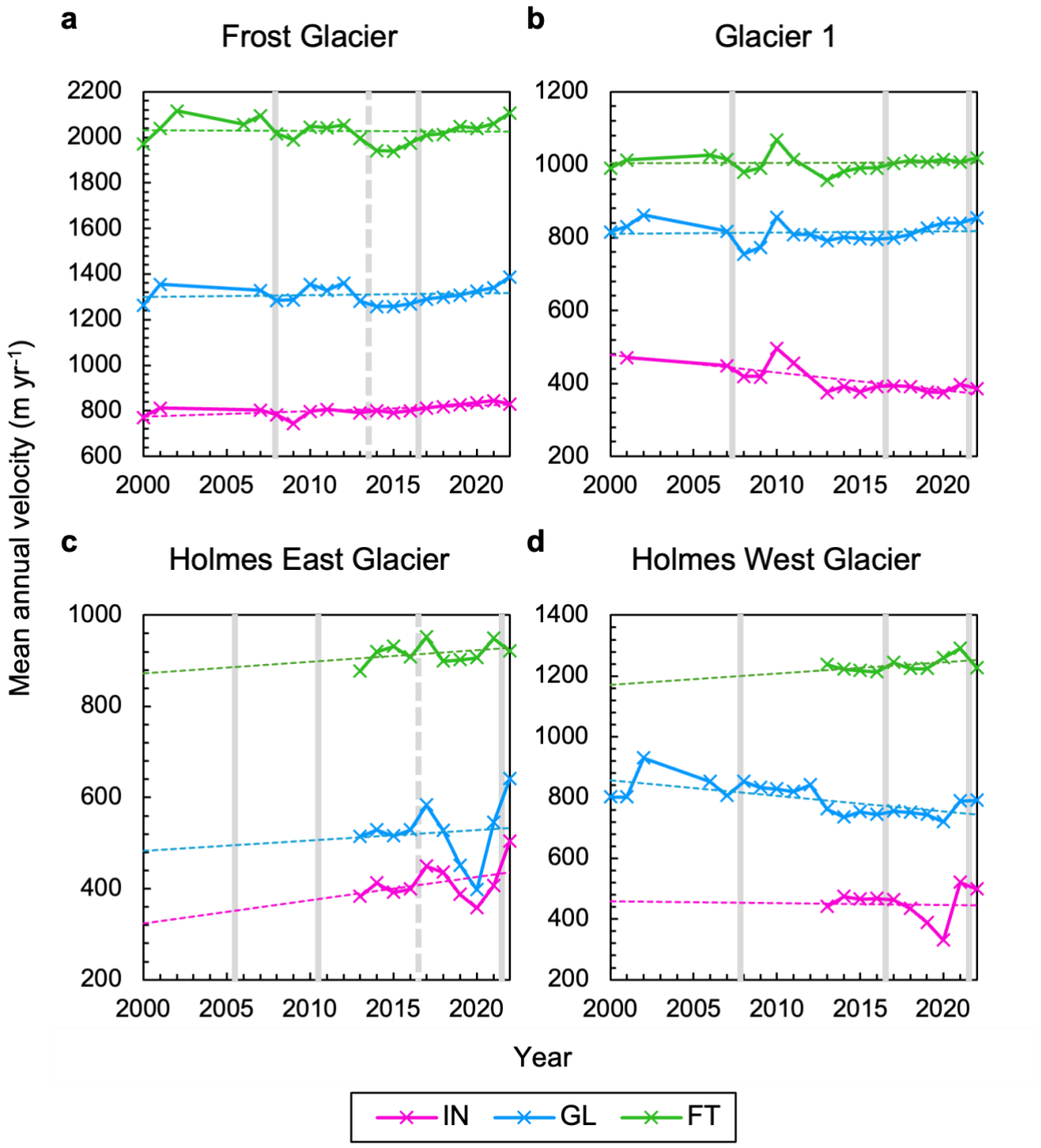

Figure 4.3: Mean annual velocity extracted from the inland (IN), grounding line (GL), and floating ice tongue (FT) boxes across (a) Frost Glacier, (b) Glacier 1, (c) Holmes East Glacier, and (d) Holmes West Glacier. Velocity data extracted from the ITS_LIVE velocity mosaic between 2000 and 2022 (Gardner et al., 2025). Dashed lines shows the linear trend. Grey lines show the timing of major calving events at the glacier ice shelf; grey dashes lines depict a partial/minor calving event. The y-axis scales are different across Figure 4.3.

4.2.2 Velocity and Ice-Shelf Position

Some of the outlet glaciers in Porpoise Bay displayed coincidental timing between changes in ice-shelf position and velocity (Fig. 4.3, grey). Frost Ice Shelf underwent a calving event between 2007 and 2008, after which the velocity increased 2 % to 6 % over the following two years across the glacier. Subsequently, the ice flow velocity increased following the small retreat between 2013 and 2014 and the ice-shelf calving between 2016 and 2019, increasing 3 % (IN), 10 % (GL), and 9 % (FT) over 8 years (Fig. 4.3a). The velocity across Glacier 1 increased 18 % (IN), 13 % (GL), and 9 % (FT) in the two years after the 2007 calving event, during which the ice-shelf area remained low, followed by a velocity slow down 24 % (IN), 7 % (GL), and 10 % (FT) over the three years after 2010, as the ice shelf regrew (Fig. 4.3b). However, there is a lack of velocity response to the latter two major calving events from Glacier 1. Following the 2016 calving event, Holmes East Glacier displayed an increase in velocity of 13 % (IN), 10 % (GL), and 5 % (FT) between 2016 and 2017 (Fig. 4.3c). The glacier showed limited velocity response to the 2021 calving event; the velocity continued its upward trend. Holmes West Ice Shelf underwent a calving event between 2007 and 2008, during which a 6 % increase in velocity was recorded across the grounding line (Fig. 4.3d). The subsequent 2016–2017 calving event is coincidental with a 3 % increase in velocity across the floating tongue. Conversely, the subsequent 2021 calving event is followed by a 5 % decline in ice velocity across the floating tongue and further inland. Overall, the outlet glaciers display some changes in velocity that correspond to changes at the ice-shelf edge, but there is not a consistent response to every calving event.

4.3 Ice Surface Elevation Change

There was general agreement between the two ice surface elevation datasets provided by Nilsson et al. (2023) and Schröder et al. (2019b) across the GL and IN boxes, especially after *ca.* 2003, when the uncertainties also decrease. Indeed, the datasets are associated with high levels of uncertainty in the 1990s and early 2000s. Across the IN boxes, a clear and consistent trend of thinning was observed across all four glaciers, with Holmes East and West thinning more rapidly than Frost and Glacier 1 (Fig. 4.4). Between 2003 and 2017, Schröder et al. (2019b) and Nilsson et al. (2023) observed elevation change at an average rate of −0.41 and −0.35 m yr^{-1} for Holmes East Glacier and −0.04 and −0.34 m yr^{-1} for Holmes West Glacier (values relative to 09/1992). Contrastingly, Frost Glacier and Glacier 1 displayed very little thinning between 2003 and 2017, with elevation change rates

calculated at an average of −0.01 and 0.003 m yr^{-1} for Frost and −0.16 and −0.01 m yr^{-1} for Glacier 1 from Schröder et al. (2019b) and Nilsson et al. (2023).

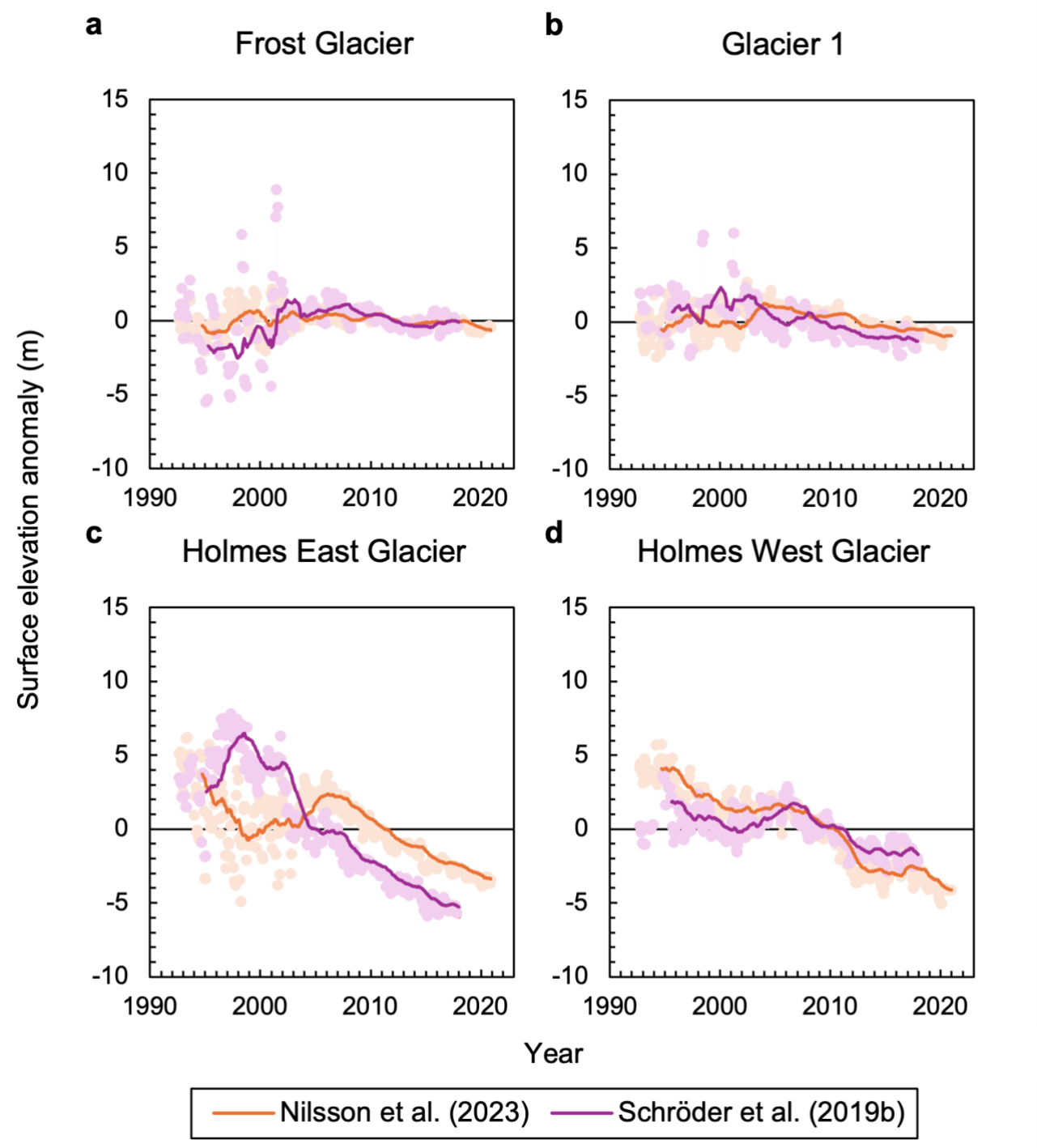

Figure 4.4: Monthly surface elevation anomalies observed in each IN box at (a) Frost Glacier, (b) Glacier 1, (c) Holmes East Glacier, and (d) Holmes West Glacier between 1992 and 2020. Elevation anomalies are calculated relative to the 1992–2017 mean. Bold lines display the 24-month rolling mean.

Mirroring the elevation patterns inland, observations of surface elevation across the GL boxes show rapid thinning at Holmes East and West Glaciers (Fig. 4.5). Schröder et al. (2019b) and Nilsson et al. (2023) observed elevation change at an average rate of −0.41 and −0.40 m yr^{-1} for Holmes East Glacier and Nilsson et al. (2023) observed average elevation change at a rate of −1.22 m yr^{-1} for Holmes West Glacier between 2003 and 2017. Lower rates of surface elevation loss were observed at Frost Glacier and Glacier 1. Schröder et al. (2019b) and Nilsson et al. (2023) observed elevation change at an average rate of −0.08 and −0.13 m yr^{-1} for Frost Glacier and −0.17 and 0.001 m yr^{-1} for Glacier 1.

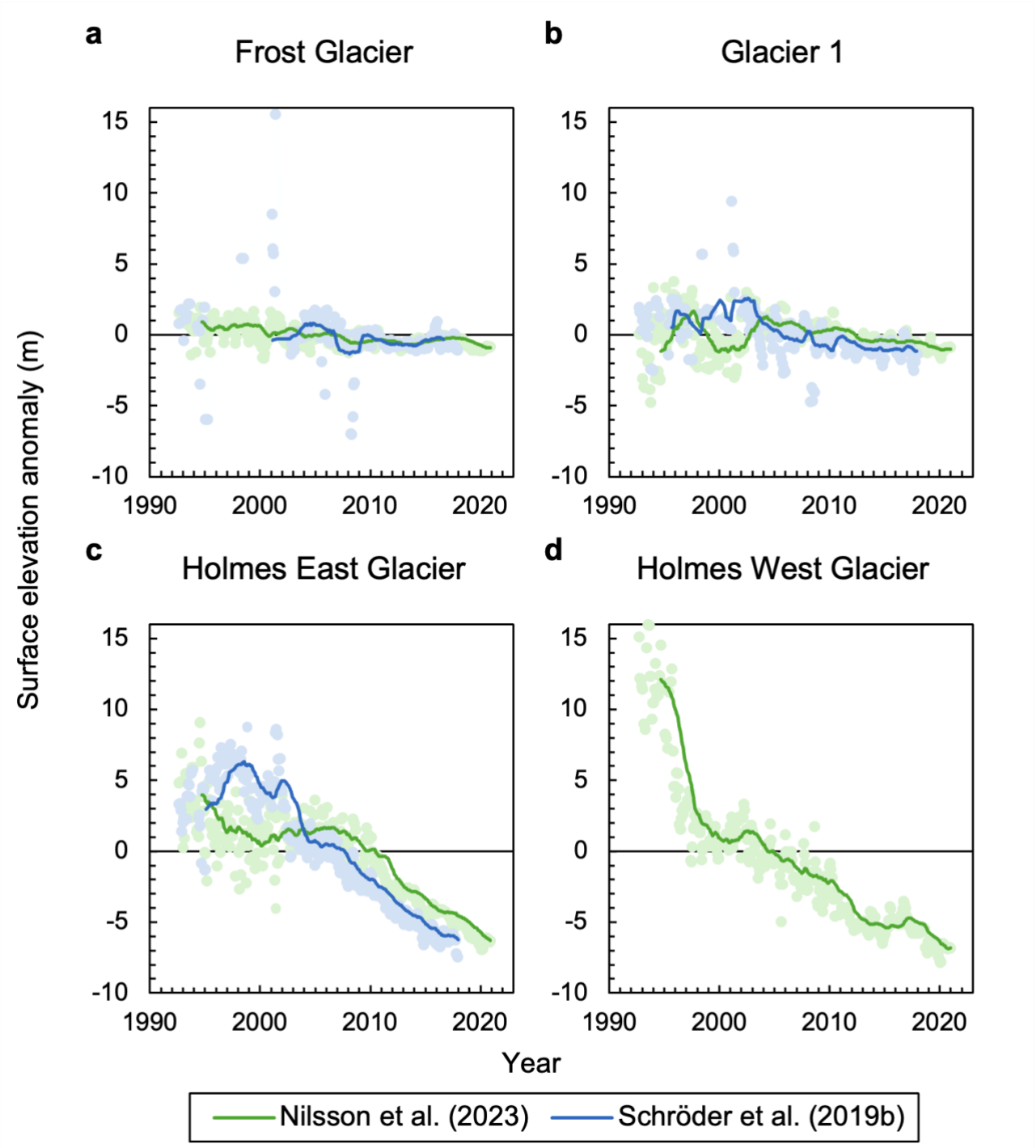

Figure 4.5: Monthly surface elevation anomalies observed in each GL box at (a) Frost Glacier, (b) Glacier 1, (c) Holmes East Glacier, and (d) Holmes West Glacier between 1992 and 2020. Elevation anomalies are calculated relative to the 1992-2017 mean. Bold lines display the 24-month rolling mean.

Similar trends are observed by Smith et al. (2020b) using ICESat- and ICESat-2-derived data (Fig. 4.6). Porpoise Bay showed an overall decrease in ice surface elevation between 2003 and 2019, with a hotspot of thinning extending across the ice shelf and grounded ice at Holmes East and West glaciers. There was a maximum surface elevation change of −1.11 m yr^{-1} on the grounded ice and −3.07 m yr^{-1} on the floating ice shelf.

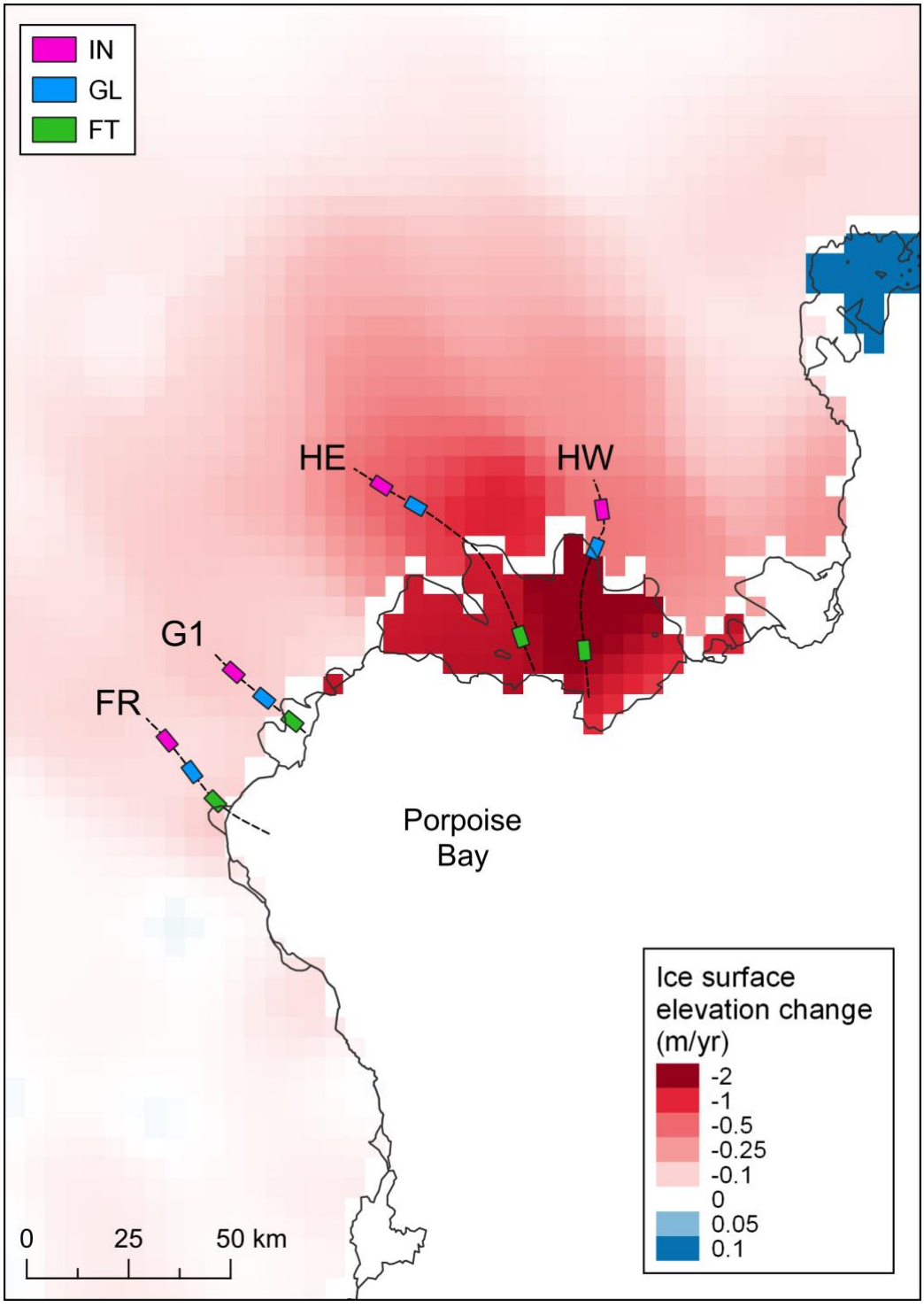

Figure 4.6: Rate of ice-surface elevation change observed inland of Porpoise Bay between 2003 and 2019, calculated by Smith et al. (2020b).

4.4 Grounding Line Position and Bathymetry

Notwithstanding some very large uncertainties (see *Section 3.4*), the highest grounding line retreat was observed at Frost and Holmes East glaciers (Fig. 4.7 and 4.8). If the MEaSUREs data from 1996 are taken at face value, Frost Glacier retreated 17.17 km between 1996 and 2014, at an average rate of −0.95 km yr^{-1} (Fig. 4.7a). This grounding line retreat occurred largely between 1996 and 2004, at an average rate of −2.14 km yr^{-1}, after which the grounding line was observed at a constant position. The grounding line retreat occurred across a largely retrograde slope, dropping in elevation from −615 m (Bedmap3)/ −587 m (BedMachine3)/ −758 m (ANTGG2021) to −982 m (Bedmap3)/ −875 m (BedMachine3), before becoming stabilised on a bedrock pinning point (Fig. 4.8a).

The grounding line position at Holmes East was observed to retreat 15.24 km between 1996 and 2001, at an average pace of −3.05 km yr^{-1} (Fig. 4.7c), where it stabilised for the following 13 years, with ASAID, and MOA datasets digitised at nearly identical locations. However, comparing across the DInSAR-derived grounding line positions, there was 3.42 km of retreat from 1996 (MEaSUREs) to 2019, at an average rate of −0.15 km yr^{-1}. The 2019 position was digitised within a 10.0 km wide buffer zone, indicating retreat within the range of 9.69 to 0.34 km, relative to 1996. The retreat continues to 2020; the findings show 5.27 km of retreat from the 1996 position, calculated at −0.22 km yr^{-1}, with a maximum of 14.65 km and minimum of 2.75 km within the 11.9 km buffer zone, at a mean rate of −0.61 km yr^{-1} to −0.11 km yr^{-1}. The grounding line retreated initially down a retrograde slope before stepping up a prograde slope (Fig. 4.8c). Taken at face value, the grounding line retreated between 1996 and 2001, remained stable between 2001 and 2014, and then advanced to 2019. The difference in grounding line position between the DInSAR and the ASAID and MOA products in Figure 4.7c highlights the uncertainty associated with comparing products delineating the hinge line from DInSAR and break-in-slope from manual delineation.

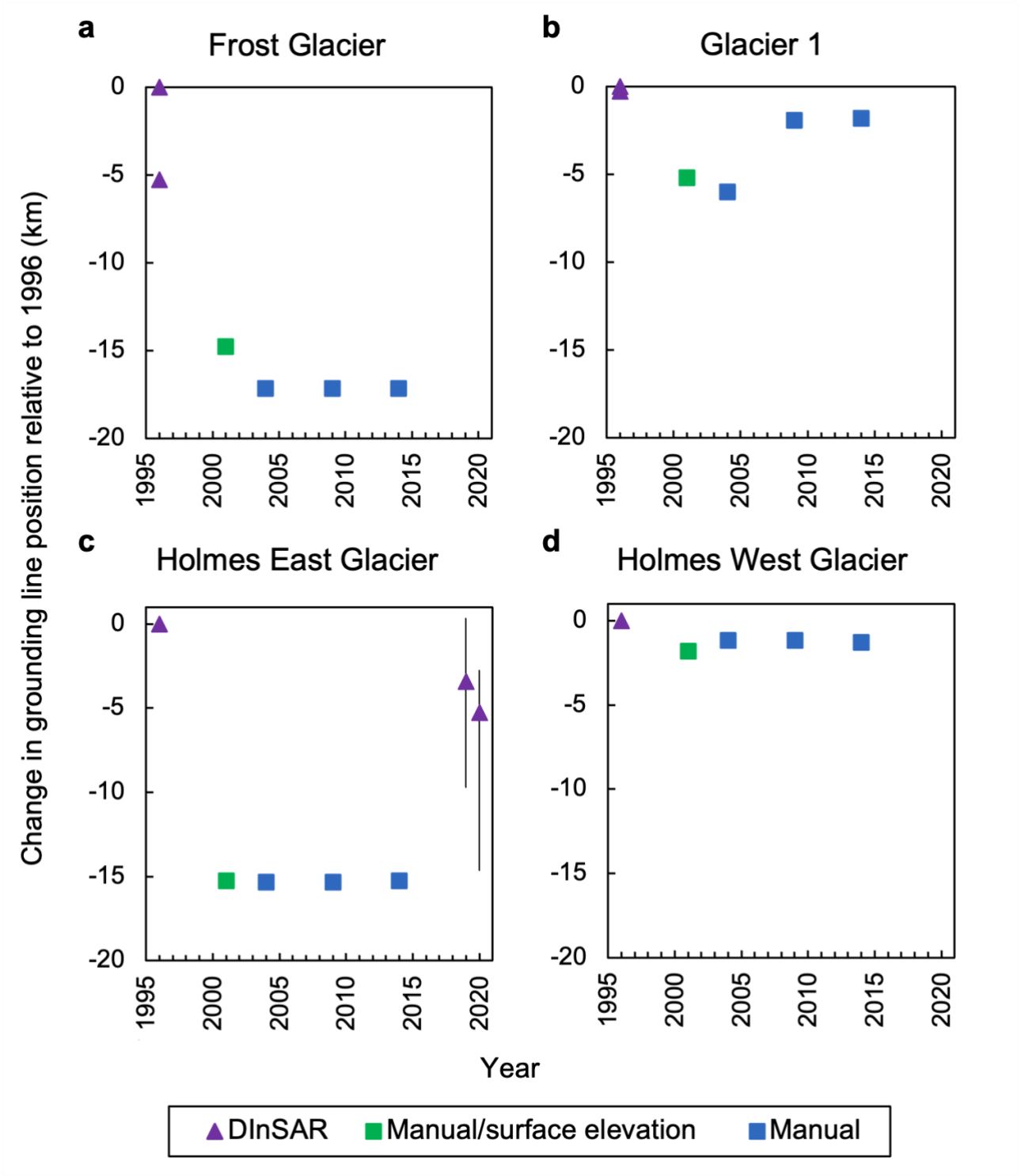

Figure 4.7: Changes in grounding line position measured relative to the 1996 position observed at (a) Frost Glacier, (b) Glacier 1, (c) Holmes East Glacier, and (d) Holmes West Glacier. The 1996 position from MEaSUREs (Rignot et al., 2016), 2001 from ASAID (Bindschadler and Choi, 2011), 2004, 2009, and 2014 from MOA (Haran et al., 2018; 2021a; 2021b), 2019 and 2020 from this paper.

In contrast, the grounding line position of Holmes West Glacier was observed to be relatively stable between 1996 and 2014; the grounding lines were digitised at very similar positions across products (Fig. 4.7d). Holmes West Glacier retreated −1.28 km between 1996 and 2014, recorded at an average rate of −0.07 km yr^{-1}. The grounding line retreated down a very shallow slope but is positioned at the edge of a significant steepening retrograde bed that continues down a reverse slope for 20 km, with the bed lowering almost 700 m along only 2 km of grounding line retreat across the flowline (Fig. 4.8d).

The grounding line position at Glacier 1 showed retreat then advance (Fig. 4.7b). Between 1996 and 2004, the grounding line position retreated −6.01 km, calculated at an average rate of −0.75 km yr^{-1}. The grounding line was subsequently observed to advance +4.18 km by 2014, at an average rate of +0.42 km yr^{-1}. Observations show an overall retreat of −1.83 km across a largely flat bedrock elevation (Fig. 4.8b).

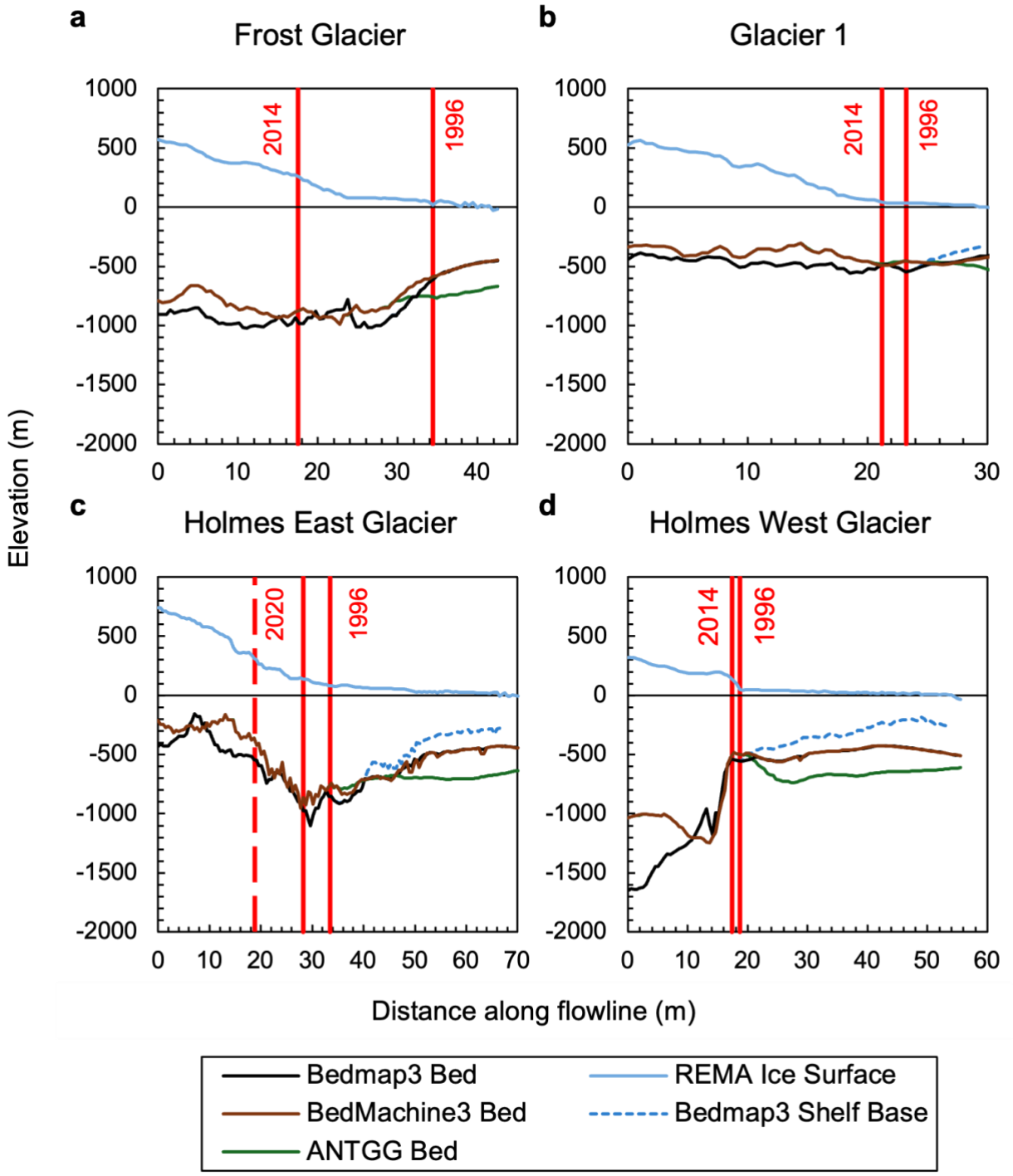

Figure 4.8: Ice surface and bed elevation profiles extracted along the central flowlines of (a) Frost Glacier, (b) Glacier 1, (c) Holmes East Glacier, and (d) Holmes West Glacier. Bed elevation: Bedmap3 (Pritchard et al., 2024), BedMachine3 (Morlighem, 2022), and ANTGG (Rignot et al., 2024), ice surface elevation: REMA (Howat et al., 2022), ice shelf base: Bedmap3 (Pritchard et al., 2024). The red lines depict the oldest and newest grounding line (dashed red in (c) shows the maximum uncertainty). Measurements are shown in the along-flow direction, in which 0 km represents the inland start point.

4.5 Variability in Ocean and Sea-Ice Conditions

Although there is substantial variability in EN4 ocean temperature over time (Fig. 4.9), these reanalysis data show warm ocean water on the continental shelf in Porpoise Bay. At the surface (shallower than 100 m depth), temperatures were recorded largely below −1°C, calculated at a mean temperature of −1.4°C between 1990 and 2025 (Fig. 4.10). There is annual or biennial seasonal warming to >0°C at depths above 50 m that last for a few summer months (Fig. 4.9). At intermediate depths (100 to 350 m depth), the mean ocean temperature was −0.7°C between 1990 and 2025 (Fig. 4.10), with seasonal cycles displaying approximately −0.5°C to −1°C in winter and 0°C to 0.5°C in summer (Fig. 4.9). At depth below 450 m, the ocean is largely warmer than 0°C with a seasonal cycle between −0.5°C (winter) and 0.5°C or warmer (summer). The mean temperature of 0.1°C was calculated for depths below 447 m between 1990 and 2025. Cooler periods were recorded, during which temperatures warmer than 0°C are not present at depths greater than 500 m across 1997–1999, 2004–2005, 2007, 2011–2015, and 2019–2021 (Fig. 4.9). No significant trend in temperature were recorded over the 1990–2025 period (Fig. 4.10).

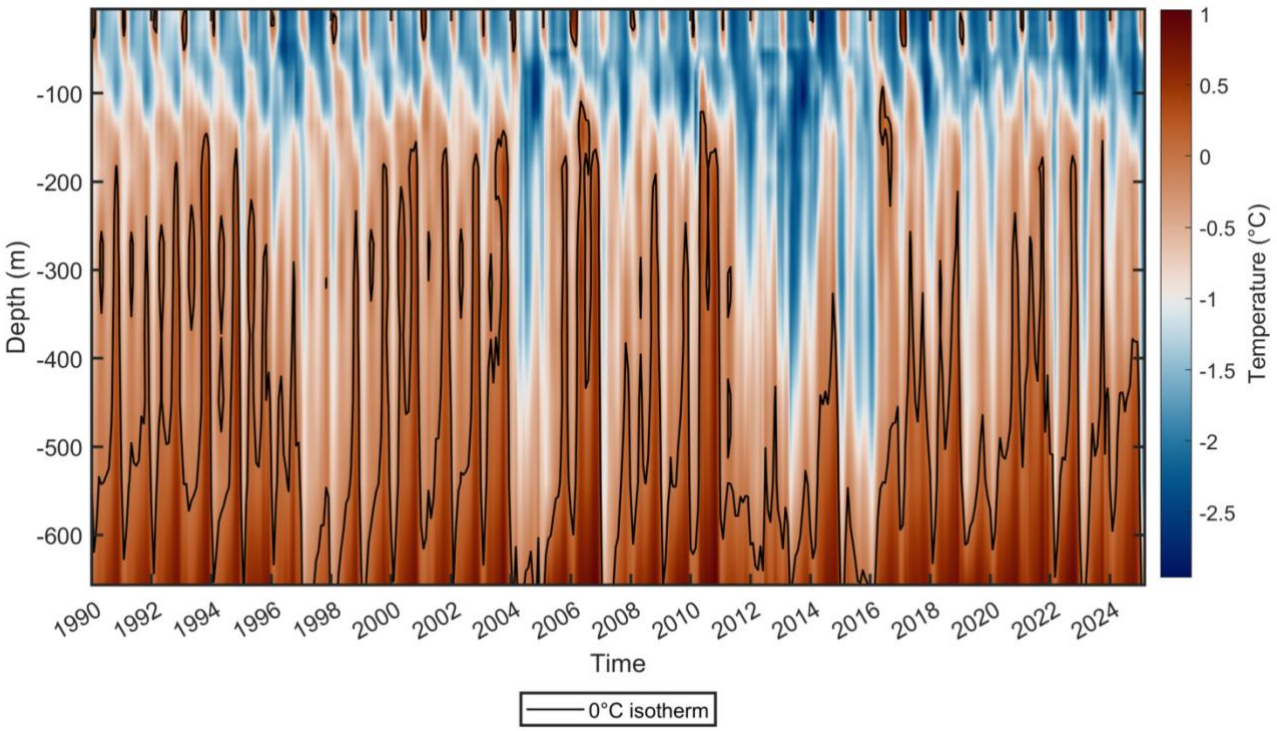

Figure 4.9: EN4 subsurface ocean temperature depth profile for 1990 to 2025 from 4 grid cells between 65° and 66°S, 127° and 128°E on the continental shelf, Porpoise Bay (Good et al., 2013).

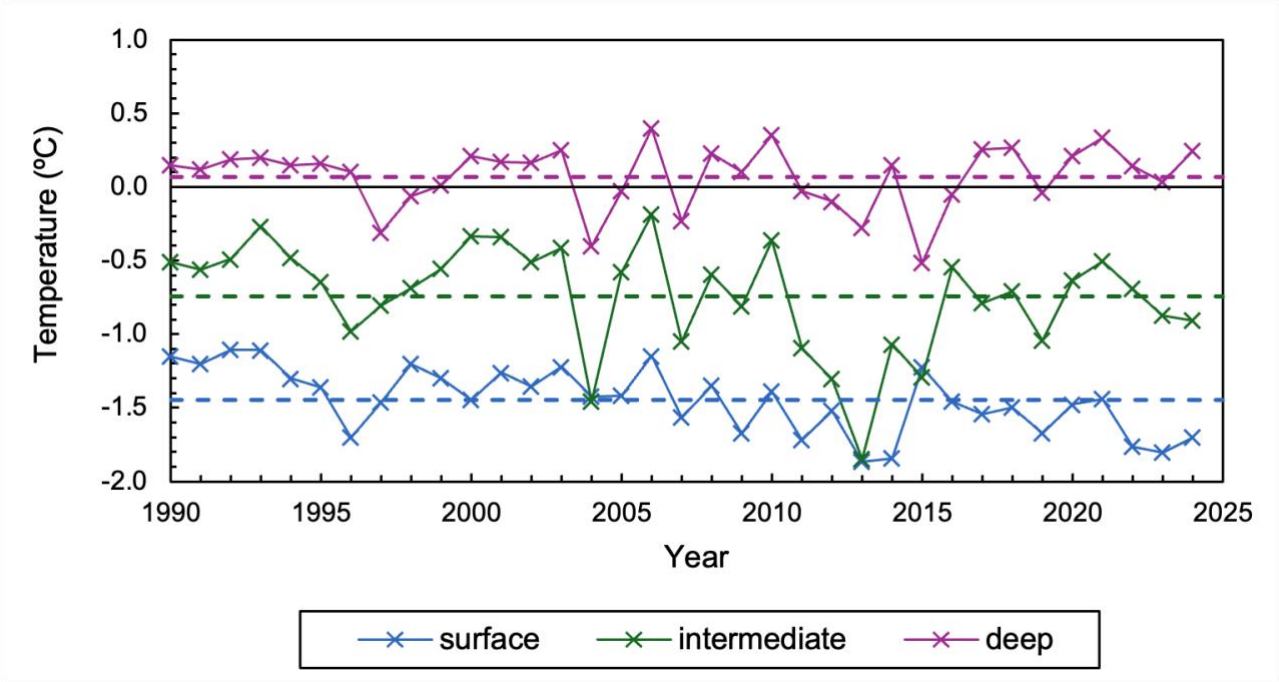

Figure 4.10: Annual EN4 subsurface ocean temperature across three depth ranges (surface: above 98 m, intermediate: between 110 m and 373 m, deep: below 447 m). Dashed lines show mean temperature at each depth.

18 MEOP casts recorded between 2004 to 2021 reveal warm, salty water between 200 m and 1,000 m depth at the continental shelf break, close to Porpoise Bay (Fig. 4.11). Further offshore, warm, salty waters are recorded over the continental slope, ranging from 0°C to 2°C (Fig. 4.11a) with salinity of around 34.8 g kg^{-1} (Fig. 4.11b) between 200 m and 1,000 m depth (Fig. 4.11c). Over the continental shelf there are relatively few MEOP casts, with none within 130 km of the ice sheet margin, possibly due to the persistence of sea ice in the region. However, *in situ* ocean temperatures on the outer continental shelf and shelf break, north-west of Porpoise Bay, are recorded above freezing at depth, with temperatures ranging from 0.19°C (at 1,000 m depth) to 0.13°C (at 918 m depth) to 0°C (at 690 m depth) (Fig. 4.11a and 4.11c). Closer to the surface, cooler temperatures were recorded −1.77°C (at 152 m depth) to −1.68°C (at 324 m depth). The casts record salinity up to 34.7 g kg^{-1} on the continental shelf, with many of the values above 34.5 g kg^{-1} (Fig. 4.11b). The presence of mCDW in East Antarctica is characterised by high salinity (>34.5 g kg^{-1}) and temperatures above freezing (Schodlok et al., 2016). The findings suggest the presence of mCDW around the continental shelf break near Porpoise Bay at depths at, or shallower than, the continental shelf edge.

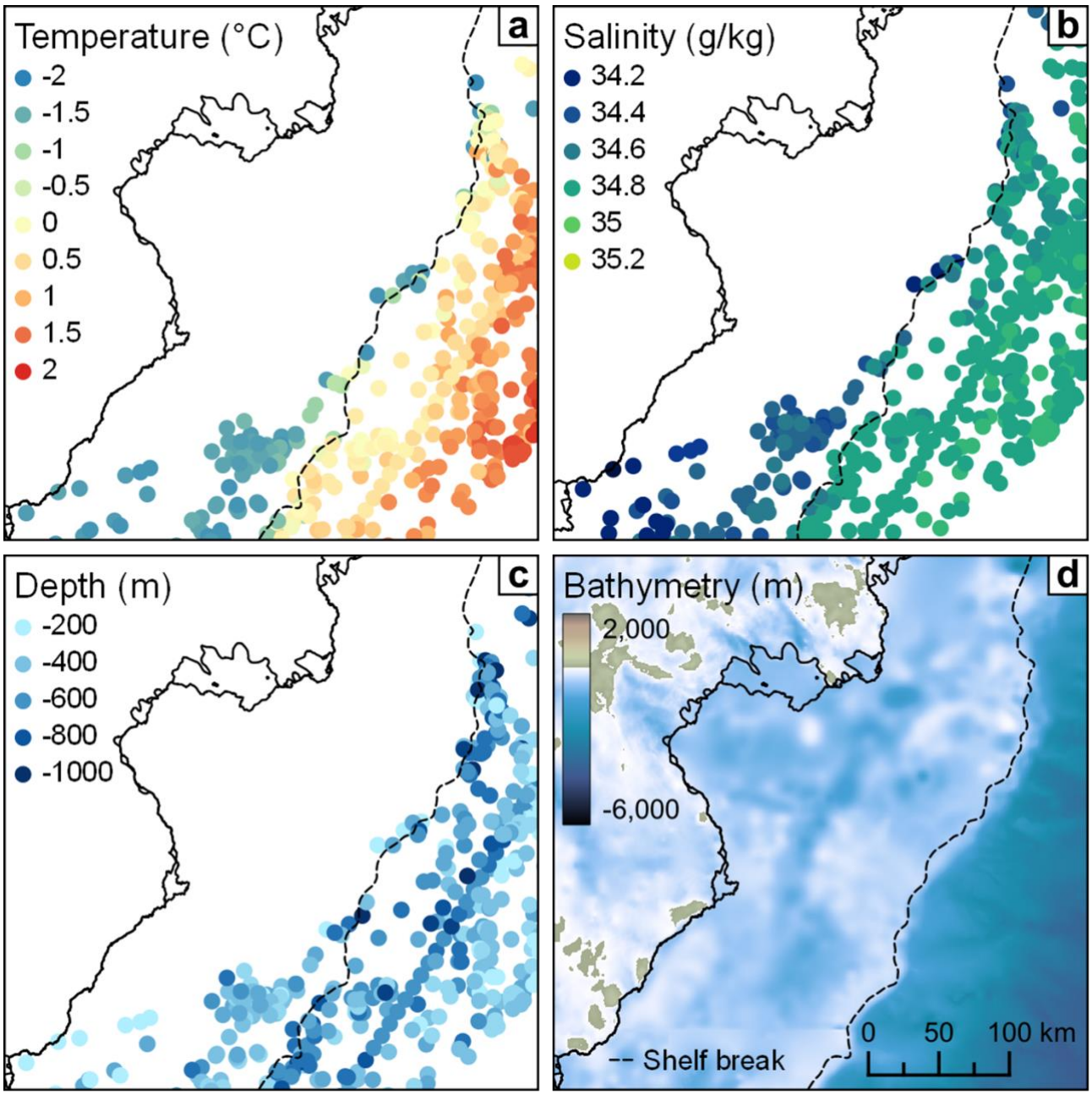

Figure 4.11: Oceanic properties derived from the MEOP casts between 2004 and 2021 near Porpoise Bay: (a) maximum conservative temperature (°C) observed below 150 m depth at each seal dive, (b) absolute salinity (g kg^{-1}) at the depth of (a), (c) depth of (a), (d) bathymetry of the continental shelf from ANTGG (Rignot et al., 2024). Dashed line shows continental shelf break from Amblas (2018) at approximately 600–800 m, solid line shows ice sheet and shelf edges from MEaSUREs (Mouginot et al., 2017).

Analysis of monthly sea-ice concentration from 1979 to 2025 reveals lower-than-average March sea-ice concentrations in 2006, 2007, 2010, 2016, 2021, and 2022 (Fig. 4.12), with very low sea-ice concentrations recorded in 2007 (38 %), 2010 (50 %), and 2021 (41 %). These abnormally low March sea-ice conditions coincide with the beginning of calving events recorded at the ice shelves (Fig. 4.2). Furthermore, the results show lower-

than-average mean sea-ice concentration in the winter-spring (June to November) of 2006, 2015, and 2020, and the summer-autumn (Dec–May) of 2007, 2016, and 2021 (Fig. 4.13). These low seasonal sea-ice conditions coincide or directly precede the calving events recorded above at Frost, Glacier 1, and Holmes West ice shelves (Fig. 4.2).

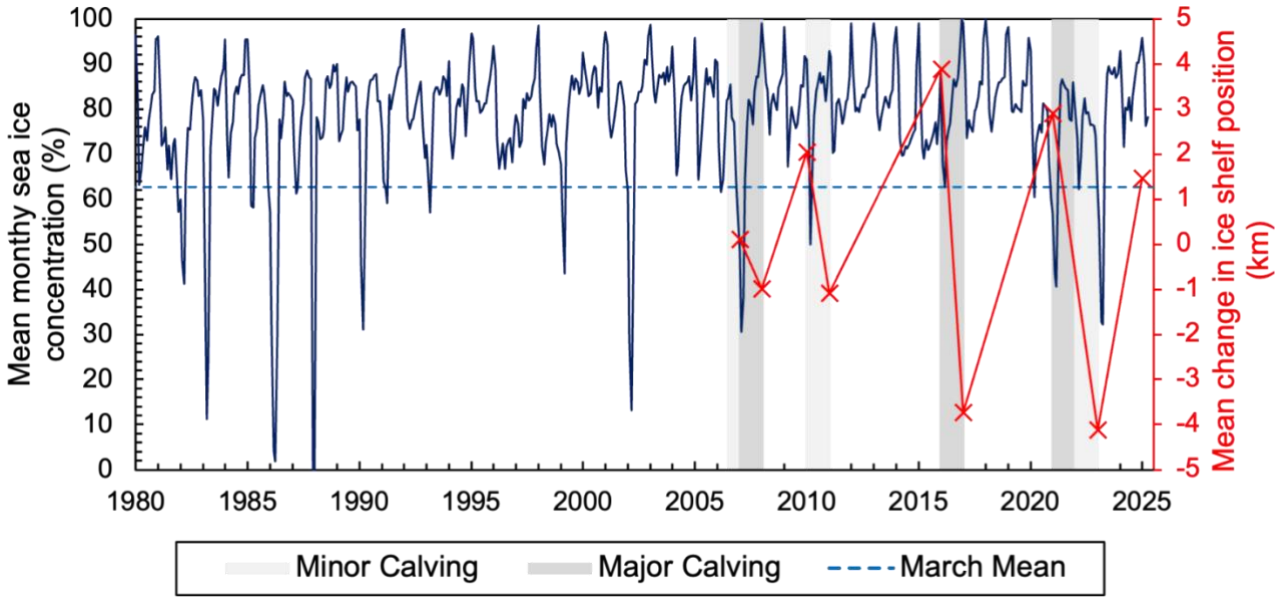

Figure 4.12: Monthly sea-ice conditions extracted from a 100 km × 125 km box extending 130 km offshore from Porpoise Bay (see Fig. 1.1a). The March mean is shown in dashed blue. Pale grey depicts when 1 glacier underwent a calving event, dark grey denotes when 3 or more glaciers calved (see Fig. 4.2). Data from Fetterer et al. (2017).

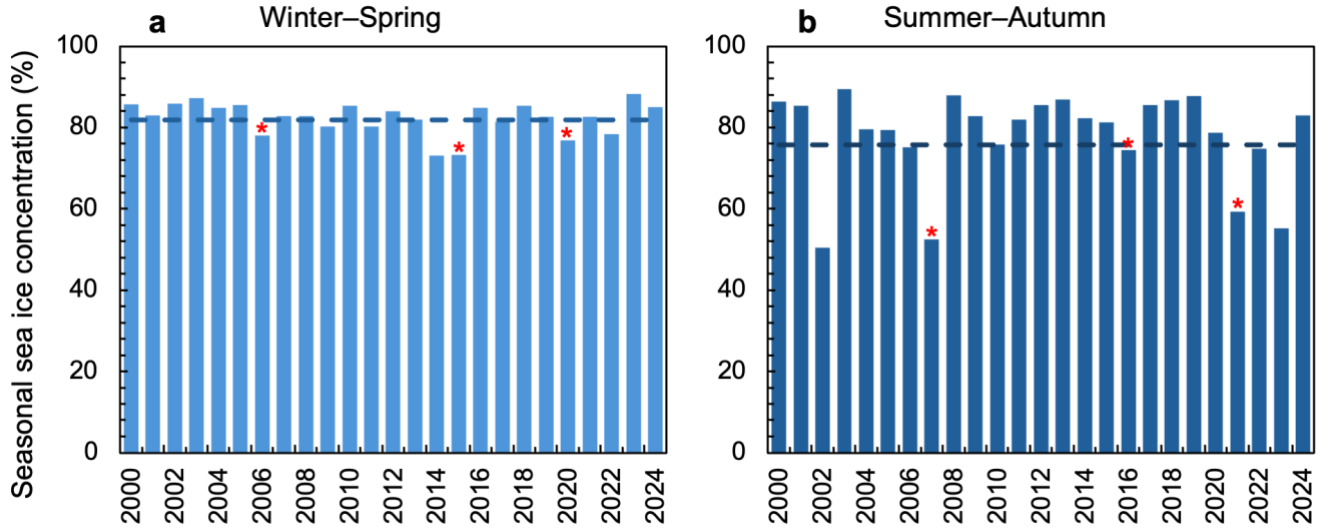

Figure 4.13: Seasonal sea-ice conditions offshore of Porpoise Bay (see Fig. 1.1a). (a) Winter–Spring (June to November). (b) Summer–Autumn (December to May). Asterisks show the key years relating to calving events at the ice-shelf fronts (Fig. 4.2). Dashed lines show the mean seasonal sea-ice concentration. Data from Fetterer et al. (2017).

4.6 Summary of Observations

Observations show notable changes at Frost, Holmes East and Holmes West glacier that are argued to be consistent with dynamic changes and mass loss observed elsewhere in Antarctica, particularly in West Antarctica (Table 4.1). Over the study period, records show grounded ice surface lowering, grounding line retreat, ice surface velocity increase, and ice-shelf retreat of varying degrees across Frost, Holmes East, and Holmes West glaciers. The highest surface elevation thinning is seen at Holmes West (−1.22 m yr^{-1}), where the grounding line retreat is modest (−70 m yr^{-1}), but where it sits on a deep bed with a retrograde bed-slope further inland. The surface elevation lowering at Frost and Holmes East is more moderate (−0.13 m yr^{-1} and −0.4 m yr^{-1}, respectively) but the grounding line retreat of both glaciers is >500 m yr^{-1}, which is high compared to most other outlet glaciers in East Antarctica (Konrad et al., 2018; Stokes et al., 2022; Picton et al., 2023). The long-term trend of ice velocity is also increasing across all three of these glaciers, albeit very slowly, with their ice front position also retreating. In contrast, the much smaller Glacier 1 shows limited evidence of dynamic change (Table 4.1).

Table 4.1: Summary statistics of each outlet glaciers. (a) Mean annual surface elevation change across the GL between 2003 and 2017 from Nilsson et al. (2023). (b) Mean annual grounding line position change between 1996 and 2014 or 2020 (maximum position within the buffer). (c) Mean annual percentage change in ice surface velocity between 2000 and 2022 (2014–2022 for HE and HW). (d) Mean annual ice-shelf calving front change between 1963 and 2025. (e) Change in bed elevation between the 2014/2020 grounding line position and 10 km inland along the flowline from Bedmap3. Statistics in red are consistent with dynamic thinning, whilst statistics in blue are less consistent.

	Frost Glacier	Glacier 1	Holmes East Glacier	Holmes West Glacier
a. surface elevation	− 0.13 m yr^{-1}	0 m yr^{-1}	− 0.4 m yr^{-1}	− 1.22 m yr^{-1}
b. grounding line position	− 950 m yr^{-1}	− 100 m yr^{-1}	− 610 m yr^{-1}	− 70 m yr^{-1}
c. ice surface velocity	+ 0.3 %	− 0.5 %	+ 1.7 %	+ 0.1 %
d. ice-shelf position	− 110 m yr^{-1}	− 17 m yr^{-1}	− 3 m yr^{-1}	− 29 m yr^{-1}
e. bed elevation	− 4 m	+ 18 m	+ 460 m	− 783 m

Chapter 5: Discussion

5.1 Grounding Line Retreat and Ice Surface Thinning

Porpoise Bay displays a pattern of localised grounding line retreat. Taken at face value, the results would make Frost one of the fastest retreating glaciers in East Antarctica on decadal timescales at an average rate of −0.95 km yr^{-1} between 1996 and 2014 (Fig. 4.7a), down a retrograde slope (Fig. 4.8a), with a more rapid rate of −2.15 km yr^{-1} between 1996 and 2001 (Fig. 4.7a). Neighbouring Holmes East Glacier underwent grounding line retreat at a maximum rate of −0.61 km yr^{-1} between 1996 and 2020 (Fig. 4.7c), observed at the maximum width of the grounding line uncertainty buffer zone. For context, only Vanderford Glacier in East Antarctica sustained similarly high rates of grounding line retreat at −0.78 km yr^{-1} (1996–2020) (Picton et al., 2023). In the WAIS, Thwaites and Pine Island glaciers in the Amundsen Sea Embayment experienced similarly rapid rates of −0.8 km yr^{-1} and −0.95 km yr^{-1} between 1992 and 2011 (Park et al., 2013; Milillo et al., 2019).

Measurements of grounding line retreat at Frost Glacier are highly uncertain due to a comparison across products that not only delineate different parts of the grounding zone (i.e., hinge line vs break-in-slope), but also use different methods (i.e., DInSAR vs manual delineation). Furthermore, the difference between the DInSAR and the ASAID and MOA positions at Holmes East Glacier (Fig. 4.7c) highlight the uncertainty between the ASAID and MOA grounding line position results at Frost Glacier (Fig. 4.7a), suggesting retreat could have been less rapid than recorded. However, even if the rates of retreat are not as high as reported in Figure 4.7a (due to uncertainties), these observations are broadly consistent with the grounding line retreat observed by Konrad et al. (2018), measured at −0.2 km yr^{-1} between 2010 and 2016 using satellite altimetry and ice geometry, suggesting that grounding line retreat is almost certainly occurring. Further identification of more recent and accurate grounding line positions at Frost Glacier are therefore a priority.

Substantial grounded ice surface elevation lowering is observed at Holmes East and West glaciers, propagating inland across datasets (Schröder et al., 2019b; Smith et al., 2020b; Nilsson et al., 2023), indicating a potential signal of dynamic thinning. Holmes West Glacier displayed thinning up to −1.22 m yr^{-1} at the grounding line (Fig. 4.5d), propagating 10 km inland at a rate of −0.34 m yr^{-1} (Fig. 4.4d). This rapid rate places Holmes West Glacier as one of the most rapidly thinning glaciers in East Antarctica over decadal timescales (Stokes et al., 2022); only at Totten Glacier are there observations of such extreme thinning, measured up to −1.9 ± 0.07 m yr^{-1} (2003–2007) (Pritchard et al., 2009), −1.22 ± 0.1 m yr^{-1} (2003–2019) (Smith et al., 2020b) and −0.72 ± 0.02 m yr^{-1} (2010–2019) (Li et al., 2023).

The results also suggest that Frost, Holmes East, and West glaciers thinned whilst ice surface velocity increased modestly (Fig. 4.3), suggesting a connection between flow regime and ice thickness that is consistent with dynamic thinning (Pritchard et al., 2009).

Further analysis suggests a relationship between grounding line retreat and ice surface thinning rates in Porpoise Bay across the study period. At Holmes East and West glaciers, the most rapid grounding line retreat took place between 1996 and 2001 (Fig. 4.7: −15.24 m and −1.81 m), during which enhanced thinning rates were recorded (Fig. 4.5: −0.63 m yr^{-1} and −2.29 m yr^{-1}). This correlates with a pan-ice sheet study by Konrad et al. (2018) that found an approximately proportional relationship between ice thickness change and grounding line migration within sections of ice flowing faster than 800 m yr^{-1}. Overall, the extreme localised grounding line retreat and the dynamic thinning, alongside ice surface velocity speed-up, are consistent with a sustained period of change in Porpoise Bay that is indicative of a dynamic response to external forcing.

5.2 Role of Ocean Forcing in Porpoise Bay Glacier Dynamics

High rates of grounding line retreat and ice surface lowering inland have been widely attributed to the intrusion of warm mCDW across the continental shelf towards Antarctic sub-ice cavities (Thoma et al., 2008; Paolo et al., 2015; Scambos et al., 2017; Rignot et al., 2019). The rates of grounding line retreat observed at Frost Glacier and Holmes East Glacier are consistent with warm mCDW incursion beneath Frost Ice Shelf and Holmes East Ice Shelf. Although the EN4 data do not depict a long-term warming trend (Fig. 4.10), recent observations of mid-depth CDW along the continental slope off East Antarctica show warming since the 1990s, which is attributed to the southwards shift in the Antarctica Circumpolar Current (ACC), potentially driven by a poleward shift in the westerlies over the Southern Ocean that is linked to a positive trend in the Southern Annular Mode (Yamazaki et al., 2021; Herraiz-Borreguero and Garabato, 2022).

18 *in situ* temperature and salinity measurements from MEOP casts indicate mCDW presence on the outer continental shelf and shelf break, and CDW offshore of the continental shelf between 2004 and 2021 (Fig. 4.11). In the absence of ocean temperature observations within 130 km of the ice-shelf margin, EN4 subsurface ocean temperatures were analysed to gain potential insight into the existence of mCDW across the continental shelf between 1990 and 2025 (Fig. 4.9). Though it is acknowledged that the nature of these data creates high uncertainty estimates, EN4 data suggest the presence of mCDW at depth across the continental shelf, with an average ocean temperature of 0.7°C below 447 m, and a seasonal cycle of 0–0.5°C at intermediate depth (100–350 m) between 1990 and 2025. The intrusion

of mCDW has the potential to cause ice-shelf melting and thinning, delivering freshwater that could inhibit the formation of dense shelf water in Porpoise Bay, strengthening water column stratification and enabling the enhanced intrusion of warm mCDW at depth (Ribeiro et al., 2021).

At Holmes Ice Shelf (East and West), high rates of ice-shelf basal melt have been estimated, which is consistent with intrusions of mCDW. Using satellite radar altimetry with satellite-derived ice velocities and a model of firn-layer evolution, Adusumilli et al. (2020) calculated an average basal melt rate of 13.3 ± 2.9 m yr^{-1} beneath the Holmes Ice Shelf between 1994 and 2018, the highest average basal melt rate of any ice shelf in East Antarctica, and fourth in Antarctica behind the ice shelves of Thwaites (26.7 ± 2.4 m yr^{-1}), Land (20.4 ± 2.7 m yr^{-1}), and Pine Island (14.0 ± 1.6 m yr^{-1}) glaciers. Adusumilli et al. (2020) reported that Holmes Ice Shelf had a higher average basal melt rate than Totten Ice Shelf (11.5 ± 2.0 m yr^{-1}), where hydrographic observations show warm mCDW at the ice front (Rintoul et al., 2016).

Studies also show that Holmes Ice Shelf has been thinning considerably. Using ICESat- and ICESat-2-derived data, Smith et al. (2020b) recorded a maximum ice surface lowering rate of −3.07 m yr^{-1} (2003–2019) on the floating ice shelf. A recent study extended this thinning record using the surface expression of pinning points as a proxy for ice-shelf thickness; Miles and Bingham (2024) found that Holmes Ice Shelf began to thin at least 50 years ago, alongside Moscow University and Totten, evinced by a reduction in pinning across three study epochs: 1973–1989, 1989–2000, and 2000–2022. Miles and Bingham (2024) concluded by noting that Holmes Ice Shelf was showing signs of acceleration and pinning-point loss and the continuation of pinning-point loss would likely reduce buttressing and cause acceleration of ice discharge and mass loss.

Porpoise Bay's pattern of localised rapid grounding line retreat and thinning is consistent with a dynamic response of glaciers flowing into thinning ice shelves due to warm mCDW intrusion. To enable mCDW to access the grounding line, sufficiently deep cross-shelf troughs must exist in front of Porpoise Bay to transfer warm water from the continental shelf break to the grounding line. Although bathymetric data are limited across Porpoise Bay, due to the persistence of sea ice in the bay, a recent study using seal data found several dives at the edge of the continental shelf, offshore from Porpoise Bay, that were up to 500 m deeper than the reported bathymetry (McMahon et al., 2023). Indeed, a trough may exist that connects the open ocean and grounding line via a deeper corridor of topography across the continental shelf that could transport mCDW (Fig. 4.11d). In addition, the ice-shelf cavity

must be sufficiently deep for mCDW to access the grounding line. Using 3D inversion, seismic, and MBES/SBES data, Rignot et al. (2024) found the bed at the ice margin of all four outlet glaciers was deeper than reported by BedMachine3 or Bedmap3, by over 200 m for several tens of kilometres along the flowlines (Fig. 4.8 and Fig. 4.12d). Visual inspection of the dataset (Rignot et al., 2024) reveals deep sub-ice-shelf cavities below Frost, Holmes East, and Holmes West glaciers, between 650 m to 750 m depth, that deepen inland (Fig. 4.8). These cavities are sufficiently large to plausibly provide a pathway for mCDW, which the EN4 and MEOP datasets suggest may exists below approximately 450 m depth (Fig. 4.9), to circulate under the ice shelves and melt the base of the ice shelves, consistent with satellite-derived high basal melt rates (Adusumilli et al., 2020) and ice-shelf thinning (Smith et al., 2020b; Miles and Bingham, 2024) reported elsewhere and likely causing the dynamic changes observed in Porpoise Bay.

The bed topography beneath the outlet glaciers may differentially enhance the impact of ocean forcing in Porpoise Bay. A sufficiently low bed elevation is recorded across the observed grounding line positions at Frost (Fig. 4.8a: below 600 m in 1996 and 900 m in 2014) and Holmes East (Fig. 4.8c: below 800 m in 1996 and 900 m in 2020) for mCDW to plausibly access the grounding line, driving grounding line retreat. Another key detail revealed by the ANTGG2021 dataset is that Holmes West Glacier has been grounded on a bedrock high between 1996 and 2014 (Rignot et al., 2024). The bed seaward of the grounding zone ranges from 600 m to 740 m depth but rises to 500 m to 485 m depth at the grounding zone (Fig. 4.8d). This bathymetry may limit warm mCDW from access the grounding line, which may explain the lower rate of grounding line retreat at Holmes West Glacier, compared to Frost and Holmes East glaciers (Fig. 4.7), whilst also explaining the rapid surface lowering observed (Fig. 4.5d), since Holmes West Glacier may flow into a rapidly thinning ice shelf, potentially caused by basal melting. Furthermore, the bed at Glacier 1 is entirely above 500 m depth, which may limit potential exposure to mCDW at the grounding line, explaining the lack of observed dynamic change at Glacier 1 (Table 4.1).

5.3 Role of Sea Ice in Driving Ice Shelf and Glacier Flow Changes

Variations in sea-ice conditions likely influenced the behaviour of calving events, ice-shelf area and ice flow in Porpoise Bay. The ice shelves underwent near-simultaneous calving events over the study period; observations show calving events in 2006–2008, 2016–2017, and 2021–2022. Recent studies around Antarctica demonstrate that the presence of sea ice and mélange may exert a resistive backstress on the ice-shelf calving front, and calving events have been linked to the removal break-up of sea ice and the removal of mélange

from the ice front (Amundson et al., 2010; Miles et al., 2017; Arthur et al., 2021; Baumhoer et al., 2021; Gomez-Fell et al., 2022; Kondo and Sugiyama, 2023; Parsons et al., 2024). Resultant ice-shelf calving can reduce their buttressing potential (Dupont and Alley, 2005; Fürst et al., 2016), which can trigger dynamic thinning and ice flow acceleration across the glacier further upstream (Reese et al., 2018; Gudmundsson et al., 2019).

The work presented here shows that all three major calving events appear to coincide with lower-than-average winter-spring sea-ice concentrations the preceding year and lower-than-average summer-autumn sea-ice conditions at the beginning of each major calving event (2006–2008, 2016–2017, and 2021–2022) (Fig. 4.13). Furthermore, the monthly sea-ice concentration was anomalously low in March 2007 and March 2021 (Fig. 4.12). This is supported by observations from Landsat-7 and Landsat-8 satellite imagery that shows the break-up and removal of the mélange and sea ice adjacent to Holmes Ice Shelf prior in 2007, 2017 and 2021. Therefore, it is likely that the break-up of sea ice and the removal of iceberg mélange reduced the stabilising backstress on the ice-shelf fronts in Porpoise Bay, culminating in major, near-synchronous calving events. This is consistent with Miles et al. (2017), who attributed the 2007 and 2016 calving events to the break-up of multi-year sea ice and suggested that atmospheric circulation anomalies caused the sea-ice break-up. Abnormally low sea-ice conditions were observed in 2002 (Fig. 4.12), when a calving event from Holmes East Ice Shelf look place(there are no positional record for the other ice shelves due to a lack of cloud-free imagery).

Porpoise Bay's ice shelves advanced and retreated quasi-cyclically, each time advancing to a similar (±1 km) maximum length prior to calving (Fig. 4.1). In a previous study of the ice shelves in Porpoise Bay, Miles et al. (2017) observed Holmes West Ice Shelf calving at the same position in each cycle and found that this took place as the glacier advanced and pushed the sea ice (attached to the ice-shelf calving front) out of the bay towards the open ocean, causing it to disintegrate. It is likely that this mechanism of ice shelves bulldozing the sea ice operated at all four glaciers and was in part facilitated by the winter-spring sea-ice conditions from the preceding years.

The findings suggest that ice-shelf calving in Porpoise Bay, alongside the intermittent loss of stabilising sea ice and mélange, had some corresponding impact on ice flow velocity for the outlet glaciers, suggesting that some of the ice shelves buttressed ice flow. This is consistent with Fürst et al. (2016), who used an ice flow model to calculate that only 18.3 % of the ice-shelf area in Porpoise Bay was passive (i.e., has no dynamical influence on ice discharge), meaning that once calving exceeds this 18.3 % of ice-shelf area, further ice-

shelf calving will have a dynamic impact inland. The most consistent velocity response followed the 2007 calving event (Fig. 4.2), after which Frost, Glacier 1, and Holmes West glaciers displayed an increased velocity response over the following few years (Fig. 4.3). Given that the calving event coincided with low sea-ice conditions (Fig. 4.12 and 4.13), these findings suggest a sea-ice-driven reduction in buttressing force, indicating that the ice shelves calved beyond the passive-ice area (Fürst et al., 2016).

The debuttressing velocity response to the 2016 calving event was more varied, with an increase in velocity observed between 2016 and 2017 at Holmes East and West glaciers (Fig. 4.3c and 16d). Given the ice-shelf retreat was relatively small at Holmes East Glacier, this debuttressing is likely caused by the sea-ice break-up and low sea-ice concentration leading up to the calving, rather than the loss of buttressing ice-shelf area. For Frost Glacier, the onset of flow speed-up coincided with a small calving event in 2013, after which the ice shelf broadly retreated, suggesting that the loss of back-stress exerted by the ice shelf is a potential driver of glacier speed-up. During high sea-ice concentrations between 2017 and 2020 (Fig. 4.13b: summer-autumn mean calculated 10 % above average) and the readvance of the ice shelves (Fig. 4.2), a decrease in ice flow velocity was recorded, with Holmes East and West slowing −32 % and −5 % across the grounding line and −20 % and −28 % across the inland ice (Fig. 4.3). This suggests the glacier flow speeds were reduced by the accumulation of sea ice and ice mélange near the glacier front. Subsequently, between 2020 and 2021, the autumn–winter and winter–spring sea-ice concentration was below average, ice-shelf retreat, and ice flow velocity increase across all sampling boxes in Holmes East and West glaciers, suggesting that the low sea-ice conditions impacted glacier dynamics before the 2021/22 ice-shelf calving event. It is difficult to assess the impact of the 2021/22 calving event on glacier flow dynamics and the impact of sea-ice-driven debuttressing that occurred due to the lack of ice flow velocity data beyond 2022.

In the future, there may be an increase in low sea-ice states that could impact the future ice-shelf stability in Porpoise Bay, as low sea-ice conditions continue to destabilise ice shelves, and drive ice flow velocity increase. The past decade has seen extreme Antarctic-wide sea-ice minima in 2017, 2022, 2023 and 2024, and a sea-ice decline in 2014–2016. Furthermore, even more extreme sea ice minima were observed in 1980s, which were likely associated with calving events. There is a growing concern that there is a structural change taking place in the Antarctic atmosphere-ocean-sea-ice system (Purich and Dodderidge, 2023; Hobbs et al., 2024), revealed by analysis of reconstructed and satellite-observed sea-ice extent that shows increasing persistence in sea-ice extent anomalies, a pattern especially clear in East Antarctica (Raphael et al., 2025).

5.4 Future Unpinning at Holmes West Glacier

The current grounding line position at Holmes West Glacier suggests that this glacier may be vulnerable to MISI in the near future. The grounding line was pinned on a local bedrock high between 1996 and 2014, which possibly inhibited mCDW from accessing the grounding line (Fig. 4.8d). The 2014 grounding line position is at the very edge of a steep retrograde bed and, over the next 2 km inland along the flowline, the bed elevation drops by 650–700 m (Morlighem, 2022, Pritchard et al., 2024). However, the reverse-sloping bed topography is subject to some uncertainty. The BedMachine3 bathymetry suggests the bed is reverse sloping for 3–4 km then stabilises; though, this bathymetry was produced using mass conservation in the absence of radar data (Morlighem et al., 2020). Comparatively, the Bedmap3 reverse slope continues inland for the next 25 km along the Holmes West Glacier flowline; this was extracted from numerous radar flight paths that intersect the trough, albeit sparsely spaced compared to Totten or Moscow University troughs (Pritchard et al., 2025). Regardless, given its current thinning rate of −1.22 m yr^{-1} at the grounding line, Holmes West Glacier will likely unground from the local bedrock high and retreat to become grounded on a bed below 1,000 m depth, where mCDW could reach the grounded ice, exposing it to rapid melting. Given the enhanced ice-shelf basal melting (Adusumilli et al., 2019), thinning across the ice shelf and grounded ice, continued grounding line retreat, and observations suggesting mCDW at depth, future grounding line retreat could theoretically be sufficient to initiate MISI at Holmes West Glacier. This is very concerning given that the Holmes catchment stores 11 cm of SLE (Rignot et al., 2019).

Furthermore, there is an adjacent 4,700 km^2 ice rise directly west along the coastline from Holmes West Glacier (Matsuoka et al., 2015) that may exert a buttressing force on the ice sheet, retarding the flow of grounded ice to the ocean and contributing to grounding line stability (Favier and Pattyn, 2015; Matsuoka et al., 2015). If the current rates of grounding line retreat (−70 m yr^{-1}) continue, Holmes West Glacier could unpin from the bedrock high in the next decade, losing contact with the stabilising ice rise, potentially resulting in threshold-like behaviour (Matsuoka et al., 2015).

Although there was greater grounding line retreat at Holmes East and Frost glaciers, the likelihood of irreversible grounding line retreat or MISI is less concerning given the elevation of the glacier troughs along the flowlines. The bed inland of the Frost Glacier grounding line is relatively flat and the bed is prograding inland of Holmes East Glacier grounding line (Fig. 4.8).

5.5 Limitations and Opportunities for Further Research

Grounding line migration is one of the key parameters that indicate dynamic imbalance in a glacier system. The DLR were able to identify grounding line positions for Holmes East Glacier for 2019 and 2020 using DInSAR. However, the grounding lines at Frost Glacier and Holmes West Glacier from secondary datasets were not verified with DInSAR due to a lack of suitable imagery. Given DInSAR is found to be the most precise and accurate grounding line position mapping technique (Rignot et al., 2014), a renewed attempt at identifying the recent grounding line position of Frost Glacier and Holmes West Glacier using DInSAR is recommended, especially at Holmes West due to the vulnerability of initiating MISI.

The findings suggest dynamic imbalance at Frost, Holmes East, and Holmes West glaciers. As a result, numerical modelling should be used to assess the potential dynamic response of these outlet glaciers to changes in grounding line position, unpinning, and ice-shelf collapse. Modelling these systems will help understand the future sea level contribution from this critical region for mass loss in East Antarctica.

SMB is an aspect of the Porpoise Bay glaciers system that was not examined in this thesis, limiting its coverage. A better understanding of how surface processes contribute to the observed dynamic changes would improve our comprehension of the glacier dynamics and drivers of change in the system.

The scarcity of ocean data in East Antarctica limited the confidence regarding the extent of mCDW intrusion to the sub-ice cavities within Porpoise Bay and the extent to which ocean forcing drives dynamic change. Given there were no observations of ocean temperature from MEOP casts within 130 km of the ice margin, EN4 subsurface ocean temperature objective analysis data was used, which contains substantial uncertainties. It is critical that direct ocean temperature observations across the continental shelf are prioritised to understand the extent of mCDW intrusion in the region.

Lastly, the continental shelf and glacier trough bathymetry is poorly sampled in Porpoise Bay. Although there are radar flight paths across the region, this is one of the most sparsely sampled area of the East Antarctic coastline, particularly given this is a critical region for mass loss in East Antarctica. It is generally understood that rates of grounding line retreat are strongly dependent on the underlying bedrock topography (Millio et al., 2019; Millan et al., 2022), so an improved understanding of the glacier trough structure inland of the grounding line is critical to estimating the vulnerability of Holmes West Glacier to future MISI. Likewise, more detailed observations of the bathymetry across the continental shelf would better show how CDW is transported over the shelf edge across to the glacier

margins. Moreover, better bathymetric data would clarify the existance of troughs under the ice sheet that connect the outlet glaciers in Porpoise Bay to the ASB. This is critically important to improving our understanding of the timescale of future sea level contributions, given that the ASB stores approximately 3.9 m of SLE (Morlighem et al., 2020) and the vulnerability of Holmes West Glacier to MISI.

Chapter 6: Conclusion

To investigate recent glacier dynamics in Porpoise Bay, Wilkes Land, East Antarctica, changes in ice-shelf calving position, ice surface velocity, grounded ice surface elevation, and grounding line position were measured across four outlet glaciers over the last three decades. The observed glacier dynamics were compared to topography, sea-ice conditions, and ocean temperatures and salinity to assess the potential forcing of any observed changes. Despite large uncertainties, the results suggest Frost and Holmes East glaciers have undergone substantial grounding line retreat, with more modest rates of grounding line retreat observed elsewhere in Porpoise Bay. Observations of surface elevation change depict considerable thinning at Frost, Holmes East, and Holmes West glaciers between 2003 and 2019, which propagated inland, with Holmes West Glacier displaying potentially one of the highest rates of thinning in East Antarctica. Furthermore, the outlet glaciers underwent moderate increases in velocity over the study period. Taken together, these findings are consistent with dynamic changes in this region, which agrees with previous work suggesting that it is losing mass and contributing to sea level rise (Rignot et al., 2019; Adusumilli et al., 2020; Smith et al., 2020a; Rignot et al., 2022). In addition, a new, previously unidentified calving event in 2021/22 is reported, alongside near-synchronous ice-shelf calving events in 2007/08 and 2016/17. As in previous work (Miles et al., 2017), the findings show that the calving events were caused by a reduction in sea ice in the preceding winter and summer and the collapse of a supportive mélange.

The findings of dynamic change are consistent with observations of mCDW at the shelf break seaward of Porpoise Bay, with EN4 ocean temperature data suggesting the presence of mCDW at depths below 450 m on the continental shelf. Bathymetric pathways were found beneath Frost, Holmes East and Holmes West glaciers could transport mCDW to the sub-ice cavities, driving high rates of basal melting that have been reported in previous work (Adusumilli et al., 2020). Furthermore, Frost and Holmes East glaciers are grounded sufficiently deep for mCDW to directly access the grounding line. In contrast, Holmes West is grounded on a local bedrock high that could inhibit year-round access of mCDW to the grounded ice, which is also consistent with its relatively low grounding line retreat rate. Of concern is that Holmes West Glacier is currently grounded at the edge of a steep retrograde bed; 2 km of retreat could see the grounding line 700 m deeper, providing access for mCDW to melt the grounded ice, which could initiate rapid and irreversible grounding line retreat down a retrograde bed that continues on a reverse slope for 25 km inland. If MISI is initiated, the retreat could rapidly drain Holmes drainage basin, contributing 11 cm to global sea level.

References

Adusumilli, S., Fricker, H.A., Medley, B., Padman, L. and Siegfried, M.R. (2020). Interannual Variations in Meltwater Input to the Southern Ocean from Antarctic Ice Shelves. *Nature Geoscience*, 13(9), pp.616–620.

Alley, K.E., Scambos, T.A., Siegfried, M.R. and Fricker, H.A. (2016). Impacts of Warm Water on Antarctic Ice Shelf Stability through Basal Channel Formation. *Nature Geoscience*, 9(4), pp.290–293.

Alley, R.B., Anandakrishnan, S., Christianson, K., Horgan, H.J., Muto, A., Parizek, B.R., Pollard, D. and Walker, R.T. (2015). Oceanic Forcing of Ice-Sheet Retreat: West Antarctica and More. *Annual Review of Earth and Planetary Sciences*, 43(1), pp.207–231.

Amblas, D. (2018). *Antarctic continental shelf break (shapefile).* [Data Set] PANGAEA, https://doi.org/10.1594/PANGAEA.890863.

Amundson, J.M., Fahnestock, M., Truffer, M., Brown, J., Lüthi, M.P. and Motyka, R.J. (2010). Ice Mélange Dynamics and Implications for Terminus stability, Jakobshavn Isbræ, Greenland. *Journal of Geophysical Research*, 115(F1).

Arthur, J.F., Stokes, C.R., Jamieson, S.S.R., Miles, B.W.J., Carr, J.R. and Leeson, A.A. (2021). The Triggers of the Disaggregation of Voyeykov Ice Shelf (2007), Wilkes Land, East Antarctica, and Its Subsequent Evolution. *Journal of Glaciology*, 67(265), pp.933–951.

Aschwanden, A., Bartholomaus, T.C., Brinkerhoff, D.J. and Truffer, M. (2021). Brief communication: a Roadmap Towards Credible Projections of Ice Sheet Contribution to Sea Level. *The Cryosphere*, 15(12), pp.5705–5715.

Bamber, J.L., Westaway, R.M., Marzeion, B. and Wouters, B. (2018). The Land Ice Contribution to Sea Level during the Satellite Era. *Environmental Research Letters*, 13(6), p.063008.

Banwell, A.F. and Macayeal, D.R. (2015). Ice-shelf Fracture Due to Viscoelastic Flexure Stress Induced by fill/drain Cycles of Supraglacial Lakes. *Antarctic Science*, 27(6), pp.587–597.

Banwell, A.F., MacAyeal, D.R. and Sergienko, O.V. (2013). Breakup of the Larsen B Ice Shelf Triggered by Chain Reaction Drainage of Supraglacial Lakes. *Geophysical Research Letters*, 40(22), pp.5872–5876.

Banwell, A.F., Willis, I.C., Macdonald, G.J., Goodsell, B. and MacAyeal, D.R. (2019). Direct

Measurements of Ice-Shelf Flexure Caused by Surface Meltwater Ponding and Drainage. *Nature Communications*, 10(1).

Barnett, R.L., Austermann, J., Dyer, B., Telfer, M.W., Barlow, N., Boulton, S.J., Carr, A.S. and Creel, R. (2023). Constraining the Contribution of the Antarctic Ice Sheet to Last Interglacial Sea Level. *Science Advances*, 9(27).

Bassis, J.N. and Walker, C.C. (2012). Upper and Lower Limits on the Stability of Calving Glaciers from the Yield Strength Envelope of Ice. *Proceedings of the Royal Society A: Mathematical, Physical and Engineering Sciences*, 468(2140), pp.913–931.

Baumhoer, C.A., Dietz, A.J., Kneisel, C., Paeth, H. and Kuenzer, C. (2021). Environmental Drivers of circum-Antarctic Glacier and Ice Shelf Front Retreat over the Last Two Decades. *The Cryosphere*, 15(5), pp.2357–2381.

Berthier, E., Scambos, T.A. and Shuman, C.A. (2012). Mass Loss of Larsen B Tributary Glaciers (Antarctic Peninsula) Unabated since 2002. *Geophysical Research Letters*, 39(13), pp.1–6.

Bindschadler, R. and Choi, H. (2011) *High-resolution Image-derived Grounding and Hydrostatic Lines for the Antarctic Ice Sheet*. [Data Set] U.S. Antarctic Program (USAP) Data Center. https://doi.org/10.7265/N56T0JK2

Bindschadler, R., Choi, H., Wichlacz, A., Bingham, R., Bohlander, J., Brunt, K.M., Corr, H., Drews, R., Fricker, H.A., Hall, M., Hindmarsh, R., Kohler, J., Padman, L., Rack, W., Rotschky, G., Urbini, S., Vornberger, P. and Young, N.S. (2011). Getting around Antarctica: New high-resolution Mappings of the Grounded and freely-floating Boundaries of the Antarctic Ice Sheet Created for the International Polar Year. *The Cryosphere*, 5(3), pp.569–588.

Black, T.E. and Joughin, I. (2022). Multi-decadal Retreat of marine-terminating Outlet Glaciers in Northwest and central-west Greenland. *The Cryosphere*, 16(3), pp.807–824.

Bradley, S.L., Siddall, M., Milne, G.A., Masson-Delmotte, V. and Wolff, E. (2012). Where Might We Find Evidence of a Last Interglacial West Antarctic Ice Sheet Collapse in Antarctic Ice Core records? *Global and Planetary Change*, 88-89, pp.64–75.

Brancato, V., Rignot, E., Milillo, P., Morlighem, M., Mouginot, J., An, L., Scheuchl, B., Jeong, S., Rizzoli, P., Bueso Bello, J.L. and Prats-Iraola, P. (2020). Grounding Line Retreat of Denman Glacier, East Antarctica, Measured with COSMO-SkyMed Radar Interferometry Data. *Geophysical Research Letters*, 47(7).

Brooks, R.L., Campbell, W.J., Ramseier, R.O., Stanley, H.R., Zwally, H.J. (1978). Ice sheet

topography by satellite altimetry. *Nature,* 274, pp.539–543.

Cavalieri, D.J., St. Germain, K.M. and Swift, C.T. (1995). Reduction of Weather Effects in the Calculation of sea-ice Concentration with the DMSP SSM/I. *Journal of Glaciology*, 41(139), pp.455–464.

Charrassin, R., Millan, R., Rignot, E. and Scheinert, M. (2025). Bathymetry of the Antarctic Continental Shelf and Ice Shelf Cavities from Circumpolar Gravity Anomalies and Other Data. *Scientific Reports*, 15(1).

Chen, J.L., Wilson, C.R., Blankenship, D. and Tapley, B.D. (2009). Accelerated Antarctic Ice Loss from Satellite Gravity Measurements. *Nature Geoscience*, 2(12), pp.859–862.

Cheng, Y., Xia, M., Qiao, G., Li, Y., Hai, G. and Die Lv (2021). Calving Cycle of Ninnis Glacier over the Last 60 Years. *International journal of applied earth observation and geoinformation*, 105, pp.102612–102612.

Christianson, K., Bushuk, M., Dutrieux, P., Parizek, B.R., Joughin, I.R., Alley, R.B., Shean, D.E., Abrahamsen, E.P., Anandakrishnan, S., Heywood, K.J., Kim, T.-W., Lee, S.H., Nicholls, K., Stanton, T., Truffer, M., Webber, B.G.M., Jenkins, A., Jacobs, S., Bindschadler, R. and Holland, D.M. (2016). Sensitivity of Pine Island Glacier to Observed Ocean Forcing. *Geophysical Research Letters*, 43(20), pp.10, 817–10, 825.

Cook, C.P., van de Flierdt, T., Williams, T., Hemming, S.R., Iwai, M., Kobayashi, M., Jimenez-Espejo, F.J., Escutia, C., González, J.J., Khim, B.-K., McKay, R.M., Passchier, S., Bohaty, S.M., Riesselman, C.R., Tauxe, L., Sugisaki, S., Lopez Galindo, A., Patterson, M.O., Sangiorgi, F., Pierce, E.L., Brinkhuis, H., Klaus, A., Fehr, A., Bendle, J.A.P., Bijl, P.K., Carr, S.A., Dunbar, R.B., Flores, J.A., Hayden, T.G., Katsuki, K., Kong, G.S., Nakai, M., Olney, M.P., Pekar, S.F., Pross, J., Röhl, U., Sakai, T., Shrivastava, P.K., Stickley, C.E., Tuo, S., Welsh, K., and Yamane, M. (2013). Dynamic Behaviour of the East Antarctic Ice Sheet during Pliocene Warmth. *Nature Geoscience*, 6(9), pp.765–769.

Cook, A.J., Vaughan, D.G., Luckman, A.J. and Murray, T. (2014). A New Antarctic Peninsula Glacier Basin Inventory and Observed Area Changes since the 1940s. *Antarctic Science*, 26(6), pp.614–624.

Cook, A.J., Holland, P.R., Meredith, M.P., Murray, T., Luckman, A. and Vaughan, D.G. (2016). Ocean Forcing of Glacier Retreat in the Western Antarctic Peninsula. *Science*, 353(6296), pp.283–286.

DeConto, R.M. and Pollard, D. (2016). Contribution of Antarctica to past and Future sea-

level Rise. *Nature*, 531(7596), pp.591–597.

DeConto, R.M., Pollard, D., Alley, R.B., Velicogna, I., Gasson, E., Gomez, N., Sadai, S., Condron, A., Gilford, D.M., Ashe, E.L., Kopp, R.E., Li, D. and Dutton, A. (2021). The Paris Climate Agreement and Future sea-level Rise from Antarctica. *Nature*, 593(7857), pp.83–89.

Depoorter, M.A., Bamber, J.L., Griggs, J.A., Lenaerts, J.T.M., Ligtenberg, S.R.M., van den Broeke, M.R. and Moholdt, G. (2013). Calving Fluxes and Basal Melt Rates of Antarctic Ice Shelves. *Nature*, 502(7469), pp.89–92.

Dorschel, B., Hehemann, L., Viquerat, S., Warnke, F., Dreutter, S., Schulze Tenberge, Y., Accettella, D., An, L., Barrios, F., Bazhenova, E., Black, J., Bohoyo, F., Davey, C., De Santis, L., Escutia Dotti, C., Fremand, A.C., Fretwell, P.T., Gales, J.A., Gao, J., Gasperini, L., Greenbaum, J.S., Jencks, J.H., Hogan, K., Hong, J.K., Jakobsson, M., Jensen, L., Kool, J., Larin, S., Larter, R.D., Leitchenkov, G., Loubrieu, B., Mackay, K., Mayer, L., Millan, R., Morlighem, M., Navidad, F., Nitsche, F.O., Nogi, Y., Pertuisot, C., Post, A.L., Pritchard, H.D., Purser, A., Rebesco, M., Rignot, E., Roberts, J.L., Rovere, M., Ryzhov, I., Sauli, C., Schmitt, T., Silvano, A., Smith, J., Snaith, H., Tate, A.J., Tinto, K., Vandenbossche, P., Weatherall, P., Wintersteller, P., Yang, C., Zhang, T., and Arndt, J.E. (2022). The International Bathymetric Chart of the Southern Ocean Version 2. *Scientific Data*, 9(1).

Dow, C.F., Sang Lee, W., Greenbaum, J.S., Greene, C.A., Blankenship, D.D., Poinar, K., Forrest, A.L., Young, D. and Zappa, C.J. (2018). Basal channels drive active surface hydrology and transverse ice shelf fracture. *Science Advances*, 4(6).

Dupont, T.K. and Alley, R.B. (2005). Assessment of the Importance of Ice-Shelf Buttressing to Ice-Sheet Flow. *Geophysical Research Letters*, 32(4).

Durand, G., Gagliardini, O., de Fleurian, B., Zwinger, T. and Le Meur, E. (2009). Marine Ice Sheet dynamics: Hysteresis and Neutral Equilibrium. *Journal of Geophysical Research*, 114(F3).

Dutrieux, P., De Rydt, J., Jenkins, A., Holland, P.R., Ha, H.K., Lee, S.H., Steig, E.J., Ding, Q., Abrahamsen, E.P. and Schroder, M. (2014). Strong Sensitivity of Pine Island Ice-Shelf Melting to Climatic Variability. *Science*, 343(6167), pp.174–178.

Dutton, A., Carlson, A.E., Long, A.J., Milne, G.A., Clark, P.U., DeConto, R., Horton, B.P., Rahmstorf, S. and Raymo, M.E. (2015a). Sea-level Rise Due to Polar Ice-Sheet Mass Loss during past Warm Periods. *Science*, 349(6244).

Dutton, A., Webster, J.M., Zwartz, D., Lambeck, K. and Wohlfarth, B. (2015b). Tropical Tales

of Polar Ice: Evidence of Last Interglacial Polar Ice Sheet Retreat Recorded by Fossil Reefs of the Granitic Seychelles Islands. *Quaternary Science Reviews*, 107, pp.182–196.

Edwards, T.L., Nowicki, S., Marzeion, B., Hock, R., Goelzer, H., Seroussi, H., Jourdain, N.C., Slater, D.A., Turner, F.E., Smith, C.J., McKenna, C.M., Simon, E., Abe-Ouchi, A., Gregory, J.M., Larour, E., Lipscomb, W.H., Payne, A.J., Shepherd, A., Agosta, C., Alexander, P., Albrecht, T., Anderson, B., Asay-Davis, X., Aschwanden, A., Barthel, A., Bliss, A., Calov, R., Chambers, C., Champollion, N., Choi, Y., Cullather, R., Cuzzone, J., Dumas, C., Felikson, D., Fettweis, X., Fujita, K., Galton-Fenzi, B.K., Gladstone, R., Golledge, N.R., Greve, R., Hattermann, T., Hoffman, M.J., Humbert, A., Huss, M., Huybrechts, P., Immerzeel, W., Kleiner, T., Kraaijenbrink, P., Le clec'h, S., Lee, V., Leguy, G.R., Little, C.M., Lowry, D.P., Malles, J.-H., Martin, D.F., Maussion, F., Morlighem, M., O'Neill, J.F., Nias, I., Pattyn, F., Pelle, T., Price, S.F., Quiquet, A., Radić, V., Reese, R., Rounce, D.R., Rückamp, M., Sakai, A., Shafer, C., Schlegel, N.-J., Shannon, S., Smith, R.S., Straneo, F., Sun, S., Tarasov, L., Trusel, L.D., Van Breedam, J., van de Wal, R., van den Broeke, M., Winkelmann, R., Zekollari, H., Zhao, C., Zhang, T., and Zwinger, T. (2021). Projected Land Ice Contributions to twenty-first-century Sea Level Rise. *Nature*, 593(7857), pp.74–82.

Favier, L. and Pattyn, F. (2015). Antarctic Ice Rise formation, evolution, and Stability. *Geophysical Research Letters*, 42(11), pp.4456–4463.

Feldmann, J. and Levermann, A. (2015). Collapse of the West Antarctic Ice Sheet after Local Destabilization of the Amundsen Basin. *Proceedings of the National Academy of Sciences*, 112(46), pp.14191–14196.

Fetterer, F., Knowles, K., Meier, W. N., Savoie, M. and Windnagel, A. K. (2017). *Sea Ice Index*. [Data Set]. Boulder, Colorado USA. National Snow and Ice Data Center. https://doi.org/10.7265/N5K072F8.

Flament, T. and Rémy, F. (2012). Dynamic Thinning of Antarctic Glaciers from Along-track Repeat Radar Altimetry. *Journal of Glaciology*, 58(211), pp.830–840.

Fogt, R.L. and Bromwich, D.H. (2006). Decadal Variability of the ENSO Teleconnection to the High-Latitude South Pacific Governed by Coupling with the Southern Annular Mode. *Journal of Climate*, 19(6), pp.979–997.

Fogt, R.L. and Marshall, G.J. (2020). The Southern Annular Mode: Variability, trends, and Climate Impacts across the Southern Hemisphere. *WIREs Climate Change*, 11(4).

Fox-Kemper, B., H.T. Hewitt, C. Xiao, G. Aðalgeirsdóttir, S.S. Drijfhout, T.L. Edwards, N.R.

Golledge, M. Hemer, R.E. Kopp, G. Krinner, A. Mix, D. Notz, S. Nowicki, I.S. Nurhati, L. Ruiz, J.-B. Sallée, A.B.A. Slangen, and Y. Yu. (2021) Ocean, Cryosphere and Sea Level Change. In *Climate Change 2021: The Physical Science Basis. Contribution of Working Group I to the Sixth Assessment Report of the Intergovernmental Panel on Climate Change.* Cambridge: Cambridge University Press, pp. 1211–1362,

Fürst, J.J., Durand, G., Gillet-Chaulet, F., Tavard, L., Rankl, M., Braun, M. and Gagliardini, O. (2016). The Safety Band of Antarctic Ice Shelves. *Nature Climate Change*, 6(5), pp.479–482.

Gardner, A. S., Fahnestock, M. and Scambos, T. (2025). *MEaSUREs ITS_LIVE Regional Glacier and Ice Sheet Surface Velocities*. (NSIDC-0776, Version 1). [Data Set]. Boulder, Colorado USA. NASA National Snow and Ice Data Center Distributed Active Archive Center. https://doi.org/10.5067/6II6VW8LLWJ7.

Gardner, A.S., Moholdt, G., Scambos, T., Fahnstock, M., Ligtenberg, S., van den Broeke, M. and Nilsson, J. (2018). Increased West Antarctic and Unchanged East Antarctic Ice Discharge over the Last 7 Years. *The Cryosphere*, 12(2), pp.521–547.

Gasson, E. and Keisling, B. (2020). The Antarctic Ice Sheet: A Paleoclimate Modeling Perspective. *Oceanography*, 33(2).

Gasson, E., DeConto, R.M., Pollard, D. and Levy, R.H. (2016). Dynamic Antarctic Ice Sheet during the Early to mid-Miocene. *Proceedings of the National Academy of Sciences*, 113(13), pp.3459–3464.

Glasser, N.F. and Scambos, T.A. (2008). A Structural Glaciological Analysis of the 2002 Larsen B ice-shelf Collapse. *Journal of Glaciology*, 54(184), pp.3–16.

Glasser, N.F., Scambos, T.A., Bohlander, J., Truffer, M., Pettit, E. and Davies, B.J. (2011). From Ice-Shelf Tributary to Tidewater Glacier: Continued Rapid Recession, Acceleration and Thinning of Röhss Glacier following the 1995 Collapse of the Prince Gustav Ice Shelf, Antarctic Peninsula. *Journal of Glaciology*, 57(203), pp.397–406.

Golledge, N.R., Kowalewski, D.E., Naish, T.R., Levy, R.H., Fogwill, C.J. and Gasson, E.G.W. (2015). The Multi-Millennial Antarctic Commitment to Future Sea-Level Rise. *Nature*, 526(7573), pp.421–425.

Gomez-Fell, R., Rack, W., Purdie, H. and Marsh, O. (2022). Parker Ice Tongue Collapse, Antarctica, Triggered by Loss of Stabilizing Land-Fast Sea Ice. *Geophysical Research Letters*, 49(1).

Good, S.A., Martin, M.J. and Rayner, N.A. (2013). EN4: Quality Controlled Ocean Temperature and Salinity Profiles and Monthly Objective Analyses with Uncertainty

Estimates. *Journal of Geophysical Research: Oceans*, 118(12), pp.6704–6716.

Grant, G.R., Naish, T.R., Dunbar, G.B., Stocchi, P., Kominz, M.A., Kamp, P.J.J., Tapia, C.A., McKay, R.M., Levy, R.H. and Patterson, M.O. (2019). The Amplitude and Origin of sea-level Variability during the Pliocene Epoch. *Nature*, 574(7777), pp.237–241.

Greenbaum, J.S., Blankenship, D.D., Young, D.A., Richter, T.G., Roberts, J.L., Aitken, A.R.A., Legresy, B., Schroeder, D.M., Warner, R.C., van Ommen, T.D. and Siegert, M.J. (2015). Ocean Access to a Cavity beneath Totten Glacier in East Antarctica. *Nature Geoscience*, 8(4), pp.294–298.

Greene, C.A., Gardner, A.S., Schlegel, N.-J. and Fraser, A.D. (2022). Antarctic Calving Loss Rivals Ice-Shelf Thinning. *Nature*, 609(7929), pp.948–953.

Gudmundsson, G.H., Paolo, F.S., Adusumilli, S. and Fricker, H.A. (2019). Instantaneous Antarctic Ice Sheet Mass Loss Driven by Thinning Ice Shelves. *Geophysical Research Letters*, 46(23), pp.13903–13909.

Gulick, S.P.S., Shevenell, A.E., Montelli, A., Fernandez, R., Smith, C., Warny, S., Bohaty, S.M., Sjunneskog, C., Leventer, A., Frederick, B. and Blankenship, D.D. (2017). Initiation and Long-Term Instability of the East Antarctic Ice Sheet. *Nature*, 552(7684), pp.225–229.

Gwyther, D.E., O'Kane, T.J., Galton-Fenzi, B.K., Monselesan, D.P. and Greenbaum, J.S. (2018). Intrinsic Processes Drive Variability in Basal Melting of the Totten Glacier Ice Shelf. *Nature Communications*, 9(1).

Hansen, N., Langen, P.L., Boberg, F., Forsberg, R., Simonsen, S.B., Thejll, P., Vandecrux, B. and Mottram, R. (2021). Downscaled Surface Mass Balance in Antarctica: Impacts of Subsurface Processes and large-scale Atmospheric Circulation. *The Cryosphere*, 15(9), pp.4315–4333.

Haran, T., Bohlander, J., Scambos, T., Painter, T. and Fahnestock, M. (2021a). *MODIS Mosaic of Antarctica 2003-2004 (MOA2004) Image Map*. (NSIDC-0280, Version 2). [Data Set]. Boulder, Colorado USA. NASA National Snow and Ice Data Center Distributed Active Archive Center. https://doi.org/10.5067/68TBT0CGJSOJ.

Haran, T., Bohlander, J., Scambos, T., Painter, T. and Fahnestock, M. (2021b). *MODIS Mosaic of Antarctica 2008-2009 (MOA2009) Image Map*. (NSIDC-0593, Version 2). [Data Set]. Boulder, Colorado USA. NASA National Snow and Ice Data Center Distributed Active Archive Center. https://doi.org/10.5067/4ZL43A4619AF.

Haran, T., Klinger, M., Bohlander, J., Fahnestock, M., Painter, T. and Scambos, T. (2018). *MEaSUREs MODIS Mosaic of Antarctica 2013-2014 (MOA2014) Image Map*.

(NSIDC-0730, Version 1). [Data Set]. Boulder, Colorado USA. NASA National Snow and Ice Data Center Distributed Active Archive Center. https://doi.org/10.5067/RNF17BP824UM.

Harig, C. and Simons, F.J. (2015). Accelerated West Antarctic Ice Mass Loss Continues to Outpace East Antarctic Gains. *Earth and Planetary Science Letters*, 415, pp.134–141.

Haywood, A.M., Dowsett, H.J. and Dolan, A.M. (2016). Integrating Geological Archives and Climate Models for the mid-Pliocene Warm Period. *Nature Communications*, 7(1), p.10646.

Herraiz-Borreguero, L. and Naveira Garabato, A.C. (2022). Poleward Shift of Circumpolar Deep Water Threatens the East Antarctic Ice Sheet. *Nature Climate Change*, 12, pp.728–734.

Hirano, D., Tamura, T., Kusahara, K., Fujii, M., Yamazaki, K., Nakayama, Y., Ono, K., Itaki, T., Aoyama, Y., Simizu, D., Mizobata, K., Ohshima, K.I., Nogi, Y., Rintoul, S.R., van Wijk, E., Greenbaum, J.S., Blankenship, D.D., Saito, K. and Aoki, S. (2023). On-Shelf Circulation of Warm Water toward the Totten Ice Shelf in East Antarctica. *Nature Communications*, 14(1).

Hobbs, W., Spence, P., Meyer, A., Schroeter, S., Fraser, A.D., Reid, P., Tian, T.R., Wang, Z., Liniger, G., Doddridge, E.W. and Boyd, P.W. (2024). Observational Evidence for a Regime Shift in Summer Antarctic Sea Ice. *Journal of Climate*, 37.

Holt, T. O., Glasser, N. F., Quincey, D. J., and Siegfried, M. R. (2013). Speedup and fracturing of George VI Ice Shelf, Antarctic Peninsula. *The Cryosphere*, 7, pp.797–816.

Howat, I., Porter, C., Noh, M.-J., Husby, E., Khuvis, S., Danish, E., Tomko, K., Gardiner, J., Negrete, A., Yadav, B., Klassen, J., Kelleher, C., Cloutier, M., Bakker, J., Enos, J., Arnold, G., Bauer, G. and Morin, P. (2022). *The Reference Elevation Model of Antarctica - Mosaics, Version 2*. [Data Set] Harvard Dataverse. https://doi.org/10.7910/dvn/x7ndny.

Howat, I.M., Porter, C., Smith, B.E., Noh, M.-J. and Morin, P. (2019). The Reference Elevation Model of Antarctica. *The Cryosphere*, 13(2), pp.665–674.

Hulbe, C.L., Scambos, T.A., Youngberg, T. and Lamb, A.K. (2008). Patterns of Glacier Response to Disintegration of the Larsen B Ice shelf, Antarctic Peninsula. *Global and Planetary Change*, 63(1), pp.1–8.

Joughin, I. and Alley, R.B. (2011). Stability of the West Antarctic Ice Sheet in a Warming World. *Nature Geoscience*, 4(8), pp.506–513.

Joughin, I., Smith, B.E. and Medley, B. (2014). Marine Ice Sheet Collapse Potentially Under Way for the Thwaites Glacier Basin, West Antarctica. *Science*, 344(6185), pp.735–738.

Kim, K., Jezek, K.C. and Liu, H. (2007). Orthorectified Image Mosaic of Antarctica from 1963 Argon Satellite photography: Image Processing and Glaciological Applications. *International Journal of Remote Sensing*, 28(23), pp.5357–5373.

King, M.A., Lyu, K. and Zhang, X. (2023). Climate Variability a Key Driver of Recent Antarctic ice-mass Change. *Nature Geoscience*, 16(12), pp.1128–1135.

Kondo, K. and Sugiyama, S. (2023). Calving, Ice flow, and Thickness of Outlet Glaciers Controlled by land-fast Sea Ice in Lützow-Holm Bay, East Antarctica. *Journal of Glaciology*, 69(278), pp.1–13.

Konrad, H., Shepherd, A., Gilbert, L., Hogg, A.E., McMillan, M., Muir, A. and Slater, T. (2018). Net Retreat of Antarctic Glacier Grounding Lines. *Nature Geoscience*, 11(4), pp.258–262.

Lau, S., Wilson, N.G., Golledge, N.R., Naish, T., Watts, P.C., Silva, C., Cooke, I., Allcock, A.L., Mark, F.C., Linse, K. and Strugnell, J.M. (2023). Genomic Evidence for West Antarctic Ice Sheet Collapse During the Last Interglacial. *Science*, 382(6677), pp.1384–1389.

Lea, J.M. (2018). The Google Earth Engine Digitisation Tool (GEEDiT) and the Margin Change Quantification Tool (MaQiT) – Simple Tools for the Rapid Mapping and Quantification of Changing Earth Surface Margins. *Earth Surface Dynamics*, 6(3), pp.551–561.

Leeson, A.A., Forster, E., Rice, A., Gourmelen, N. and Wessem, J.M. (2020). Evolution of Supraglacial Lakes on the Larsen B Ice Shelf in the Decades before It Collapsed. *Geophysical Research Letters*, 47(4).

Levy, R., Harwood, D., Florindo, F., Sangiorgi, F., Tripati, R., von Eynatten, H., Gasson, E., Kuhn, G., Tripati, A., DeConto, R., Fielding, C., Field, B., Golledge, N., McKay, R., Naish, T., Olney, M., Pollard, D., Schouten, S., Talarico, F., Warny, S., Willmott, V., Acton, G., Panter, K., Paulsen, T., Taviani, M., and SMS Science Team (2016). Antarctic Ice Sheet Sensitivity to Atmospheric CO2 Variations in the Early to mid-Miocene. *Proceedings of the National Academy of Sciences*, 113(13), pp.3453–3458.

Lewis, A.R., Marchant, D.R., Ashworth, A.C., Hedenäs, L., Hemming, S.R., Johnson, J.V., Leng, M.J., Machlus, M.L., Newton, A.E., Raine, J.I., Willenbring, J.K., Williams, M. and Wolfe, A.P. (2008). Mid-Miocene Cooling and the Extinction of Tundra in

Continental Antarctica. *Proceedings of the National Academy of Sciences*, 105(31), pp.10676–10680.

Lhermitte, S., Sun, S., Shuman, C., Wouters, B., Pattyn, F., Wuite, J., Berthier, E. and Nagler, T. (2020). Damage Accelerates Ice Shelf Instability and Mass Loss in Amundsen Sea Embayment. *Proceedings of the National Academy of Sciences*, 117(40), pp.24735–24741.

Li, T., Dawson, G.J., Chuter, S.J. and Bamber, J.L. (2023). Grounding Line Retreat and tide-modulated Ocean Channels at Moscow University and Totten Glacier Ice shelves, East Antarctica. *The Cryosphere*, 17(2), pp.1003–1022.

Li, X., Rignot, E., Mouginot, J. and Scheuchl, B. (2016). Ice Flow Dynamics and Mass Loss of Totten Glacier, East Antarctica, from 1989 to 2015. *Geophysical Research Letters*, 43(12), pp.6366–6373.

Lowry, D.P., Krapp, M., Golledge, N.R. and Alevropoulos-Borrill, A. (2021). The Influence of Emissions Scenarios on Future Antarctic Ice Loss Is Unlikely to Emerge This Century. *Communications Earth & Environment*, 2(1), pp.1–14.

Luthcke, S.B., Sabaka, T.J., Loomis, B.D., Arendt, A., McCarthy, J. and Camp, J. (2013). Antarctica, Greenland and Gulf of Alaska Land-Ice Evolution from an Iterated GRACE Global Mascon Solution. *Journal of Glaciology*, 59(216), pp.613–631.

Marshall, G.J., Thompson, D.W.J. and van den Broeke, M.R. (2017). The Signature of Southern Hemisphere Atmospheric Circulation Patterns in Antarctic Precipitation. *Geophysical Research Letters*, 44(22), pp.11580–11589.

Massom, R.A., Giles, A.B., Warner, R., Fricker, H.A., Legresy, B., Hyland, G., Lescarmontier, L. and Young, N.W. (2015). External Influences on the Mertz Glacier Tongue (East Antarctica) in the Decade Leading up to Its Calving in 2010. *Journal Of Geophysical Research: Earth Surface*, 120(3), pp.490–506.

Massom, R.A., Scambos, T.A., Bennetts, L.G., Reid, P., Squire, V.A. and Stammerjohn, S.E. (2018). Antarctic Ice Shelf Disintegration Triggered by Sea Ice Loss and Ocean Swell. *Nature*, 558(7710), pp.383–389.

Matsuoka, K., Hindmarsh, R., Moholdt, G., Bentley, M.J., Pritchard, H.D., Brown, J.S., Conway, H., Drews, R., Durand, G., Goldberg, D.E., Hattermann, T., Kingslake, J., Lenaerts, J., Martin, C., Mulvaney, R., Nicholls, K.W., Pattyn, F., Ross, N., Scambos, T. and Whitehouse, P.L. (2015). Antarctic Ice Rises and rumples: Their Properties and Significance for ice-sheet Dynamics and Evolution. *Earth-Science Reviews*, 150, pp.724–745.

McMahon, C.R., Hindell, M.A., Charrassin, J.B., Coleman, R., Guinet, Christophe., Harcourt, R., Labrousse, S., Raymond, B., Sumner, M. and Ribeiro, N. (2023). Southern Ocean Pinnipeds Provide Bathymetric Insights on the East Antarctic Continental Shelf. *Communications Earth & Environment*, 4(1).

McMillan, M., Shepherd, A., Sundal, A., Briggs, K., Muir, A., Ridout, A., Hogg, A. and Wingham, D. (2015). Increased Ice Losses from Antarctica Detected by CryoSat-2. *Geophysical Research Letters*, 41(11), pp.3899–3905.

Medley, B. and Thomas, E.R. (2019). Increased Snowfall over the Antarctic Ice Sheet Mitigated Twentieth-century Sea-level Rise. *Nature Climate Change*, 9(1), pp.34–39.

Medley, B., Joughin, I., Smith, B.E., Das, S.B., Steig, E.J., Conway, H., Gogineni, S., Lewis, C., Criscitiello, A.S., McConnell, J.R., van den Broeke, M.R., Lenaerts, J.T.M., Bromwich, D.H., Nicolas, J.P. and Leuschen, C. (2014). Constraining the Recent Mass Balance of Pine Island and Thwaites glaciers, West Antarctica, with Airborne Observations of Snow Accumulation. *The Cryosphere*, 8(4), pp.1375–1392.

Mercer, J.H. (1978). West Antarctic Ice Sheet and CO2 Greenhouse effect: a Threat of Disaster. *Nature*, 271(5643), pp.321–325.

Miles, B.W.J. and Bingham, R.G. (2023) *Landsat mosaics of Antarctic Ice Shelves from 1973 and 1989.* [Data Set] Edinburgh DataShare. http://doi/org/10.7488/ds/3810

Miles, B.W.J. and Bingham, R.G. (2024). Progressive Unanchoring of Antarctic Ice Shelves since 1973. *Nature*, 626(8000), pp.785–791.

Miles, B.W.J., Stokes, C.R. and Jamieson, S.S.R. (2016). Pan–ice-sheet Glacier Terminus Change in East Antarctica Reveals Sensitivity of Wilkes Land to sea-ice Changes. *Science Advances*, 2(5), p.e1501350.

Miles, B.W.J., Stokes, C.R. and Jamieson, S.S.R. (2017). Simultaneous Disintegration of Outlet Glaciers in Porpoise Bay (Wilkes Land), East Antarctica, Driven by Sea Ice Break-Up. *The Cryosphere*, 11(1), pp.427–442.

Miles, B.W.J., Stokes, C.R. and Jamieson, S.S.R. (2018). Velocity Increases at Cook Glacier, East Antarctica, Linked to Ice Shelf Loss and a Subglacial Flood Event. *The Cryosphere*, 12(10), pp.3123–3136.

Miles, B.W.J., Stokes, C.R., Jenkins, A., Jordan, J.R., Jamieson, S.S.R. and Gudmundsson, G.H. (2020). Intermittent Structural Weakening and Acceleration of the Thwaites Glacier Tongue between 2000 and 2018. *Journal of Glaciology*, 66(257), pp.485–495.

Miles, B.W.J., Jordan, J.R., Stokes, C.R., Jamieson, S.S.R., Gudmundsson, G.H. and Jenkins, A. (2021). Recent Acceleration of Denman Glacier (1972–2017), East

Antarctica, Driven by Grounding Line Retreat and Changes in Ice Tongue Configuration. *The Cryosphere*, 15(2), pp.663–676.

Miles, B.W.J., Stokes, C.R., Jamieson, S.S.R., Jordan, J.R., Gudmundsson, G.H. and Jenkins, A. (2022). High Spatial and Temporal Variability in Antarctic Ice Discharge Linked to Ice Shelf Buttressing and Bed Geometry. *Scientific Reports*, 12(1).

Milillo, P., Rignot, E., Rizzoli, P., Scheuchl, B., Mouginot, J., Bueso-Bello, J. and Prats-Iraola, P. (2019). Heterogeneous Retreat and Ice Melt of Thwaites Glacier, West Antarctica. *Science Advances*, 5(1).

Millan, R., Mouginot, J., Derkacheva, A., Rignot, E., Milillo, P., Ciraci, E., Dini, L. and Bjørk, A. (2022). Ongoing Grounding Line Retreat and Fracturing Initiated at the Petermann Glacier Ice shelf, Greenland, after 2016. *The Cryosphere*, 16(7), pp.3021–3031.

Mohajerani, Y., Velicogna, I. and Rignot, E. (2018). Mass Loss of Totten and Moscow University Glaciers, East Antarctica, Using Regionally Optimized GRACE Mascons. *Geophysical Research Letters*, 45(14), pp.7010–7018.

Moon, T. and Joughin, I. (2008). Changes in ice front position on Greenland's outlet glaciers from 1992 to 2007. *Journal of Geophysical Research*, 113(F02022).

Morlighem, M. (2022). *MEaSUREs BedMachine Antarctica*. (NSIDC-0756, Version 3). [Data Set]. Boulder, Colorado USA. NASA National Snow and Ice Data Center Distributed Active Archive Center. https://doi.org/10.5067/FPSU0V1MWUB6.

Morlighem, M., Goldberg, D., Barnes, J.M., Bassis, J.N., Benn, D.I., Crawford, A.J., Gudmundsson, G.H. and Seroussi, H. (2024). The West Antarctic Ice Sheet May Not Be Vulnerable to Marine Ice Cliff Instability during the 21st Century. *Science Advances*, 10(34).

Morlighem, M., Rignot, E., Binder, T., Blankenship, D., Drews, R., Eagles, G., Eisen, O., Ferraccioli, F., Forsberg, R., Fretwell, P., Goel, V., Greenbaum, J. S., Gudmundsson, H., Guo, J., Helm, V., Hofstede, C., Howat, I., Humbert, A., Jokat, W., Karlsson, N. B., Lee, W. S., Matsuoka, K., Millan, R., Mouginot, J., Paden, J., Pattyn, F., Roberts, J., Rosier, S., Ruppel, A., Seroussi, H., Smith, E. C., Steinhage, D., Sun, B., Broeke, M. R. van den, Ommen, T. D., van Wessem, M., and Young, D. A. (2020). Deep Glacial Troughs and Stabilizing Ridges Unveiled beneath the Margins of the Antarctic Ice Sheet. *Nature Geoscience*, 13.

Mottram, R., van den Broeke, M., Meijers, A., Rodehacke, C., Dell, R.L., Hogg, A.E., Davison, B.J., Lhermitte, S., Hansen, N., Torres Alavez, J.A. and Olesen, M. (2024). Determining the Freshwater Fluxes from Antarctica with Earth Observation Data,

Models, and In Situ Measurements: Uncertainties, Knowledge Gaps, and Prospects for New Advances. *Bulletin of the American Meteorological Society*, 105(7), pp.1371–1379.

Mouginot, J., Rignot, E. and Scheuchl, B. (2014). Sustained Increase in Ice Discharge from the Amundsen Sea Embayment, West Antarctica, from 1973 to 2013. *Geophysical Research Letters*, 41(5), pp.1576–1584.

Naish, T.R., Woolfe, K.J., Barrett, P.J., Wilson, G.S., Atkins, C., Bohaty, S.M., Bücker, C.J., Claps, M., Davey, F.J., Dunbar, G.B., Dunn, A.G., Fielding, C.R., Florindo, F., Hannah, M.J., Harwood, D.M., Henrys, S.A., Krissek, L.A., Lavelle, M., van der Meer, J. McIntosh, W.C., Niessen, F., Passchier, S., Powell, R.D., Roberts, A.P., Sagnotti, L., Scherer, R.P., Strong, C.P., Talarico, F., Verosub, K.L., Villa, G., Watkins, D.K., Webb, Peter-N. and Wonik, T. (2001). Orbitally Induced Oscillations in the East Antarctic Ice Sheet at the Oligocene/Miocene Boundary. *Nature*, 413(6857), pp.719–723.

Naughten, K.A., Holland, P.R. and De Rydt, J. (2023). Unavoidable Future Increase in West Antarctic ice-shelf Melting over the twenty-first Century. *Nature Climate Change*, 13(1), pp.1–7.

Nilsson, J., Gardner, A. S. and Paolo, F. (2023). *MEaSUREs ITS_LIVE Antarctic Grounded Ice Sheet Elevation Change*. (NSIDC-0782, Version 1). [Data Set]. Boulder, Colorado USA. NASA National Snow and Ice Data Center Distributed Active Archive Center. https://doi.org/10.5067/L3LSVDZS15ZV.

Nilsson, J., Gardner, A.S. and Paolo, F.S. (2022). Elevation Change of the Antarctic Ice Sheet: 1985 to 2020. *Earth System Science Data*, 14(8), pp.3573–3598.

Otosaka, I. N., Shepherd, A., Ivins, E. R., Schlegel, N.-J., Amory, C., van den Broeke, M. R., Horwath, M., Joughin, I., King, M. D., Krinner, G., Nowicki, S., Payne, A. J., Rignot, E., Scambos, T., Simon, K. M., Smith, B. E., Sørensen, L. S., Velicogna, I., Whitehouse, P. L., A, G., Agosta, C., Ahlstrøm, A. P., Blazquez, A., Colgan, W., Engdahl, M. E., Fettweis, X., Forsberg, R., Gallée, H., Gardner, A., Gilbert, L., Gourmelen, N., Groh, A., Gunter, B. C., Harig, C., Helm, V., Khan, S. A., Kittel, C., Konrad, H., Langen, P. L., Lecavalier, B. S., Liang, C.-C., Loomis, B. D., McMillan, M., Melini, D., Mernild, S. H., Mottram, R., Mouginot, J., Nilsson, J., Noël, B., Pattle, M. E., Peltier, W. R., Pie, N., Roca, M., Sasgen, I., Save, H. V., Seo, K.-W., Scheuchl, B., Schrama, E. J. O., Schröder, L., Simonsen, S. B., Slater, T., Spada, G., Sutterley, T. C., Vishwakarma, B. D., van Wessem, J. M., Wiese, D., van der Wal, W., and Wouters, B. (2023). Mass Balance of the Greenland and Antarctic Ice Sheets from

1992 to 2020. *Earth System Science Data Discussions*, 15(4), pp.1–33.

Paolo, F.S., Fricker, H.A. and Padman, L. (2015). Volume Loss from Antarctic Ice Shelves Is Accelerating. *Science*, 348(6232), pp.327–331.

Paolo, F.S., Padman, L., Fricker, H.A., Adusumilli, S., Howard, S. and Siegfried, M.R. (2018). Response of Pacific-sector Antarctic Ice Shelves to the El Niño/Southern Oscillation. *Nature Geoscience*, 11(2), pp.121–126.

Park, J.W., Gourmelen, N., Shepherd, A., Kim, S.W., Vaughan, D.G. and Wingham, D.J. (2013). Sustained Retreat of the Pine Island Glacier. *Geophysical Research Letters*, 40(10), pp.2137–2142.

Parsons, R., Sun, S., Gudmundsson, G.H., Wuite, J. and Nagler, T. (2024). Quantifying the Buttressing Contribution of Landfast Sea Ice and Melange to Crane Glacier, Antarctic Peninsula. *The Cryosphere*, 18(12), pp.5789–5801.

Passchier, S., Browne, G., Field, B., Fielding, C.R., Krissek, L.A., Panter, K. and Pekar, S.F. (2011). Early and Middle Miocene Antarctic Glacial History from the Sedimentary Facies Distribution in the AND-2A Drill hole, Ross Sea, Antarctica. *Geological Society of America Bulleti*n, 123(11-12), pp.2352–2365.

Pattyn, F. (2018). The Paradigm Shift in Antarctic Ice Sheet Modelling. *Nature Communications*, 9(1).

Pattyn, F. and Morlighem, M. (2020). The Uncertain Future of the Antarctic Ice Sheet. *Science*, 367(6484), pp.1331–1335.

Paul, F., Bolch, T., Briggs, K., Kääb, A., McMillan, M., McNabb, R., Nagler, T., Nuth, C., Rastner, P., Strozzi, T. and Wuite, J. (2017). Error Sources and Guidelines for Quality Assessment of Glacier area, Elevation change, and Velocity Products Derived from Satellite Data in the Glaciers_cci Project. *Remote Sensing of Environment*, 203, pp.256–275.

Paxman, G.J.G., Gasson, E.G.W., Jamieson, S.S.R., Bentley, M.J. and Ferraccioli, F. (2020). Long-Term Increase in Antarctic Ice Sheet Vulnerability Driven by Bed Topography Evolution. *Geophysical Research Letters*, 47(20).

Pelle, T., Morlighem, M. and McCormack, F.S. (2020). Aurora Basin, the Weak Underbelly of East Antarctica. *Geophysical Research Letters*, 47(9).

Pelle, T., Morlighem, M., Nakayama, Y. and Seroussi, H. (2021). Widespread Grounding Line Retreat of Totten Glacier, East Antarctica, Over the 21st Century. *Geophysical Research Letters*, 48(17).

Picton, H.J., Stokes, C.R., Jamieson, S.S.R., Floricioiu, D. and Krieger, L. (2023). Extensive

and Anomalous Grounding Line Retreat at Vanderford Glacier, Vincennes Bay, Wilkes Land, East Antarctica. *The Cryosphere*, 17(8), pp.3593–3616.

Pollard, D., DeConto, R.M. and Alley, R.B. (2015). Potential Antarctic Ice Sheet Retreat Driven by Hydrofracturing and Ice Cliff Failure. *Earth and Planetary Science Letters*, 412, pp.112–121.

Pritchard, H.D., Arthern, R.J., Vaughan, D.G. and Edwards, L.A. (2009). Extensive Dynamic Thinning on the Margins of the Greenland and Antarctic Ice Sheets. *Nature*, 461(7266), pp.971–975.

Pritchard, H.D., Ligtenberg, S.R.M., Fricker, H.A., Vaughan, D.G., van den Broeke, M.R. and Padman, L. (2012). Antarctic ice-sheet loss driven by basal melting of ice shelves. *Nature*, 484(7395), pp.502–505.

Pritchard, H. D., Fretwell, P., Fremand, A. C., Bodart, J., Bamber, J. L., Bell, R., Bianchi, C., Bingham, R. G., Blankenship, D. D., Casassa, G., Catania, G., Christianson, K., Conway, H., Corr, H. F. J., Cui, X., Damaske, D., Damm, V., Drews, R., Eagles, G., Eisen, O., Eisermann, H., Ferraccioli, F., Forsberg, R., Franke, S., Fujita, S., Gim, Y., Goel, V., Gogineni, P., Greenbaum, J., Hills, B., Hindmarsh, R. C. A., Holmlund, P., Holschuh, N., Holt, J. W., Humbert, A., Jacobel, R. W., Jansen, D., Jenkins, A., Jokat, W., Jordan, T., King, E. C., Kohler, J., Krabill, W., Langley, K. A., Lee, J., Leitchenkov, G., Leuschen, C., Luyendyk, B. P., MacGregor, J., MacKie, E., Matsuoka, K., Mouginot, J., Nitsche, F. O., Nogi, Y., Nost, O. A., Paden, J. D., Pattyn, F., Popov, S. V., Kusk-Gillespie, M., Rignot, E., Rippin, D. M., Rivera, A., Ross, N., Ruppel, A., Schroeder, D. M., Siegert, M. J., Smith, A. M., Steinhage, D., Studinger, M., Sun, B., Tabacco, I., Tinto, B. K., Urbini, S., Vaughan, D. G., Welch, B. C., Wilson, D., Young, D. A., Zirizzotti, A., Aitken, A., Roberts, R., Kirkham, J. D., Dorschel, B., Field, E., Hoffman, A. O., Horlings, A. N., and Moholdt, G. (2024) *BEDMAP3 – Ice thickness, bed and surface elevation for Antarctica – gridded products (Version 1.0*), [Data Set]. NERC EDC UK Polar Data Centre. https://doi.org/10.5285/2d0e4791-8e20-46a3-80e4-f5f6716025d2.

Pritchard, H.D., Fretwell, P.T., Fremand, A.C., Bodart, J.A., Kirkham, J.D., Aitken, A., Bamber, J., Bell, R., Bianchi, C., Bingham, R.G., Blankenship, D.D., Casassa, G., Christianson, K., Conway, H., Corr, H.F.J., Cui, X., Damaske, D., Damm, V., Dorschel, B. and Drews, R. (2025). Bedmap3 Updated Ice bed, Surface and Thickness Gridded Datasets for Antarctica. *Scientific Data*, 12(1).

Purich, A. and Doddridge, E.W. (2023). Record Low Antarctic Sea Ice Coverage Indicates a

New Sea Ice State. *Communications Earth & Environment*, 4(1).

Ramanath, S., Krieger, L., Floricioiu, D., Diaconu, C.-A., and Heidler, K. (2025). Automatic grounding line delineation of DInSAR interferograms using deep learning, *The Cryosphere*, 19(7), pp.2431–2455.

Raphael, M.N., Maierhofer, T.J., Fogt, R.L., Hobbs, W.R. and Handcock, M.S. (2025). A twenty-first Century Structural Change in Antarctica's Sea Ice System. *Communications Earth & Environment*, 6(1).

Reese, R., Gudmundsson, G.H., Levermann, A. and Winkelmann, R. (2018). The Far Reach of Ice-Shelf Thinning in Antarctica. *Nature Climate Change*, 8(1), pp.53–57.

Rémy, F. and Parouty, S. (2009). Antarctic Ice Sheet and Radar Altimetry: A Review. *Remote Sensing*, 1(4), pp.1212–1239.

Ribeiro, N., Herraiz-Borreguero, L., Rintoul, S.R., McMahon, C.R., Hindell, M., Harcourt, R. and Williams, G. (2021). Warm Modified Circumpolar Deep Water Intrusions Drive Ice Shelf Melt and Inhibit Dense Shelf Water Formation in Vincennes Bay, East Antarctica. *Journal of Geophysical Research: Oceans*, 126(8).

Rignot, E. and Thomas, R.H. (2002). Mass Balance of Polar Ice Sheets. *Science*, 297(5586), pp.1502–1506.

Rignot, E., G. Casassa, P. Gogineni, W. Krabill, A. Rivera, and R. Thomas (2004). Accelerated ice discharge from the Antarctic Peninsula following the collapse of Larsen B ice shelf, *Geophysical Research Letters*, 31(18), pp.L18401.

Rignot, E., Velicogna, I., van den Broeke, M.R., Monaghan, A. and Lenaerts, J.T.M. (2011). Acceleration of the Contribution of the Greenland and Antarctic Ice Sheets to Sea Level Rise. *Geophysical Research Letters*, 38(5).

Rignot, E., Jacobs, S., Mouginot, J. and Scheuchl, B. (2013). Ice-Shelf Melting Around Antarctica. *Science*, 341(6143), pp.266–270.

Rignot, E., Mouginot, J., Morlighem, M., Seroussi, H. and Scheuchl, B. (2014). Widespread, Rapid Grounding Line Retreat of Pine Island, Thwaites, Smith, and Kohler glaciers, West Antarctica, from 1992 to 2011. *Geophysical Research Letters*, 41(10), pp.3502–3509.

Rignot, E., Mouginot, J. and Scheuchl, B. (2016). *MEaSUREs Antarctic Grounding Line from Differential Satellite Radar Interferometry*. (NSIDC-0498, Version 2). [Data Set]. Boulder, Colorado USA. NASA National Snow and Ice Data Center Distributed Active Archive Center. https://doi.org/10.5067/IKBWW4RYHF1Q.

Rignot, E., Mouginot, J., Scheuchl, B., van den Broeke, M., van Wessem, M.J. and

Morlighem, M. (2019). Four Decades of Antarctic Ice Sheet Mass Balance from 1979–2017. *Proceedings of the National Academy of Sciences*, 116(4), pp.1095–1103.

Rignot, E., Mouginot, J., Scheuchl, B. and Jeong, S. (2022). Changes in Antarctic Ice Sheet Motion Derived from Satellite Radar Interferometry between 1995 and 2022. *Geophysical Research Letters*, 49(23).

Rignot, E., Millan, R., Charrassin, R. and Scheinert, M. (2024). *Bathymetry of the Antarctic continental shelf and ice shelf cavities from a 3D inversion of circumpolar gravity anomalies constrained by other data*. [Data Set]. Dryad, https://doi.org/10.5061/dryad.rbnzs7hkc.

Rintoul, S.R., Silvano, A., Pena-Molino, B., van Wijk, E., Rosenberg, M., Greenbaum, J.S. and Blankenship, D.D. (2016). Ocean Heat Drives Rapid Basal Melt of the Totten Ice Shelf. *Science Advances*, 2(12), p.e1601610.

Rohling, E.J., Hibbert, F.D., Grant, K.M., Galaasen, E.V., Irvalı, N., Kleiven, H.F., Marino, G., Ninnemann, U., Roberts, A.P., Rosenthal, Y., Schulz, H., Williams, F.H. and Yu, J. (2019). Asynchronous Antarctic and Greenland ice-volume Contributions to the Last Interglacial sea-level Highstand. *Nature Communications*, 10(1), p.5040.

Roquet, F., Williams, G., Hindell, M.A., Harcourt, R., McMahon, C., Guinet, C., Charrassin, J.-B., Reverdin, G., Boehme, L., Lovell, P. and Fedak, M. (2014). A Southern Indian Ocean Database of Hydrographic Profiles Obtained with Instrumented Elephant Seals. *Scientific Data*, 1(1).

Ross, N., Milillo, P. and Dini, L. (2024). Automated Grounding Line Delineation Using Deep Learning and Phase gradient-based Approaches on COSMO-SkyMed DInSAR Data. *Remote Sensing of Environment*, 315, p.114429.

Rott, H., Skvarca, P. and Nagler, T. (1996). Rapid Collapse of Northern Larsen Ice Shelf, Antarctica. *Science*, 271(5250), pp.788–792.

Saunderson, D., Mackintosh, A., McCormack, F., Jones, R.S. and Picard, G. (2022). Surface Melt on the Shackleton Ice Shelf, East Antarctica (2003–2021). *The Cryosphere*, 16(10), pp.4553–4569.

Scambos, T. A., Bell, R. E., Alley, R. B., Anandakrishnan, S., Bromwich, D. H., Brunt, K., Christianson, K., Creyts, T., Das, S.B., DeConto, R., Dutrieux, P., Fricker, H. A., Holland, D., MacGregor, J., Medley, B., Nicolas, J. P., Pollard, D., Siegfried, M. R., Smith, A. M., Steig, E. J., Trusel, L. D., Vaughan, D. G., and Yager, P. L. (2017) How Much, How Fast?: A Science Review and Outlook for Research on the Instability of Antarctica's Thwaites Glacier in the 21st century. *Global and Planetary Change,* 153,

pp.16–34.

Scambos, T., Hulbe, C. and Fahnestock, M. (2003). Climate-Induced Ice Shelf Disintegration in the Antarctic Peninsula, in Domack, E., Levente, A., Burnet A., Bindschadler, R., Convey, R. and Kirby, M. (ed.) *Antarctic Peninsula Climate Variability: Historical and Paleoenvironmental Perspectives.* Washington, D.C., American Geophysical Union, pp. 79-92.

Scambos, T.A., Bohlander, J.A., Shuman, C.A. and Skvarca, P. (2004). Glacier Acceleration and Thinning after Ice Shelf Collapse in the Larsen B embayment, Antarctica. *Geophysical Research Letters*, 31(18).

Scambos, T.A., Hulbe, C., Fahnestock, M. and Bohlander, J. (2000). The Link between Climate Warming and Break-Up of Ice Shelves in the Antarctic Peninsula. *Journal of Glaciology*, 46(154), pp.516–530.

Scherer, R.P., DeConto, R.M., Pollard, D. and Alley, R.B. (2016). Windblown Pliocene Diatoms and East Antarctic Ice Sheet Retreat. *Nature Communications*, 7(1).

Schoof, C. (2007). Ice Sheet Grounding Line Dynamics: Steady States, Stability, and Hysteresis. *Journal of Geophysical Research*, 112(3), pp.1–19.

Schröder, L., Horwath, M., Dietrich, R., Helm, V., van den Broeke, M.R. and Ligtenberg, S.R.M. (2019a). Four Decades of Antarctic Surface Elevation Changes from Multi-Mission Satellite Altimetry. *The Cryosphere*, 13(2), pp.427–449.

Schröder, L., Horwath, M., Dietrich, R., Helm, V., van den Broeke, M. R., and Ligtenberg, S. R. M. (2019b) *Gridded surface elevation changes from multi-mission satellite altimetry 1978-2017*. PANGEA. https://doi.org/10.1594/PANGAEA.897390, 2019b.

Seroussi, H., Nowicki, S., Payne, A.J., Goelzer, H., Lipscomb, W.H., Abe-Ouchi, A., Agosta, C., Albrecht, T., Asay-Davis, X., Barthel, A., Calov, R., Cullather, R., Dumas, C., Galton-Fenzi, B.K., Gladstone, R., Golledge, N.R., Gregory, J.M., Greve, R., Hattermann, T., Hoffman, M.J., Humbert, A., Huybrechts, P., Jourdain, N.C., Kleiner, T., Larour, E., Leguy, G.R., Little, C.M., Morlighem, M., Pattyn, F., Pelle, T., Price, S.F., Quiquet, A., Reese, R., Schlegel, N.-J., Shepherd, A., Simon, E., Smith, R.S., Straneo, F., Sun, S., Trusel, L.D., Van Breedam, J., van de Wal, R.S.W., Winkelmann, R., Zhao, C., Zhang, T., and Zwinger, T. (2020). ISMIP6 Antarctica: a multi-model Ensemble of the Antarctic Ice Sheet Evolution over the 21st Century. *The Cryosphere*, 14(9), pp.3033–3070.

Seroussi, H., Pelle, T., Lipscomb, W.H., Abe-Ouchi, A., Albrecht, T., Alvarez-Solas, J., Asay-Davis, X., Barre, J.-B., Berends, C.J., Bernales, J., Blasco, J., Caillet, J., Chandler,

D.M., Coulon, V., Cullather, R., Dumas, C., Galton-Fenzi, B.K., Garbe, J., Gillet-Chaulet, F., Gladstone, R., Goelzer, H., Golledge, N., Greve, R., Gudmundsson, G.H., Han, H.K., Hillebrand, T.R., Hoffman, M.J., Huybrechts, P., Jourdain, N.C., Klose, A.K., Langebroek, P.M., Leguy, G.R., Lowry, D.P., Mathiot, P., Montoya, M., Morlighem, M., Nowicki, S., Pattyn, F., Payne, A.J., Quiquet, A., Reese, R., Robinson, A., Saraste, L., Simon, E.G., Sun, S., Twarog, J.P., Trusel, L.D., Urruty, B., Van Breedam, J., van de Wal, R.S.W., Wang, Y., Zhao, C., and Zwinger, T. (2024). Evolution of the Antarctic Ice Sheet over the next Three Centuries from an ISMIP6 Model Ensemble. *Earths Future*, 12(9).

Shepherd, A., Wingham, D. and Rignot, E. (2004). Warm Ocean Is Eroding West Antarctic Ice Sheet. *Geophysical Research Letters*, 31(23).

Shepherd, A., Gilbert, L., Muir, A.S., Konrad, H., McMillan, M., Slater, T., Briggs, K.H., Sundal, A.V., Hogg, A.E. and Engdahl, M.E. (2019). Trends in Antarctic Ice Sheet Elevation and Mass. *Geophysical Research Letters*, 46(14), pp.8174–8183.

Silvano, A., Rintoul, S. and Herraiz-Borreguero, L. (2016). Ocean-Ice Shelf Interaction in East Antarctica. *Oceanography*, 29(4), pp.130–143.

Silvano, A., Rintoul, S.R., Peña-Molino, B. and Williams, G.D. (2017). Distribution of Water Masses and Meltwater on the Continental Shelf near the Totten and Moscow University Ice Shelves. *Journal of Geophysical Research: Oceans*, 122(3), pp.2050–2068.

Smith, B., Fricker, H.A., Gardner, A.S., Medley, B., Nilsson, J., Paolo, F.S., Holschuh, N., Adusumilli, S., Brunt, K., Csatho, B., Harbeck, K., Markus, T., Neumann, T., Siegfried, M.R. and Zwally, H.J. (2020a). Pervasive Ice Sheet Mass Loss Reflects Competing Ocean and Atmosphere Processes. *Science*, 368(6496), pp.1239–1242.

Smith, B., Fricker, H. A., Gardner, A. S., Medley, B., Nilsson, J., Paolo, F. S., Holschuh, N., Adusumilli, S., Brunt, K., Csatho, B., Harbeck, K., Markus, T., Neumann, T., Siegfried, M. R.,and Zwally, H. J. (2020b) I*ce-sheet height and thickness changes from ICE-Sat to ICESat-2.* [Data Set]. ResearchWorks Archive http://hdl. handle.net/1773/45388.

Spreen, G., Kaleschke, L. and Heygster, G. (2008). Sea Ice Remote Sensing Using AMSR-E 89-GHz Channels. *Journal of Geophysical Research*, 113(2).

Stokes, C.R., Abram, N.J., Bentley, M.J., Edwards, T.L., England, M.H., Foppert, A., Jamieson, S.S.R., Jones, R.S., King, M.A., Lenaerts, J.T.M., Medley, B., Miles, B.W.J., Paxman, G.J.G., Ritz, C., van de Flierdt, T. and Whitehouse, P.L. (2022).

Response of the East Antarctic Ice Sheet to Past and Future Climate Change. *Nature*, 608(7922), pp.275–286.

Stokes, C.R., Bamber, J.L., Dutton, A. and DeConto, R.M. (2025). Warming of +1.5 °C Is Too High for Polar Ice Sheets. *Communications Earth & Environment*, 6(1).

Tamsitt, V., England, M.H., Rintoul, S.R. and Morrison, A.K. (2021). Residence Time and Transformation of Warm Circumpolar Deep Water on the Antarctic Continental Shelf. *Geophysical Research Letters*, 48(20).

The IMBIE Team (2018). Mass Balance of the Antarctic Ice Sheet from 1992 to 2017. *Nature*, 558(7709), pp.219–222.

Thoma, M., Jenkins, A., Holland, D. and Jacobs, S. (2008). Modelling Circumpolar Deep Water Intrusions on the Amundsen Sea Continental shelf, Antarctica. *Geophysical Research Letters*, 35(18).

Thompson, A., Stewart, A.K., Spence, P. and Heywood, K.J. (2018). The Antarctic Slope Current in a Changing Climate. *Reviews of Geophysics*, 56(4), pp.741–770.

Thompson, D.W.J. and Solomon, S. (2002). Interpretation of Recent Southern Hemisphere Climate Change. *Science*, 296(5569), pp.895–899.

Treasure, A.M., Roquet, F., Ansorge, I.J., Bester, M.N., Boehme, L., Bornemann, H., Charrassin, J.-B., Chevallier, D., Costa, D.P., Fedak, M.A., Guinet, C., Hammill, M.O., Harcourt, R.G., Hindell, M.A., Kovacs, K.M., Lea, M.-A., Lovell, P., Lowther, A.D., Lydersen, C., McIntyre, T., McMahon, C.R., Muelbert, M.M.C., Nicholls, K., Picard, B., Reverdin, G., Trites, A.W., Williams, G.D., and de Bruyn, P.J.N. (2017). Marine Mammals Exploring the Oceans Pole to Pole: A Review of the MEOP Consortium. *Oceanography*, 30(2), pp.132–138.

Turney, C.S.M., Fogwill, C.J., Golledge, N.R., McKay, N.P., van Sebille, E., Jones, R.T., Etheridge, D., Rubino, M., Thornton, D.P., Davies, S.M., Bronk Ramsey, C., Thomas, Z.A., Bird, M.I., Munksgaard, N.C., Kohno, M., Woodward, J., Winter, K., Weyrich, L.S., Rootes, C.M., Millman, H., Albert, P.G., Rivera, A., van Ommen, T., Curran, M., Moy, A., Rahmstorf, S., Kawamura, K., Hillenbrand, C.-D., Weber, M.E., Manning, C.J., Young, J., and Cooper, A. (2020). Early Last Interglacial Ocean Warming Drove Substantial Ice Mass Loss from Antarctica. *Proceedings of the National Academy of Sciences*, 117(8), pp.3996–4006.

van den Broeke, M.R. and van Lipzig, N.P.M. (2004). Changes in Antarctic Temperature, Wind and Precipitation in Response to the Antarctic Oscillation. *Annals of Glaciology*, 39, pp.119–126.

van den Broeke, M. (2005). Strong Surface Melting Preceded Collapse of Antarctic Peninsula Ice Shelf. Geophysical Research Letters, 32(12).

van Lipzig, N.P.M., Marshall, G.J., Orr, A. and King, J.C. (2008). The Relationship between the Southern Hemisphere Annular Mode and Antarctic Peninsula Summer Temperatures: Analysis of a High-Resolution Model Climatology. *Journal of Climate*, 21(8), pp.1649–1668.

Vannitsem, S., Dalaiden, Q. and Goosse, H. (2019). Testing for Dynamical Dependence: Application to the Surface Mass Balance Over Antarctica. *Geophysical Research Letters*, 46(21), pp.12125–12135.

Velicogna, I. (2009). Increasing Rates of Ice Mass Loss from the Greenland and Antarctic Ice Sheets Revealed by GRACE. *Geophysical Research Letters*, 36(19).

Velicogna, I. and Wahr, J. (2006). Measurements of Time-Variable Gravity Show Mass Loss in Antarctica. *Science*, 311(5768), pp.1754–1756.

Velicogna, I., Sutterley, T.C. and van den Broeke, M.R. (2014). Regional Acceleration in Ice Mass Loss from Greenland and Antarctica Using GRACE time-variable Gravity Data. *Geophysical Research Letters*, 41(22), pp.8130–8137.

Walker, C.C. and Gardner, A.S. (2017). Rapid Drawdown of Antarctica's Wordie Ice Shelf Glaciers in Response to ENSO/Southern Annular Mode-driven Warming in the Southern Ocean. *Earth and Planetary Science Letters*, 476, pp.100–110.

Walker, C.C., Millstein, J.D., Miles, B., Cook, S., Fraser, A.D., Colliander, A., Misra, S., Trusel, L.D., Adusumilli, S., Roberts, C. and Fricker, H.A. (2024). Multi-Decadal Collapse of East Antarctica's Conger–Glenzer Ice Shelf. *Nature Geoscience*, 17.

Wang, L., Davis, J.L. and Howat, I.M. (2021). Complex Patterns of Antarctic Ice Sheet Mass Change Resolved by Time-Dependent Rate Modeling of GRACE and GRACE Follow-On Observations. *Geophysical Research Letters*, 48(1).

Weatherley, M., Stokes, C.R., Jamieson, S.S.R., Ramanath, S. and Silvano, A. (2025) 'Dynamic thinning and grounding line retreat in Porpoise Bay, Wilkes Land, East Antarctica', *EGUsphere* [preprint]. https://doi.org/10.5194/egusphere-2025-4100.

Weertman, J. (1974). Stability of the Junction of an Ice Sheet and an Ice Shelf. *Journal of Glaciology*, 13(67), pp.3–11.

Wille, J.D., Favier, V., Jourdain, N.C., Kittel, C., Turton, J.V., Agosta, C., Gorodetskaya, I.V., Picard, G., Codron, F., Santos, C.L.-D., Amory, C., Fettweis, X., Blanchet, J., Jomelli, V. and Berchet, A. (2022). Intense Atmospheric Rivers Can Weaken Ice Shelf Stability at the Antarctic Peninsula. *Communications Earth & Environment*, 3(1), pp.1–14.

Wingham, D.J., Ridout, A.J., Scharroo, R., Arthern, R.J. and Shum, C.K. (1998). Antarctic Elevation Change from 1992 to 1996 . *Science*, 282(5388), pp.456–458.

Wingham, D.J., Shepherd, A., Muir, A. and Marshall, G.J. (2006). Mass Balance of the Antarctic Ice Sheet. *Philosophical Transactions of the Royal Society A: Mathematical, Physical and Engineering Sciences*, 364(1844), pp.1627–1635.

Xia, Y., Gwyther, D.E., Galton-Fenzi, B., Cougnon, E.A., Fraser, A.D. and Moore, J.C. (2023). Eddy and Tidal Driven Basal Melting of the Totten and Moscow University Ice Shelves. *Frontiers in Marine Science*, 10.

Yamazaki, K., Aoki, S., Katsumata, K., Hirano, D. and Nakayama, Y. (2021). Multidecadal Poleward Shift of the Southern Boundary of the Antarctic Circumpolar Current off East Antarctica. *Science Advances*, 7(24).

Young, D.A., Wright, A.P., Roberts, J.L., Warner, R.C., Young, N.W., Greenbaum, J.S., Schroeder, D.M., Holt, J.W., Sugden, D.E., Blankenship, D.D., van Ommen, T.D. and Siegert, M.J. (2011). A Dynamic Early East Antarctic Ice Sheet Suggested by Ice-Covered Fjord Landscapes. *Nature*, 474(7349), pp.72–75.

Yu, H., Rignot, E., Seroussi, H. and Morlighem, M. (2018). Retreat of Thwaites Glacier, West Antarctica, over the next 100 Years Using Various Ice Flow models, Ice Shelf Melt Scenarios and Basal Friction Laws. *The Cryosphere*, 12(12), pp.3861–3876.

Zachos, J., Pagani, M., Sloan, L., Thomas, E. and Billups, K. (2001). Trends, Rhythms, and Aberrations in Global Climate 65 Ma to Present. *Science*, 292(5517), pp.686–693.

Zachos, J.C., Lohmann, K.C., Walker, J.C.G. and Wise, S.W. (1993). Abrupt Climate Change and Transient Climates during the Paleogene: A Marine Perspective. *The Journal of Geology*, 101(2), pp.191–213.

Zwally, H. J., R. A. Bindschadler, A. C. Brenner, T. V. Martin, and R. H. Thomas (1983), Surface elevation contours of greenland and Antarctic Ice Sheets, *Journal of Geophysical Research*, 88(C3), pp.1589–1596.

Zwally, H.J., Giovinetto, M.B., Li, J., Cornejo, H.G., Beckley, M.A., Brenner, A.C., Saba, J.L. and Yi, D. (2005). Mass Changes of the Greenland and Antarctic Ice Sheets and Shelves and Contributions to sea-level rise: 1992–2002. *Journal of Glaciology*, 51(175), pp.509–527.